Exploring the aqueous dissolution-precipitation mechanism of Ca-Si-Na-O containing reactants to form crystalline calcium silicate hydrates in carbonated environments

A

Dissertation

Presented to

the faculty of the School of Engineering and Applied Science

University of Virginia

in partial fulfilment
of the requirements for the degree
Doctor of Philosophy
by

Coleman Tolliver

May 2023

APPROVAL SHEET

This Dissertation
is submitted in partial fulfillment of the requirements
for the degree of
Doctor of Philosophy

Author Signature: ____________________

This Dissertation has been read and approved by the examining committee:

Advisor: Elizabeth Opila

Committee Member: Prasanna Balachandran

Committee Member: Andres Clarens

Committee Member: Tao Sun

Committee Member: Dan Plattenberger

Accepted for the School of Engineering and Applied Science:

Jennifer L. West, School of Engineering and Applied Science

May 2019

Acknowledgements

This thesis is a part of the Reinventing CEMENT project funded through ARPA-E on Grant Award DE-AR0001858. I would like to thank the GEM consortium and the Bridge to the Doctorate Programs for proving me fellowships through my graduate experience. I also would like to thank the staff members in both the UVA Graduate & Postdoctoral Diversity Programs and the Engineering Center for Diversity for all their guidance and assistance. Thank you to Dr. Bill Epling for your time and fun conversations through the Mentorship Institute. Thank you to Drs. Beth Opila and Andres Clarens for advising me and helping me complete this degree. Finally, thank you to the many members of the Opila and Clarens research groups, past and present, for all your support and friendship.

List of acronyms and mineral names

Aragonite - $CaCO_3$, orthorhombic

Calcite – $CaCO_3$, trigonal

Vaterite – $CaCO_3$, hexagonal

CSH gel – amorphous calcium silicate hydrate

CCSH – crystalline calcium silicate hydrates

CCASH - crystalline calcium aluminum silicate hydrates

CNASH - crystalline sodium aluminum silicate hydrates

OPC – Ordinary Portland Cement

Portlandite – $Ca(OH)_2$, trigonal

Pwol – pseudowollastonite: $Ca_3Si_3O_9$ or $CaSiO_3$ empirically, monoclinic

Wollastonite - $Ca_3Si_3O_9$ or $CaSiO_3$ empirically, triclinic

Tobermorites

- Tobermorite 11Å – ($Ca_5Si_6H_2O_{18} \bullet 4H_2O$), monoclinic
- Tobermorite 12.5Å - $Ca_{7.76}\ Si_{6.76}O_{18.8}(OH)_{4.88}(H_2O)_{7.84}$, monoclinic
- Tobermorite 13Å - $Ca_{12}(Si_8O_{28})(H_2O)_{13}$, monoclinic

CCSH phases

- Gyrolite - $Ca_4(Si_6O_{15})(OH)_2 \cdot 3H_2O$, triclinic
- Rhodesite – $(Ca,K,Na)_8Si_{16}O_{40} \bullet 11H_2O$, Orthorhombic
- Pectolite - $NaCa_2Si_3O_8(OH)$, Triclinic

CNASH phases

- Analcime – $K_{0.19}Na_{7.69}Ca_{0.06}Al_8Si_{16}O_{48}(H_2O)_8$, triclinic
- Gismondine-Na – $Na_{3.6}Al_{3.6}Si_{12.4}O_{32} \bullet 14H_2O$, tetragonal
- Montmorillonite – $(Ca,Na)_{0.3}Al_2(Si,Al)_4O_{10}(OH)_2 \bullet xH_2O$, monoclinic

1. Introduction

1.0 Conventional OPC and its issues

Ordinary Portland Cement (OPC) is made by mixing ground calcium carbonate, aluminosilicate, and ferrosilicate feedstocks, heating to about 1450 ˚C, and then air quenching to 1200 ˚C to stabilize the more reactive phases. The primary components of OPC are tricalcium silicate ($(CaO)_3 \cdot SiO_2$), dicalcium silicate ($(CaO)_2 \cdot SiO_2$), tricalcium aluminate ($(CaO)_3 \cdot Al_2O_3$), and tetracalcium ferroaluminate ($(CaO)_4 \cdot Al_2O_3 \cdot Fe_2O_3$). The fired product, called clinker, is mixed with gypsum ($CaSO_4 \cdot 2\,H_2O$), and then ground to the desired particle size for the intended use.[1] Clinker is then used to make mortar, hydrated mixtures of cement and sand, or concrete, hydrated mixtures of cement, sand, and aggregate.

OPC is a hydraulic cement, meaning it cures in the presence of water to attain its maximum strength after about 28 days. Up to 81% of OPC is comprised of dicalcium and tricalcium silicate, according to ASTM C150,[2] which react with water to form **calcium silicate hydrate (CSH)** and portlandite ($Ca(OH)_2$).[1, 3] CSH is the primary phase attributed to the strength of OPC mortars and concretes and is comprised of tetrahedral silica chains sandwiching layers of calcium and oxygen. The CSH phase is chemically and morphologically inconsistent, resulting in a poorly crystalline matrix that is referred to as a gel. When OPC is used in concrete or mortar, the CSH gel forms a matrix that surrounds sand or aggregate grains to create high strength composites, which can be further reinforced with fibers or steel. Gel forms is not well understood, but strength varies with the interactions between semicrystalline nanoparticles of CSH, amorphous gel, and the distribution of pores and voids in the matrix.[3]

OPC is inexpensive with abundant feedstock, making it a great structural material, despite the short lifetimes of 50 years. The hydration of OPC is difficult to predict because of the variance in initial feedstock and the inconsistencies of the CSH gel matrix. While the CSH gel is the preferred hydration product, the reaction also produces portlandite ($Ca(OH)_2$) at 20-30% of the hydrated mass.[1] Portlandite provides no benefits to the overall strength and instead can be a pathway for calcium to leach out of the system if submerged or exposed to marine environments. The leached calcium leads to shorter silica chains and a less cohesive matrix. Portlandite is also prone to calcium removal by carbonating via atmospheric CO_2 and forming calcite. Both of the crystalline phases portlandite and calcite pose additional problems because they will dissolve in the presence of acids like those found in acid rain,[4] leading to voids and further infiltration pathways.

The production of OPC also presents environment issues, producing about 8% of global CO_2.[5] The thermal degradation of calcium carbonate into CaO and gaseous CO_2 accounts for about 50% of OPC emissions alone. Another 40% of emissions comes from burning fossil fuels to heat billions of tons of material to 1450 ˚C, with transportation and plant electricity accounting for the last 10%.[6] Cement producers are exploring green energy options for their furnaces, but removing CO_2 from calcium carbonate will still contribute significantly to global emissions.

The cement industry has partially addressed their emissions problem by mixing waste products from the energy or metallurgy sectors, like fly ash or slag, with OPC. These waste materials reduce the amount of OPC needed and are pozzolans: they are not cementitious materials on their own, but react with portlandite to form cementitious products.[7] The pozzolans improve strength and durability of OPC by reducing the chemical attack pathway and by forming a **calcium aluminum silicate hydrate (CASH)** gel,[8] which is more stable than its CSH counterpart.[9] CASH is structurally similar to CSH but has alumina substitutions in the silica chains. Its stability is particularly useful in marine environments to resist attacks from sulfates and other salts.[10] However, environmental regulations and the move to greener energy sources has decreased the production of these waste products, like fly ash from coal, rendering them a temporary solution.

1.1 Tobermorite and ancient Roman concretes

Another way to improve OPC is to strengthen the CSH gel by forming **crystalline calcium silicate hydrates (CCSH)**, like tobermorite. Tobermorites are sought after precipitate phases in cement research due to the high strengths they provide relative to CSH gel. Ideal tobermorite ($Ca_5Si_6H_2O_{18} \bullet 4H_2O$), also known as tobermorite 11 Å, is comprised of silica chains sandwiching calcium oxide layers and interlayers of Ca^{2+} and water, as seen in Figure 1.1. Tobermorite can be described as an ordered form of the CSH gels produced in OPC. However, CCSHs are not found in conventional OPC structures because they form hydrothermally in the temperature range of 80-180 ˚C.[11]

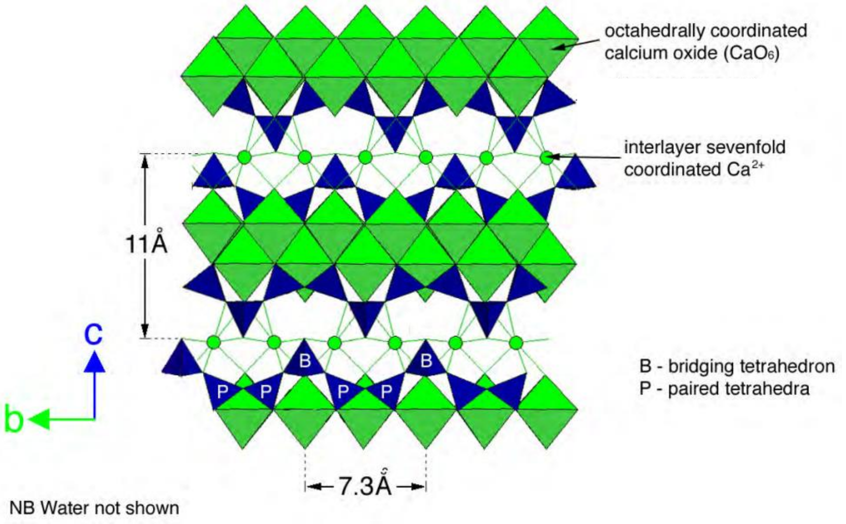

Figure 1.1. Structure of tobermorite 11 Å($Ca_5Si_6H_2O_{18} \bullet 4H_2O$)).[12]

Tobermorite synthesis experiments often use mixtures of CaO and a finely ground SiO_2 source, like quartz or amorphous SiO_2, at a Ca:Si molar ratio of 5:6 to match the stoichiometry of the phase. CaO and SiO_2 react to form CSH gel, described notionally in Equation 1.1.

$$xCaO_{(s)} + ySiO_{2(am)} + zH_2O_{(l)} \xleftrightarrow{time,temp} xCaO \cdot ySiO_2 \cdot zH_2O_{am}^{\delta} \tag{1.1}$$

Here, the stoichiometry is undefined, and the δ charge indicates the variable charge which is experienced locally in the CSH gel. The CSH gel then orders into crystalline form at temperatures above 80 ˚C, described in Equation 1.2

$$xCaO \cdot ySiO_2 \cdot zH_2O_{am}^{\delta} \xleftrightarrow{time,temp} Ca_5Si_6O_{16}(OH)_2 \cdot 4H_2O_{(s)} \tag{1.2}$$

There are many phases in the tobermorite family, differentiated by the amounts of bonded water, the amount of calcium in the interlayers, and the orientations of the silica tetrahedra. A list of variations of tobermorites described in this work can be found on page iv. This body of work will focus on tobermorite – 11 Å, referred to simply as tobermorite, as model CCSHs for precipitation.

Aluminum substituted tobermorite – 11Å (Al-tobermorite) is one variation in the larger tobermorite family. Al-tobermorite can be differentiated from tobermorite by the substitution of Al^{3+} for Si^{4+}, most commonly at the bridging sites,[13] as circled in Figure 1.2.

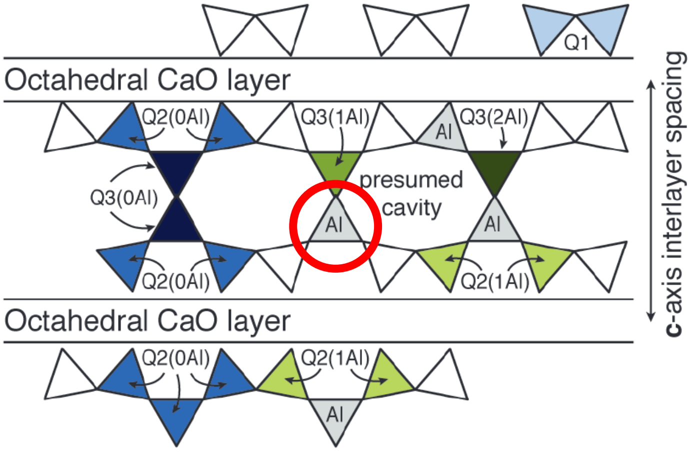

Figure 1.2. Locations of aluminum substitution in Al-tobermorite, with the bridging site circled in red. Here, Q"X" notes the number of bonds to other tetrahedra and ("Y"Al) notes how many of the X bonds are to alumina tetrahedra.[13]

Al-tobermorite has been studied because of its contributions to the longevity and strength of ancient Roman marine concretes. These concretes were made using lime, volcanic ash pozzolan with high sodium content from the Flegrean Fields volcanic district, and volcanic glasses as aggregate.[13-16] Unlike modern methods used to form tobermorites, Roman concretes were not autoclaved. Instead, the heat necessary for the hydrothermal reaction came via the reaction of lime with seawater to form portlandite, estimated to reach up to 97 ˚C.[13] The portlandite would then react with the volcanic ashes to form CASH, Al-tobermorite, and other crystalline phases. Another key feature of Roman concrete is its high porosity,[15] a trait that is minimized in conventional cements to prevent degradation. The high porosity allowed the influx of sea water that slowly dissolved glass aggregates. The resulting alkali rich pore solution further facilitated the growth of Al-tobermorite over several years.[15] The result was a concrete that "can neither be dissolved in the waves, nor by the power of water" [Vitruvius, de Architectura, 30 BCE].

Al-tobermorite is also studied for its improved sorption properties for long term storage of radioactive metals, like Cs Rb, using cement. The charge imbalance caused by the Al_2O_3 tetrahedra substituting for silica allows for greater ion exchange with solutions.[17, 18] Tobermorite synthesis studies use Al_2O_3 to form Al-tobermorite, which generally decreases growth rates compared to ideal tobermorite. Small molar additions of α or γ phase Al_2O_3 (5% Al/(Si+Al)), have been shown to decrease the crystallinity of tobermorite.[19] In a study by Gabrovsek, Al_2O_3 dissolution was predicted to slow precipitation of tobermorite by negatively impact aqueous SiO_2 solubility.[20]

The addition of Na^+, usually in the form of NaOH, has been shown to improve sorption of to Al-tobermorite, but negatively impacts the crystallinity.[17, 18, 20, 21] Increasing concentrations of NaOH have also been shown to decrease crystallinity of ideal tobermorite when CaO and SiO_2 are reactants by stabilizing the CSH gel formed.[21] However, NaOH, Na_2CO_3, and $NaHCO_3$, have all been shown to increase to tobermorite precipitation when calcium silicates or calcium aluminum silicates are used as reactants.[22–25]

1.2 Alternative cements

One viable climate solution of recent focus is CO_2 mineralization, where gaseous carbon is converted to carbonate salts using materials like calcium and magnesium silicates. $Ca_3Si_3O_9$ ($CaSiO_3$ empirically), the line compound in the CaO-SiO_2 system shown in Figure 1.3, has shown promise in carbonation research for its reactivity. Coincidentally, the $CaSiO_3$ phase wollastonite (wol) also has great potential as an alternative cement, producing high strengths when carbonated for as short as 3 days.[26] Unlike the CSH gel of OPC, the wol cement strength is attributed to the formation of calcium carbonate crystalline networks, primarily calcite.[27]

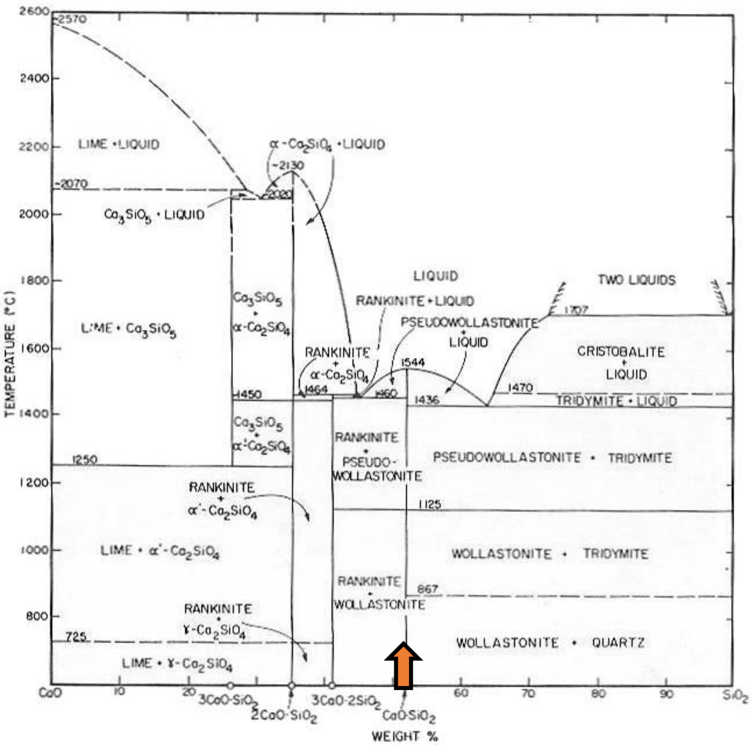

Figure 1.3. A phase diagram of the CaO-SiO$_2$ system, with the orange arrow indicating the line compound for CaSiO$_3$.[28]

Pseudowollastonite (pwol), the polymorph of wollastonite that forms above 1125 ˚C, has also been shown to have a high conversion to calcium carbonates. Additionally, in the presence of NaOH, pwol is also able to produce CCSHs, particularly in the tobermorite family.[23, 25, 29, 30] The combination of CCSH phases alongside carbonates in pwol mortar samples has been shown to improve both compressive strength and acid resistance when compared to pure calcium carbonate mortar from wollastonite cement,[30] as seen in Figure 1.4. These mortar samples were produced via a two-step curing process in which cast mortar is placed into a dry and wet curing environment, outlined by Plattenberger.[30]

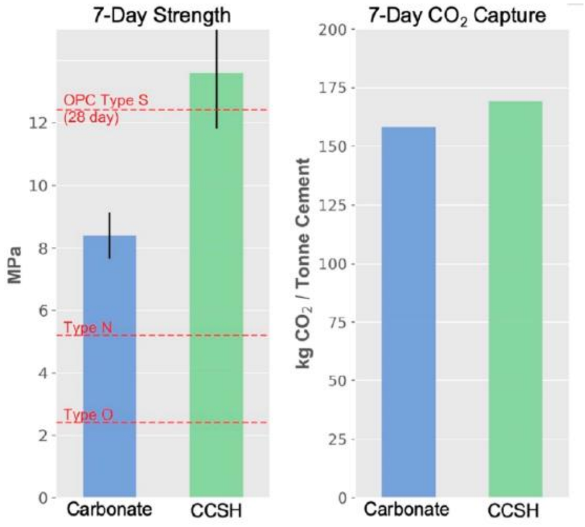

Figure 1.4. A compressive strength plot of pwol mortar where carbonate is pwol cement without NaOH, only forming calcium carbonates, CCSH indicates pwol and NaOH to form unidentified crystalline phases, and the Type S, N and O are different commercially available OPC blends with reported mortar strength data.[30]

The work presented in this thesis was a part of work done on the Reinventing CEMENT grant, which was funded by ARPA-E based on the pwol research of Plattenberger.[25, 29, 30] The overarching goal of the project was to design novel techniques to produce a low carbon emission, cementitious material with CCSH phases to increase strength and durability. Lifetime cycle analysis based on data collected previously by Plattenberger[30] indicates that precast concrete structures made with pwol cement would have a significantly smaller CO_2 footprint compared to OPC concrete,[31] as seen in Figure 1.5. The largest offsets would come from reducing emissions from cement production and CO_2 uptake during curing. Cement production would require less consumption of calcium carbonate than OPC because pwol has less calcium than dicalcium or tricalcium silicate. Additionally, pwol can be synthesized at 1125 ˚C, requiring significantly less energy compared the OPC synthesis temperature of 1450 ˚C.

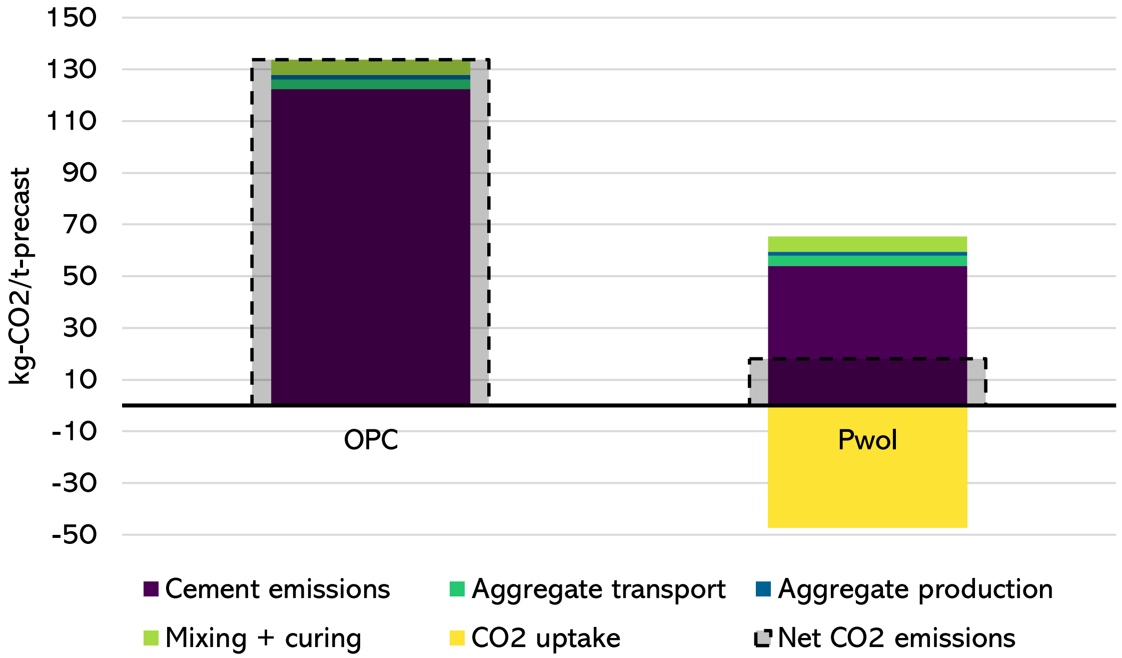

Figure 1.5. A CO_2 emissions plot comparing production of OPC precast to predicted pwol precast using data from Plattenberger.[30, 31]

While pwol is predicted to have lower emissions than OPC, we estimate that pwol precast structures would be over twice as expensive as OPC precast. The largest majority of the increase comes from purchasing, running, and maintaining autoclaves at the necessary CO_2 pressure for curing pwol cement. In order to design a low carbon footprint material with competitive costs to OPC, the Reinventing CEMENT project aimed to use cheaper waste slags or ashes to produce cementitious materials. **Pwol was used as a model calcium silicate to research aqueous chemistry and develop techniques to eventually apply to the more complex systems presented in waste materials.**

Initial research pointed to the pwol crystal structure and dissolution as a major factor in CCSH precipitation. Figure 1.6 shows that pwol has three-member silicate rings that dissolve congruently, unlike, the silicate chains that dissolve incongruently from wol.[32] The higher concentration of aqueous silica in solution from pwol dissolution is hypothesized to facilitate

CCSH precipitation after the system is saturated with calcium carbonates. In pwol mortar samples, CCSH phases have been shown to form in the pores and greatly reduce the permeability of the material and prevent acid infiltration.[25] Networks of plate and needle like crystals, hypothesized to be CCSHs, can be seen in Figure 1.7.

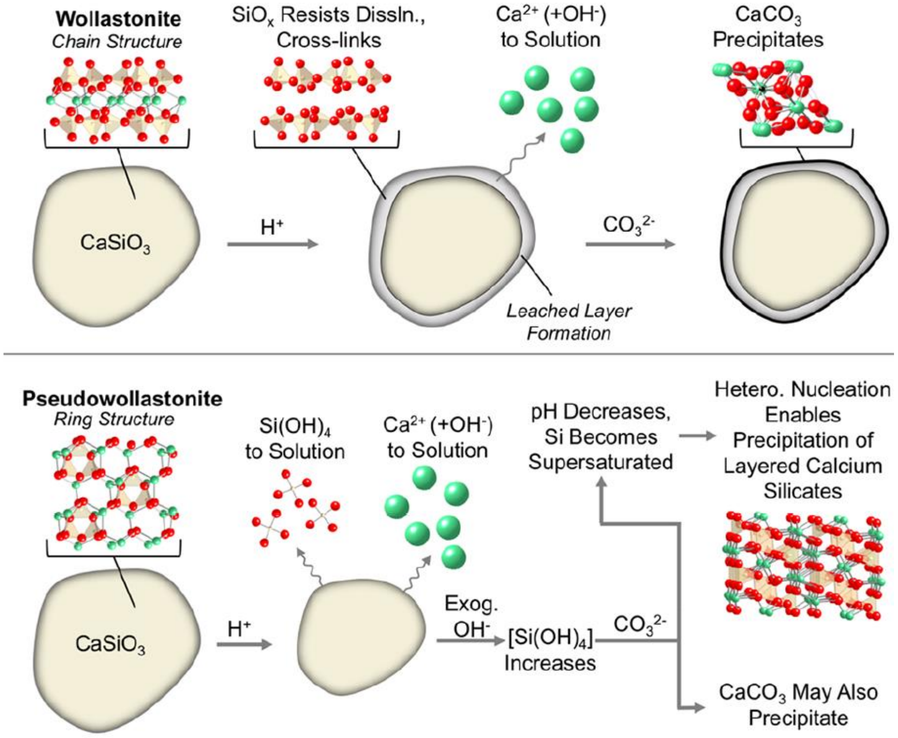

Figure 1.6. Different dissolution/precipitation mechanism proposed for the polymorphs wollastonite and pwol in the presence of CO_2 and form precipitates.[25]

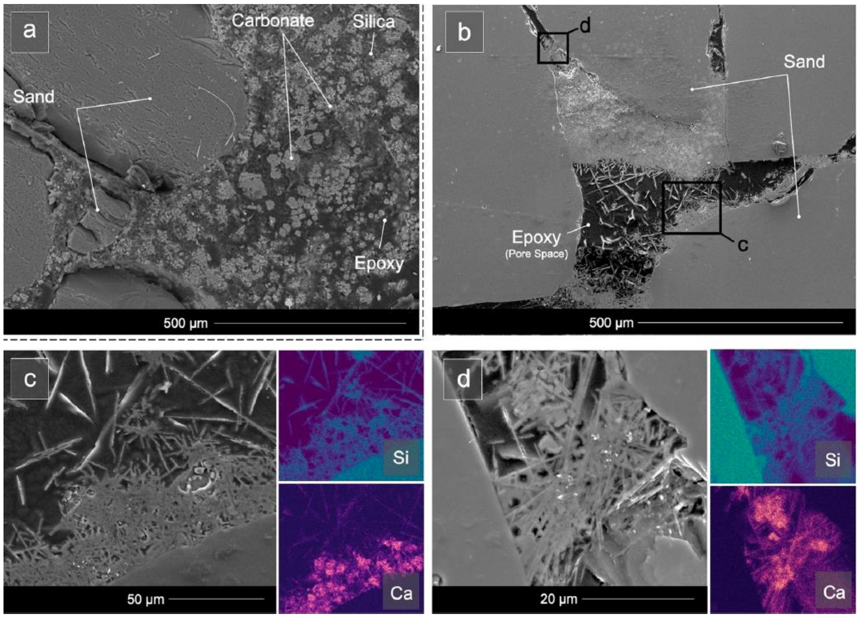

Figure 1.7. Scanning electron micrographs of CO_2 flow through pwol mortar samples. a. indiscriminate precipitation of calcium carbonates throughout matrix. b. plate and needle phases precipitating in pore throats. c, d. energy dispersive spectroscopy maps indicating the plate and needle phases contain both Ca and Si.[25]

CCSH phases were shown to precipitate from pwol in mortar experiments done in prior work done by Plattenberger,[23] however, the crystalline phases found have not been identified.[25, 29, 30] Continuation experiments were conducted around the mortar mix designs and curing conditions over two years that improved the compressive strength significantly. However, attempts to characterize bulk powder filtered from crushed mortar samples via **X-ray diffraction (XRD)** and **thermogravimetric analysis (TGA)** indicated the powder was primarily unreacted pwol and the calcium carbonate phases calcite and aragonite; there were no CCSH phases detected in these samples. Additionally, the experiments and data collected did little to elucidate the pwol to CCSH mechanism, as seen by the possible pathways proposed in Figure 1.8. A new approach was required to clarify the mechanism because the evolution of the chemistry inside the mortar pores could not be monitored, especially at pressure and temperature. **Thus, the major**

goal of this thesis was to identify chemical pathways to form measurable amounts of CCSH from pwol in carbonated environments.

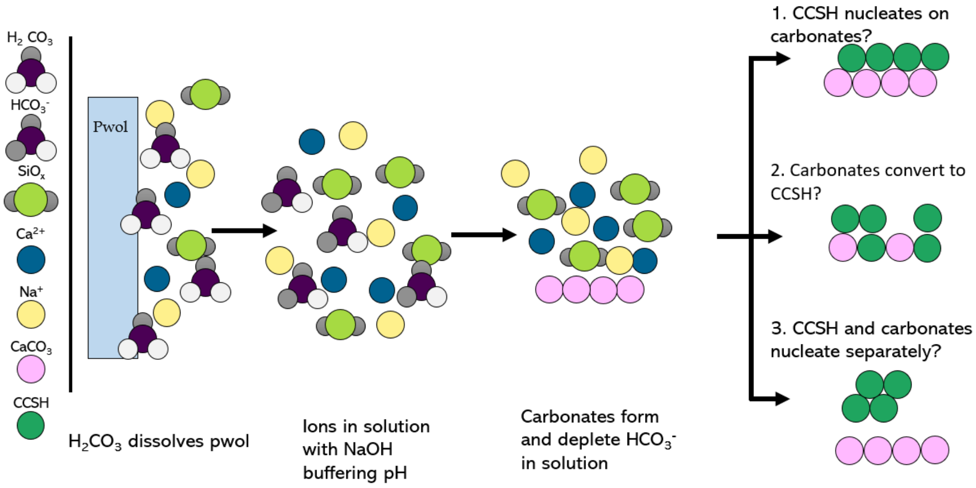

Figure 1.8. Schematic diagram of possible pwol dissolution and tobermorite precipitation mechanism.

2. Preliminary exploration of CCSH precipitation from pure reactants

2.0 Background

The first step in understanding how **crystalline calcium silicate hydrates (CCSHs)** precipitated from **pseudowollastonite (pwol)** was to start with pure reactants and define the key variables necessary for precipitation under similar conditions to that of the prior pwol mortar experiments. This Chapter explores the precipitation of tobermorite, as a model CCSH, from combinations of CaO and SiO_2 or CaO and **tetraethyl ortho silicate (TEOS)** and the resulting solution chemistry required. The effects of amorphous versus aqueous silica sources, the presence of NaOH and α-Al_2O_3, and, through serendipity, the **partial pressure of CO_2 (P_{CO_2})** at 150°C were investigated. Contrary to previous studies using CaO and SiO_2, positive relationships between tobermorite precipitation and the presence of NaOH were found using micro silica, while Al_2O_3 improved tobermorite precipitation from TEOS. The reaction pathway for CaO and SiO_2 to tobermorite are rewritten below as Equations 2.1 and 2.2 for convenience.

$$5CaO_{(s)} + 6SiO_{2(am)} + 5H_2O_{(l)} \xleftrightarrow{time,temp} 5CaO \cdot 6SiO_2 \cdot 5H_2O^{\delta}_{am} \tag{2.1}$$

$$5CaO \cdot 6SiO_2 \cdot 5H_2O^{\delta}_{am} \xleftrightarrow{time,temp} Ca_5Si_6O_{16}(OH)_2 \cdot 4H_2O_{(s)} \tag{2.2}$$

2.1 Research questions

i. What is the reaction timeframe for CCSH precipitation?

ii. How does the presence of NaOH affect this reaction?

iii. How does the presence of Al_2O_3 affect this reaction?

iv. How does the P_{CO_2} affect this reaction?

v. How do the solution chemistry and precipitates from micro silica and TEOS reactants vary?

2.2 Methods

2.2.1 Experimental setup

The commercially available powders used were CaO (Fisher, 99.95% pure), Elkem micro silica 965 (95% pure), and α-phase Al_2O_3 (Fisher, 99.9% pure). Powders were combined at a Ca:Si ratio of 5:6 or a Ca:(Si+Al) of 5:6 with an Al/(Si+Al) = 0.05 where applicable.[33-35] The total powder mass was 2 g. The powders were put into 25 mL borosilicate glass test tubes (Fisher) and vortexed (Fisher Scientific Vortex Mixer) for 15 seconds. The importance of SiO_2 solubility on the precipitation rate was explored using TEOS as an alternative reactant. TEOS (Sigma Aldrich) was added at 8.318 mL to 2 g of CaO powder, both with and without Al_2O_3 at the same molar ratio. **Deionized (DI)** water or 0.1 M NaOH (Fisher) solution was added to the SiO_2 and TEOS experiments to reach a volume of 20 mL and vortexed again. Table 2.1 lists all the variations of experiments completed and highlights which experiments produced tobermorites or other CCSHs, all of which were identified by X-ray diffraction (XRD, Malvern-Panalytical Empyrean, Worcestershire, UK) analysis and are shown in Chapter 2.3. It should be noted that the combination of CaO, TEOS, and α-Al_2O_3 was not run in the initial 3 days – additional carbonation (AC) trial, which cannot be accurately replicated. The abbreviations AC and no carbonation (NC) will be explained in Chapter 2.1.2.

Table 2.1. Products phases produced in 150 °C exposure. 3 days – AC is Additional Carbonation and 3 days – NC is No Carbonation. Phases were identified via XRD.

DI water							
Reactants	1 hour	6 hours	24 hours	3 days - AC	3 days	3 days - NC	7 days
CaO + micro SiO_2	⬜	⬜	⬜	⬜	⬜	⬜	⬜
CaO + micro SiO_2 + α-Al_2O_3	⬜	⬜	⬜	⬜	⬜	⬜	⬜
CaO + TEOS	⬜	⬜	⬜	⬜	🟦	⬜	🟩
CaO + TEOS + α-Al_2O_3	⬜	⬜	⬜	☒	🟦	⬜	🟩

0.1 M NaOH							
CaO + micro SiO_2	⬜	⬜	⬜	🟦	🟦	⬜	🟩
CaO + micro SiO_2 + α-Al_2O_3	⬜	⬜	⬜	🟦	🟦	⬜	🟩
CaO + TEOS	⬜	⬜	⬜	⬜	⬜	⬜	🟩
CaO + TEOS + α-Al_2O_3	⬜	⬜	⬜	☒	🟦	🟦	🟩

⬜ No Tobermorite 🟦 Tobermorite 🟩 Tobermorite and CCSH ☒ Not conducted

2.2.2 Hydrothermal experiments and CO_2 exposure

Test tubes were placed into a test tube rack and sealed in a pressure vessel with 1.5 L of water, then heated in an oven at 150 °C (± 3 °C) for 1 hour, 6 hours, 24 hours, 3 days, or 7 days of curing. All sample compositions at a given timestep were cured together in the same pressure vessel along with preliminary experiments for Chapter 3 of this work.

An initial 3-day experiment was run to confirm that tobermorite would be produced with the reactant combinations in Table 2.1, excluding the combination of TEOS, CaO, and Al_2O_3. In this first experiment, all samples were exposed to an unknown, additional quantity of gaseous CO_2, referred to as the Additional Carbonation (AC) condition. Here, the pressure vessel was initially sealed by connecting a line to a syringe pump (Teledyne ISCO 500D, Lincoln, NE, US) to monitor the pressure, illustrated in Figure 2.1a. This experiment was repeated without gaseous exposure for consistency, but the AC experiments will be included in this work. Because samples were cured alongside preliminary experiments from Objective 4 that contained fixed amounts of Na_2CO_3 (Fisher), it was also discovered that CO_2 was released and contaminated experiments due to the high temperature decreasing the gas solubility in solution. Using the ideal gas law at 150 °C, the P_{CO_2} potentially increased from 0.008 psi from atmospheric CO_2 to a maximum of 1.15 psi if all the CO_2 were to leave the Na_2CO_3 solutions. All timesteps were completed with the CO_2 exposure from Na_2CO_3, and this will be referred to as the standard condition. One final repeat was run for 3 days without the Na_2CO_3 experiments, noted as No Carbonation (NC).

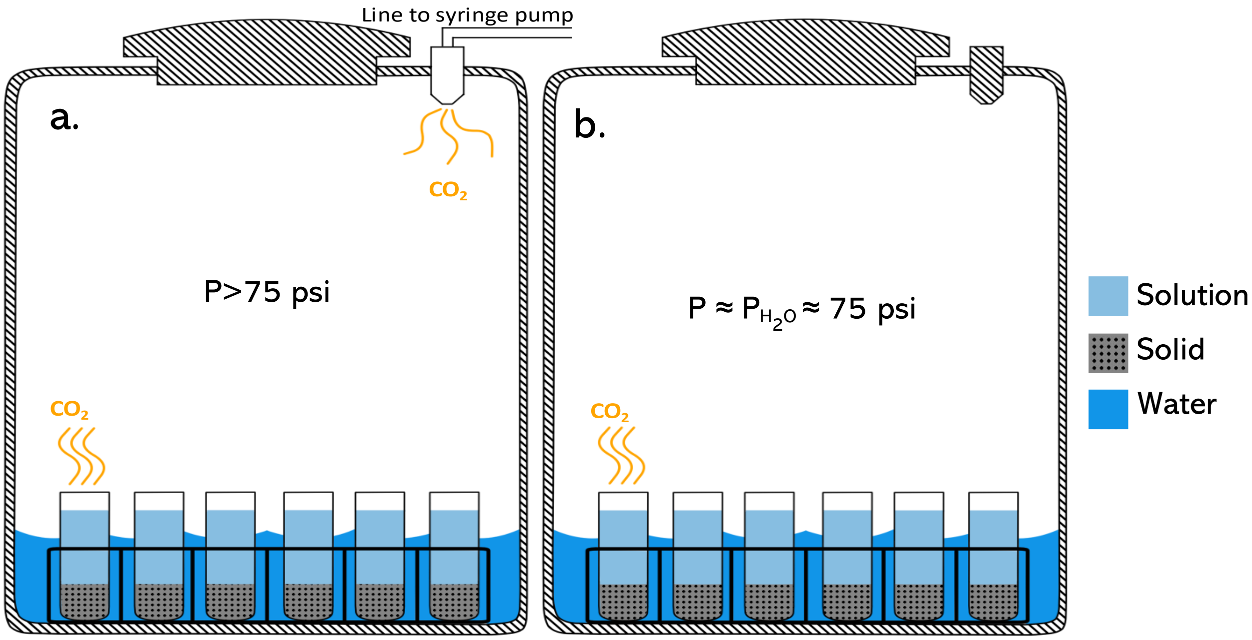

Figure 2.1 a. the initial experimental set up where samples were exposed to Additional Carbonation (AC) for 3 days at 150 °C. b. The standard setup for all timesteps.

The pressure vessels were removed from the oven and were naturally cooled to room temperature before removing the test tubes. The supernatant was separated from the micro silica experiments using 25 µm filter paper (Whatman) after curing and were stored for future analysis; the TEOS experiments formed gels after curing and did not have supernatant remaining for collection. The remaining powders were acidified with 0.1 M acetic acid, filtered, dried at 40 °C for 24 hours, and then stored in vials for future analysis.

2.2.3 Characterization

X-ray diffraction (XRD) of the dried precipitates was conducted using the following parameters Cu Kα-radiation (λ =1.5405 Å); current = 40 mA; tension = 45 kV; GaliPIX Detector; measurement range = 4.8–55°2θ; time per step = 60 s; and step size =0.0143 °2θ. The sample stage was spun during the scans to minimize the effects of orientation. The scans were repeated 3 times and summed for analysis. The data were analyzed with Highscore Plus (Version 4.9) using the International Centre for Diffraction Data (ICDD) database to identify phases. Table 2.2 contains the mineral names, compositions, and ICDD reference codes of the phase identified in this Chapter. All referenced patterns of the major phases (>10% mass) and minor phases (2-10%) identified showed strong alignment of peak locations and intensities with data presented.

Table 2.2. A list of mineral names, chemical formulae, and ICDD reference codes for the phases identified in this work. Major phases over an estimated 10% mass are indicated by (+), minor phases from 2-10% mass by (-), and trace phases under 2% by (t).

Mineral Name	Chemical formula	ICDD reference code
Calcite (+)	$CaCO_3$	04-008-0198
Portlandite (+)	$Ca(OH)_2$	04-014-7726
α-Al_2O_3 (t)	Al_2O_3	00-005-0712
Tobermorite (+)	$Ca_4Si_6O_{16}(OH)_2 \bullet 4H_2O$	00-019-1364
Unnamed CCSH (-)	$Ca_9(Si_{16}O_{34}(OH)_{14})(H_2O)_8$	01-074-7587

Select samples were further analyzed via TGA (Netzsch STA-449 F1, Bayern, Germany) to measure the amount of hydration and carbonation. For this characterization, 100 mg of powder was placed in a Pt-Rh crucible and heated at a rate of 10 °C/min to 1000 °C. The STA-449 F1 has a mass resolution of 0.025 µg. The mass change data were collected and compared to the literature.[23, 36–38]

Five mL from all supernatants were acidified with 5 mL of a 1 M HF and 1 M HNO_3 solution. The digested samples were then diluted 200x with deionized water. Standards of Ca, Si, Na, and Al (Inorganic Ventures) were made for calibration. Supernatant concentrations were measured in triplicate using inductively coupled plasma – optical emission spectroscopy (ICP-OES, Thermofisher ICAP 6200, Waltham, Massachusetts, US).

2.3 Results

XRD data indicated the earliest tobermorite precipitation occurred between 24 and 72 hours of curing in this experimental set up, across all conditions. When cured for 168 days, the precipitates that did produce tobermorite also produced the same unnamed CCSH phase seen at 5.8° 2θ in XRD spectra.

2.3.1 Micro silica experiments

The experiments using CaO and micro silica showed a clear relationship between the presence of NaOH and CCSH precipitation, where tobermorite only precipitated in the samples containing 0.1 M NaOH between 24 and 72 hours, as seen in Figure 2.2. The sodium dependance of tobermorite was inconsistent with synthesis literature using similar reactants, where tobermorite has been shown to exhibit less crystallinity in the presence of NaOH, although precipitation occurred at a similar time frame.[20] In the micro silica precipitates, the presence of α-Al_2O_3 showed little effect on the precipitation of tobermorite in the XRD spectra in Figure 2.2 and in the TGA data (not shown). Based on the literature, Al_2O_3 was expected to decrease the amount of tobermorite precipitated, particularly in combination with NaOH. [17, 19, 20] In these and following plots calcite refers to $CaCO_3$ and portlandite to $Ca(OH)_2$.

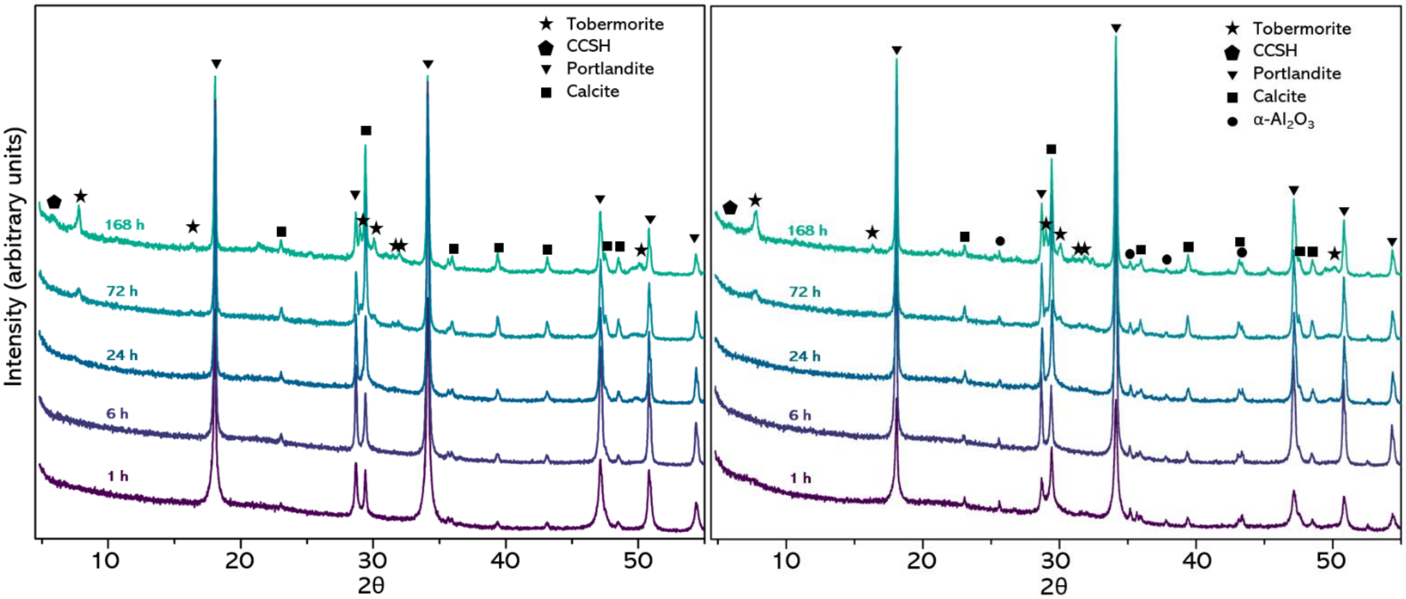

Figure 2.2. XRD time comparison plot of the micro silica and 0.1M NaOH experiments a. without a- Al_2O_3*, b. with a-*Al_2O_3 *at standard* P_{CO_2}*. Note the early peaks at 8° 2θ, indicating the 11Å basal plane of tobermorite after 72 hours. Calcite (*$CaCO_3$*), Portlandite (*$Ca(OH)_2$*)*

The P_{CO_2} had a noticeable effect on these experiments, increasing the amount of tobermorite formed with increasing CO_2, as seen clearly in Figures 2.3a and 2.3b. The XRD data also show a decrease in portlandite as it is converted to calcite with increasing P_{CO_2}.

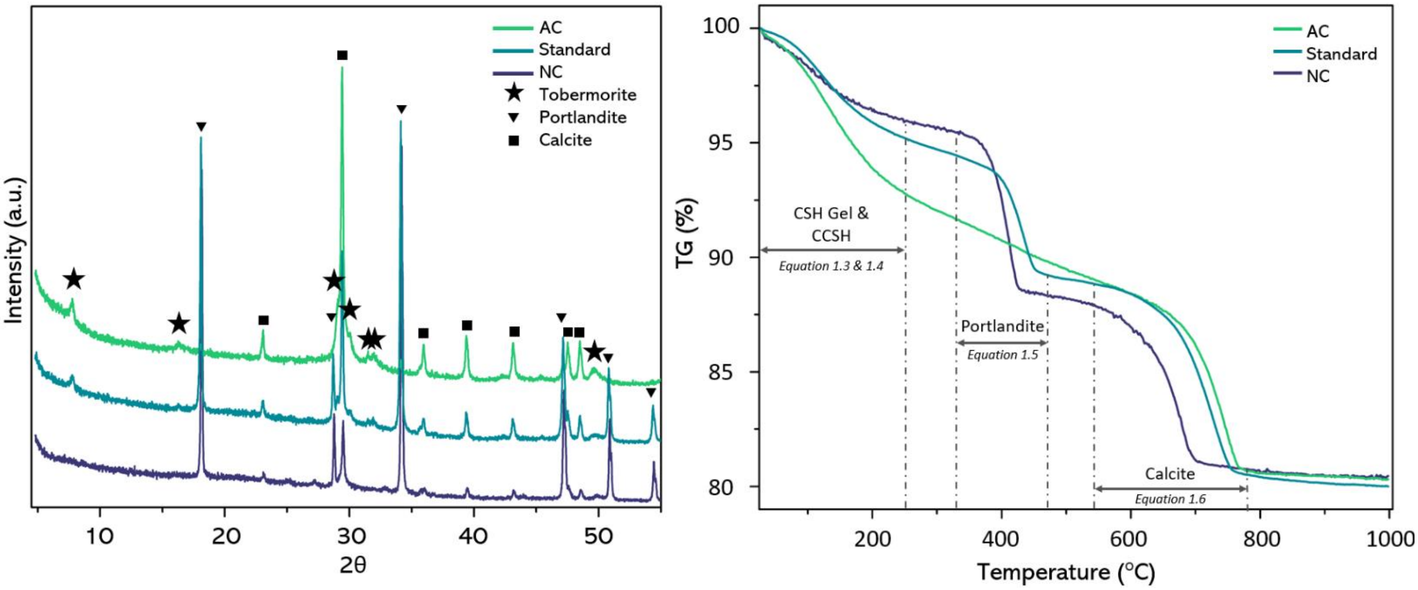

Figure 2.3. a. XRD plot and b. TG plot comparing the No Carbonation (NC), standard, and Additional Carbonation (AC) conditions at 3 days in 0.1M NaOH.

The TGA data show an increase in the dehydration of CSH gel and tobermorite from 50-250 °C[39] in Figure 2.3b, supporting the trends in XRD data. About 4.1% water vapor was lost for NC, 4.8% for standard, and 7.1% for AC. Equations 2.3 and 2.4 nominally describe the thermal decomposition of CSH and tobermorite, respectively.

$$xCaO \cdot ySiO_2 \cdot zH_2O_{am}^{\delta} \overset{\Delta h}{\rightarrow} CaSiO_3 + H_2O_{(g)} \qquad (2.3)^{39}$$

$$Tobermoite\ 11\text{Å} \overset{\Delta h}{\rightarrow} Tobermorite\ 9\text{Å} + 2H_2O_{(g)} \overset{\Delta h}{\rightarrow} CaSiO_{3(s)} + 2H_2O_{(g)} \qquad (2.4)^{40}$$

Here $CaSiO_3$ is wollastonite, and tobermorite 9Å ($Ca_5Si_6O_{16}(OH)_2 \cdot 2H_2O_{(s)}$) is the dehydrated form of tobermorite that occurs after about 250 °C. The Δh term indicates that heat is required for the thermal decomposition to occur. Tobermorite 9Å does not dehydrate at a set temperature, but instead slowly loses water from 250-800 °C and eventually transitions to wollastonite.[40] This slow dehydration can be seen in Figure 2.3b, where the AC curve shows constant mass loss without a definitive step. The increase in P_{CO_2} suppressed portlandite formation, from about 16.3% by mass in the NC condition, to 10.23% in the standard condition, and to 0% in the AC condition. The thermal decomposition of portlandite occurs around 400 °C[37] and is described below in Equation 2.5.

$$Ca(OH)_{2(s)} \overset{\Delta h}{\rightarrow} CaO_{(s)} + H_2O_{(g)} \qquad (2.5)^{37}$$

Despite the differences in calcite intensity in the XRD data, the P_{CO_2} only slight increased the amount of calcite formed from the baseline NC condition based on the TGA data. This difference in XRD spectra is likely due to the high intensity of portlandite present dominating calcite. The precipitates from the NC condition were calculated to be comprised of about 15.9% calcium carbonate, where precipitates from the standard and AC conditions were 18.8% and 18.5%, respectively. $CaCO_3$ decomposes into CaO and gaseous CO_2 around 550 °C,[38] described below in Equation 2.6.

$$CaCO_{3(s)} \overset{\Delta h}{\rightarrow} CaO_{(s)} + CO_{2(g)} \qquad (2.6)$$

ICP-OES data show the concentration of calcium ions and silicon [Si] in the supernatant at timesteps between 1 and 168 hours, seen in Figures 2.4a and 2.4b, respectively. In the experiments with NaOH, the [Ca^{2+}] stays around 50 ppm, excluding the 72-hour outlier. The [Si] values for the NaOH experiments spike at 24 hours before dropping at 3 days when tobermorite was shown to precipitate. This drop was also seen in the NC experiments where CSH gel precipitated instead of tobermorite. In the DI water samples in Figure 2.4a, the [Ca^{2+}] are higher than in the NaOH solutions but follow a similar trend by staying at similar concentrations. In these same DI water samples, the [Si] vary but stay within the same order of magnitude. The major outliers in the data are the [Ca^{2+}] of the 72 hour standard condition across all variations.

The data collected have very low statistical variance, with the error bars indicating one standard of deviation.

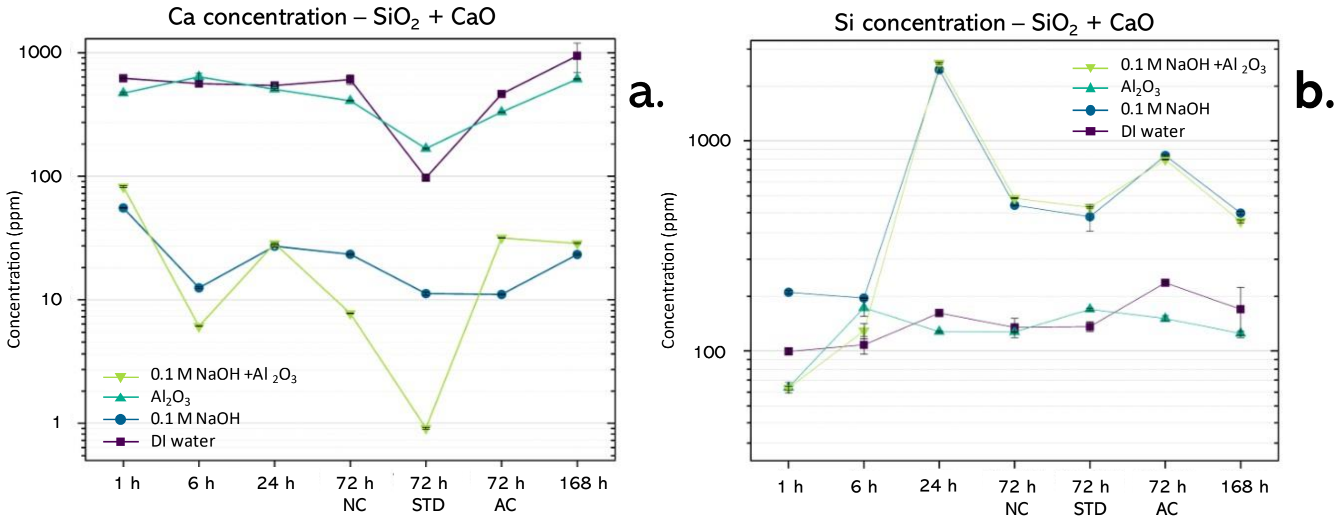

Figure 2.4. a. Logarithmic concentration plot of Ca ions from ICP OES data. Note the drop in [Ca^{2+}] when experiments include NaOH (blue, yellow green). b. Logarithmic concentration plot of Si ions from ICP OES data. Note the increase in [Si] at 24 hours and subsequent drop at 3 days when tobermorite forms in the NaOH experiments. Error bars are one standard of deviation for triplicate measurements and are often smaller than the symbol size.

2.3.2 TEOS experiments

The CaO and TEOS experiments had differing responses to the presence of NaOH, Al_2O_3, and the P_{CO_2} compared to the micro silica experiments. NaOH reduced the crystallinity of tobermorite formed for the 3-day standard precipitates observed in Figure 2.5a. The pure NaOH precipitates (second from the bottom) did not precipitate tobermorite and were the only precipitates to form portlandite. After 7 days, the NaOH precipitates show lower intensity for tobermorite than the DI waster in Figure 2.5b. The TEOS precipitates with NaOH and Al_2O_3 show greater tobermorite intensity than the pure NaOH precipitates at both 1 and 7 days. The TGA data of 7-day experiments, shown in Figures 2.5b and 2.5c, shows Al_2O_3 also improved hydration of in DI water. Figure 2.5c, the derivative of the TG plot (DTG) of 2.5b, shows that a main peak for the Al_2O_3 and DI water experiment centered at a lower temperature than the other three experiments. The shift indicates more CSH and/or **calcium aluminum silicate hydrate (CASH)** gel formed here than in the other three experiments.[23, 39] The other three sets precipitates in Figure 2.5d show similar amounts of hydration, despite differences in intensity for the XRD spectra.

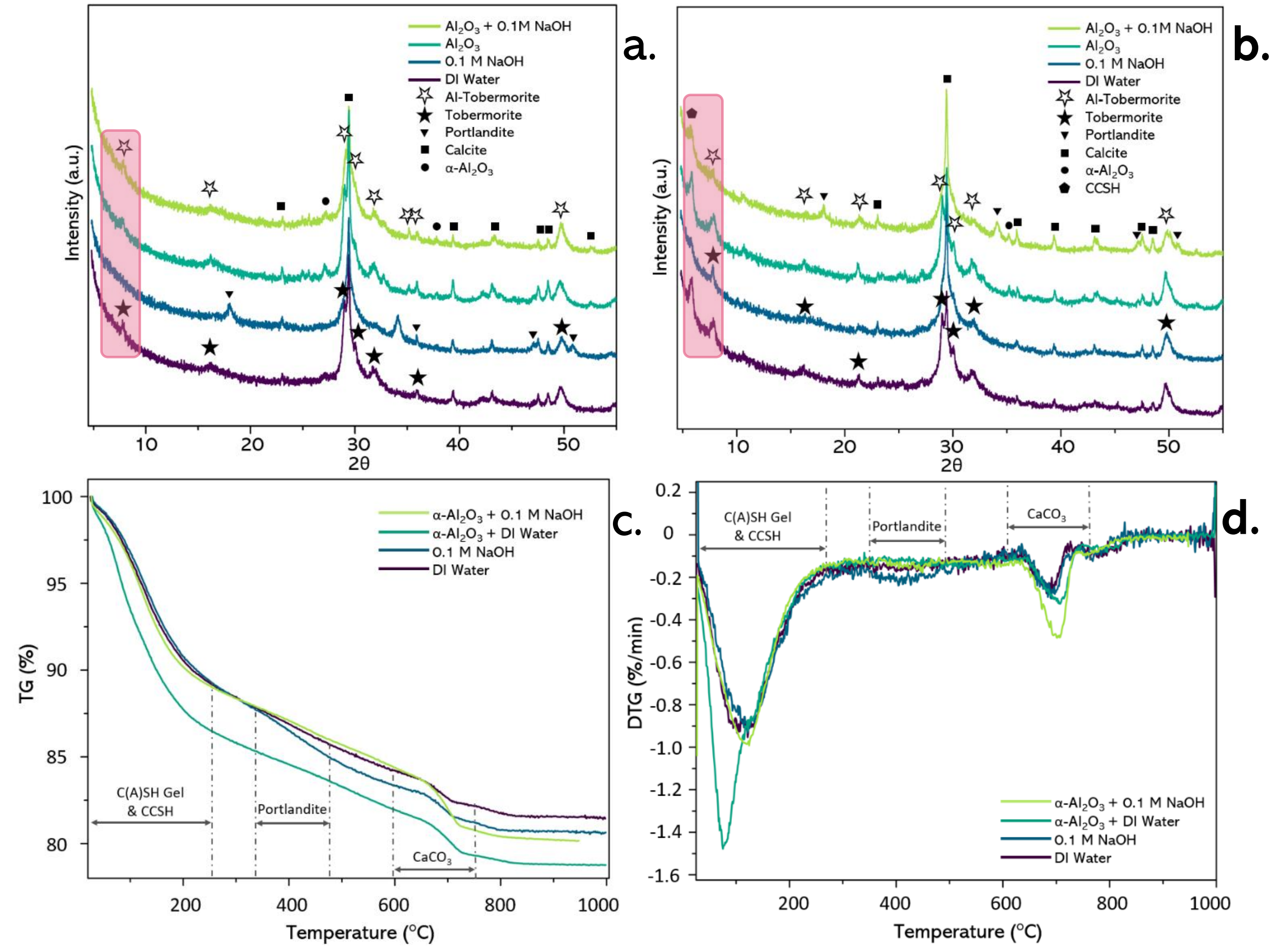

Figure 2.5. a. The XRD comparison plot of the standard CaO + TEOS experiments at 3 days b. the XRD plot of the standard CaO + TEOS experiments at 7 days. Note the intensities of peaks at 8° 2θ, indicating the 11Å spacing of tobermorite in the highlighted region. b. TG of the 7-day TEOS experiments. c. DTG of the 7-day TEOS experiments. Note the increased hydration of the DI water and Al_2O_3 precipitates and the shifted hydration peak in c.

The effect of P_{CO_2} on the TEOS samples was less consistent. The XRD data in Figures 2.6a show what phases were identified in precipitates in DI water at increasing PCO_2, and the data in

Figure 2.6b show the counterpart NaOH precipitates. Tobermorite only precipitated in DI water at the standard condition, as shown in Figure 2.6a. Interestingly, the NC experiment in DI water, bottom of Figure 2.6a, produced vaterite, an unstable, polymorph of calcite ($CaCO_3$). Only samples without Al_2O_3 are presented because, again, no TEOS + Al_2O_3 samples were run in the AC condition, which cannot be accurately replicated.

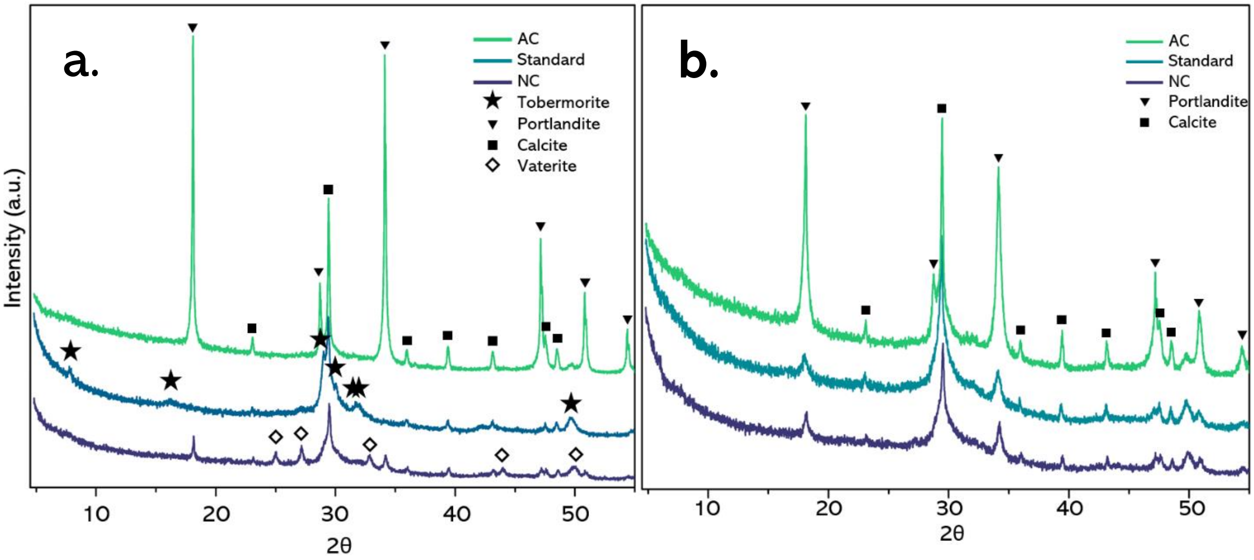

Figure 2.6 XRD spectra of TEOS samples cured for 3 days in a. DI water, b. 0.1M NaOH

2.4 Discussion

Tobermorite precipitated somewhere between 1 and 3 days at 150 °C, consistent with similar experiments conducted by Houston et al.[33] The major differences in the quantity precipitated are closely tied to the reactants. While other studies suggest crystallization of CSH gel to form tobermorite, the data indicate the micro silica experiments go through a dissolution step to provide enough silica in solution prior to the precipitation. On the other hand, it is expected that the TEOS experiments start with aqueous silica and can directly precipitate. The effects of NaOH, Al_2O_3, P_{CO_2}, and overall pH on these two experimental systems are examined through this lens of dissolution-precipitation versus only precipitation chemistry in the following sections.

2.4.1 Micro silica experiments

NaOH and P_{CO_2} were the most important factors for tobermorite precipitation from the micro silica experiments, while the presence of Al_2O_3 had no noticeable effect beyond the formation of Al-tobermorite. These observations for NaOH and Al_2O_3 are inconsistent with trends seen in tobermorite research, where additions of both compounds have been reported to decrease tobermorite crystallinity.

Focusing first on NaOH, its presence increased the concentration of aqueous silica, as shown earlier in Figure 2.4b. Silica dissolves in hydroxide solutions and forms aqueous colloids, described in Equation 2.7.

$$xSiO_{2(am)} + H_2O_{(l)} + OH^- \overset{Na^+}{\longleftrightarrow} Si_xO_y(OH)^{-\delta}_{(aq)} \tag{2.7}$$

The -δ charge indicates the variable nature of the aqueous silica compounds. Sodium ions then balance the surface charges of these silica colloids without reacting to form precipitates, thus keeping them in solution.[41] At a critical concentration of aqueous silica, observed around 24 hours based on data in Figure 2.4b, the aqueous silica structures are hypothesized to form highly reactive colloids. These colloids then readily react with Ca^{2+} and precipitate out of solution as seen in the lower $[Ca^{2+}]$ in the 0.1M NaOH experiments compared to the DI water in Figure 2.4a. It should be noted that no current explanation can be provided for the drop in $[Ca^{2+}]$ at the standard condition.

The data also indicate that increasing P_{CO_2} had a strong effect on increasing precipitation of tobermorite and CSH gel, as seen in Figure 2.3. Here it is believed CO_2 equilibrated with the solutions to produce carbonic acid (H_2CO_3) and bicarbonate ions (HCO_3^-), described in Equation 2.8.

$$CO_{2(g)} + H_2O_{(aq)} \leftrightarrow H_2CO_{3(aq)} \leftrightarrow H^+_{(aq)} + HCO^-_{3(aq)} \leftrightarrow H^+_{(aq)} + CO^{2-}_{3(aq)} \tag{2.8}$$

The increase in CO_2 dropped the pH of the solution, increasing the solubility of portlandite and thus the [Ca^{2+}]. The aqueous bicarbonate then reacted with Ca^{2+} to produce calcite, described in Equation 2.9.

$$Ca^{2+}_{(aq)} + 2HCO^-_{3(aq)} \overset{k_1}{\leftrightarrow} CaCO_{3(s)} + 2H^+ + CaO_{(aq)} + H_2O_{(aq)} + CO_{2(g)} \tag{2.9}$$

It is expected that the excess Ca^{2+} ions that were not consumed to form calcite instead reacted with the silica colloids to form tobermorite. Here calcite could be acting as a nucleation site for heterogenous nucleation of tobermorite. The formation of CSH gel and tobermorite would also explain why only minor increases in calcite concentration were seen across the three P_{CO_2} conditions, as there was not enough Ca^{2+} available to continue the precipitation of calcite.

The hypothesized aqueous reaction between Ca^{2+} and colloidal silica can be described nominally by combining Equations 2.7 – 2.9 into Equation 2.10.

$$Si_xO_y(OH)^{-\delta}_{z(aq)} + mCa^{2+}_{(aq)} + nH_2O_{(l)} \xleftrightarrow{Na^+, CO_2, time, temp} Ca_mSi_xO_y(OH)_z \cdot nH_2O_{(s)} \tag{2.10}$$

The $Ca_mSi_xO_y(OH)_z \bullet nH_2O_{(s)}$ term is used to generalize CCSH. However, this does not follow the expected gel crystallization pathway described by the majority of previous studies. One study by Houston[33] suggests that supersaturation of the bulk solution could be a pathway to tobermorite precipitation, though the data presented there also indicate that crystallization of CSH gel is simultaneously occurring.

The difference in reaction pathways seen in the experiments described in this chapter may be explained by portlandite formation. Data from Houston and similar studies show portlandite forms only during initial mixing and is quickly consumed to form CSH gel.[33] Comparatively, the presence of portlandite in this work suggests the SiO_2 was not reactive enough and needed to be ground to finer size. The powder likely clumped in storage due to the lab air humidity and negatively impacted reactivity. An accurate measure of the particle size of the unground micro silica used could not be attained as the larger clumps would not stay on a stub for scanning electron microscopy (SEM, Quanta 650). The particle size is estimated to be larger than 150 µm, as this was the sieve size the powder could not pass through. Repeat experiments were run concurrently with the 7-day standard experiments using ground micro silica that was dried at 55 °C for 24 hours, ball milled for 24 hours, sieved through to µm, and had an average size of 20.3 µm measured via image analysis of SEM micrographs (ImageJ). The repeats showed little change in XRD spectra beyond portlandite disappearing, found in Figure A.1 of the appendix. The use of ground-micro silica to increase reactivity was pursued in further depth in Chapter 2 of this work.

2.4.2 TEOS experiments

The TEOS experiments demonstrated overall that the precipitation step was much more sensitive to changes in the starting reactants than the dissolution step. TEOS reacts with water to produce aqueous SiO_2 species and ethanol, described below in the simplified Equation 2.11.[42]

$$Si(OC_2H_5)_{4(l)} + H_2O_{(l)} \rightarrow SiO_{2(aq)} + 4C_2H_4OH_{(l)} \tag{2.11}$$

Here the aqueous SiO_2 formed is hydrated and is expected to be similar to that given by Equation 2.7. This hydrolysis reaction is pH sensitive and can be increased by adding NaOH.[42] It is expected that this increase in silica hydrolysis would further promote tobermorite formation;

however, the data do not show this trend in most NaOH experiments. Figures 2.5 and 2.6 show that tobermorite only precipitated in 0.1M NaOH from TEOS at 7 days or in the presence of Al_2O_3. The relationship between NaOH and precipitation is not well understood. One possibility is that with NaOH, TEOS hydrolyzed too quickly and formed silica gel that limited ionic mobility needed to precipitate tobermorite. Similarly, the increase in ethanol in solution may have increased the evaporation rate of the solution, further promoting the formation of a gel.

The role of P_{CO_2} on the TEOS experiments shows no consistent trend. The standard experiments produced by far the most tobermorite; increasing the P_{CO_2} to the AC condition prevented tobermorite precipitation, while decreasing the P_{CO_2} to the NC condition only produced one sample with a detectable amount of tobermorite after the 3 days. Because the TEOS hydrolysis reaction is pH sensitive, the standard condition was expected to have fallen in a narrow pH narrow range where enough water remained unconsumed to allow for precipitation.

The TEOS experiments also demonstrate a clear increase in tobermorite precipitation with the addition of α-Al_2O_3. Al-tobermorite and CASH gel can be seen to consistently precipitate in greater quantities than ideal tobermorite and CSH gel in the data of Figure 2.5. As stated prior, Al_2O_3 has been shown to reduce SiO_2 solubility.[20] While this can be disadvantageous starting from solid SiO_2, the decrease in solubility may have worked in favor of precipitation from TEOS. It is expected that Al_2O_3 promoted precipitation of silica colloids out of solution to form CASH gel, which then crystallized into tobermorite.

2.5 Conclusions

The results presented in this chapter demonstrated that tobermorite precipitates from reactants between 1 and 3 days of hydrothermal curing at 150 °C. Two different reaction pathways were investigated: (1) the dissolution of amorphous SiO_2 into colloidal silica then precipitation of CSH gel/tobermorite via reaction with Ca^{2+} ions; and (2) the direct precipitation of CSH gel/tobermorite via hydrolyzed TEOS reacting with Ca^{2+} ions. NaOH was found to have a strong, but opposite, impact on both pathways, increasing tobermorite formed from amorphous SiO_2 and decreasing tobermorite from TEOS. Increasing the P_{CO_2} improved precipitation rates for both pathways, though only to a point in the direct precipitation pathway seen at the standard condition. Minor additions of Al_2O_3 showed no major effect on the dissolution-precipitation pathway but allowed for noticeably increased tobermorite from the direct precipitation.

i. *What is the reaction timeframe for CCSH precipitation?*
    a. Tobermorite precipitated between 1 and 3 days from CaO and micro silica and CaO and TEOS in the conditions tested. An unnamed CCSH phase was identified after 7 days.

ii. *How does the presence of NaOH affect this reaction?*
    a. NaOH was demonstrated as necessary for tobermorite precipitation from CaO and micro silica, while hindering precipitation from TEOS and CaO.

iii. *How does the presence of Al_2O_3 affect this reaction?*
    a. Al_2O_3 showed no noticeable effect on the CaO and micro silica precipitates, but improved crystallinity of tobermorite in the CaO and TEOS precipitates.

iv. *How does the P_{CO_2} affect this reaction?*
    a. Increased P_{CO_2} improved tobermorite precipitation from CaO and micro silica experiments and showed inconsistent effects in the CaO and TEOS experiments.

v. *How do the solution chemistry and precipitates from micro silica and TEOS reactants vary?*

a. Micro silica is hypothesized to dissolve before reacting with CaO to precipitate CSH gel or tobermorite. TEOS dissociates immediately into aqueous silica species and is expected to directly precipitate into CSH gel or tobermorite.

2.6 Future work

The relationship between tobermorite precipitation and CO_2 is explored further in Chapters 2-4, and more detailed explanations are provided. These chapters also explore how aqueous silica affects tobermorite, though not with TEOS. Experimenting with higher water to TEOS ratios to minimize total gelation could prove interesting, though not applicable to industrial processes as TEOS is an expensive reactant material relative to other cement feedstocks. Direct precipitation of tobermorite and/or cementitious materials from colloidal silica solutions would be a better avenue of investigation for technical purposes. Experimentation with higher Al_2O_3 concentrations would be beneficial as baseline research to eventually incorporate Al-rich waste products, such as red mud and slags, into tobermorite synthesis and cementitious materials.

3. The role of colloidal silica and Na^+ on CCSH formation

3.0 Background

Explorations of the tobermorite precipitation mechanism in Chapter 2 indicated both CO_2 and NaOH aided in precipitating tobermorite from CaO and micro silica, while Al_2O_3 showed little effect. We hypothesized that tobermorite was precipitating directly from solution in addition to the crystallization of CSH gel as described by the literature. However, issues with micro silica particle size render the trends and conclusions from Chapter 2 uncertain.

In this chapter, the issue of particle size is addressed by using micro silica ball milled to 15 µm. The hypothesized sodium relationship with direct precipitation was tested by curing CaO and micro silica in higher NaOH concentrations of 0.28 M and 0.56 M. The effect of CO_2 on tobermorite precipitations was explored by replacing CaO with calcite ($CaCO_3$). Additionally, the effect of the curing vessel on tobermorite precipitation was investigated, as synthesis methods in the literature typically use inert Teflon vessels rather than the borosilicate glass test tubes used in Chapter 2.

The data described in this chapter are consistent with the literature reported trends for NaOH and Al_2O_3 on tobermorite precipitation for CaO and micro silica experiments cured in Teflon. However, the CaO and micro silica experiments cured in borosilicate test tubes and all the $CaCO_3$ experiments support the hypothesis that direct precipitation of CCSH phases from solution increases with NaOH concentration.

3.1 Research questions

i. Why were CaO and micro silica experiments dependent on NaOH to precipitate tobermorite in Chapter 2 when the literature suggests otherwise?

ii. How does CCSH precipitation vary in borosilicate glass test tubes versus Teflon vessels?

iii. How does CCSH precipitation from $CaCO_3$ differ compared to CaO?

3.2 Methods

3.2.1 Hydrothermal experiments

The commercially available powders used were CaO (Fisher, 99.95% pure), $CaCO_3$ (Huber, 97% pure), Elkem micro silica 965 (95% pure), and α-phase Al_2O_3 (Fisher, 99.9% pure). The micro silica was ball milled for 24 hours and sieved to 150 μm, with an average particle size of 15 μm determined from scanning electron microscopy (FEI Quanta 650, Hillsboro, OR, US) and analysis of resulting images using ImageJ.[43] Powders were combined at a Ca:Si ratio of 5:6 or a Ca:(Si+Al) of 5:6 with an Al/(Si+Al) = 0.05 where applicable. The total powder mass for a single experiment was 2 g. The powders were put into 50 mL Teflon liners (Parr) or 25 mL borosilicate glass test tubes (Fisher), with a **chemical composition of $Ca_{0.2}K_{3.8}Na_{8.4}Al_{8.6}B_9Si_{78.8}$**, measured using inductively coupled plasma – optical emission spectroscopy (ICP-OES). NaOH (Fisher, >97% pure) solution at concentrations of DI water, 0.28 M NaOH, or 0.56 M NaOH was added to the powders at a volume of 20 mL and stirred with a glass rod when using Teflon liners or vortexed (Fisher Scientific Vortex Mixer) for 15 seconds when using borosilicate test tubes.

The liners and test tubes were placed into a rack and sealed in a 10 L pressure vessel with 2 L of water in the basin, as illustrated in Figure 3.1. Samples were then heated in an oven at 150 °C[23, 29, 33] (± 3 °C). An initial set of experiments were conducted in liners and test tubes, mixed with either DI water or 0.56 M NaOH, and cured for 3 days. Subsequent experiments were conducted in test tubes for 1 day, 3 days, or 7 days of curing. The CaO containing mixtures were cured in a separate vessel than the $CaCO_3$ containing mixtures to prevent interactions with off gassed CO_2. Additional borosilicate test tubes were filled with 20 mL of DI water, 0.28 M NaOH, or 0.56 M NaOH and run without powder under the same hydrothermal conditions and times.

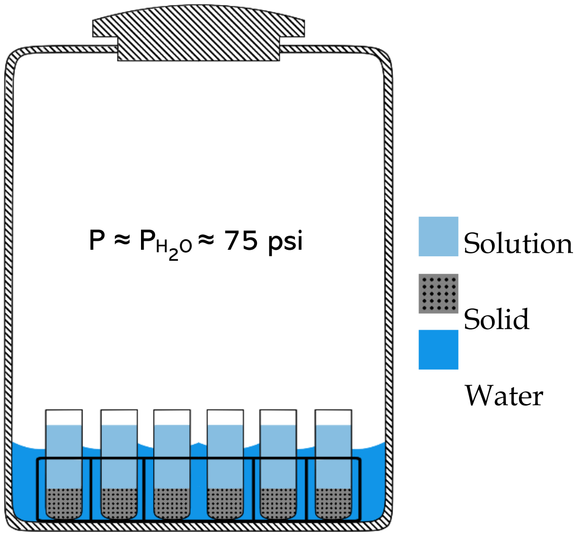

Figure 3.1.The experimental set up where samples were cured at 150 °C in a pressure vessel.

The pressure vessel was removed from the oven and was naturally cooled to room temperature before removing the liners or test tubes. The supernatants were separated using 25 µm filter paper (Whatman) after curing and stored for future ICP-OES analysis. The remaining powders were acidified with 0.1 M acetic acid (Fisher, glacial), filtered, and dried at 50 °C for 24 hours. The powders were then ground using a diamonite mortar and pestle (Fisher), sieved through a 45 µm mesh, and stored in sealed vials.

3.2.2 Characterization

X-ray powder diffraction (Malvern-Panalytical Empyrean, Worcestershire, UK) of the dried precipitates was conducted at the following parameters: Cu Kα-radiation (λ =1.5405 Å); current = 40 mA; tension = 45 kV, GaliPIX Detector scanning 501 steps at a time; measurement range = 4.8–55 °2θ; time per step = 90 s; and step size = 0.0143 °2θ. The sample stage was spun during the scans to minimize the effects of orientation. The data were analyzed with Highscore

Plus (Version 4.9), using the International Centre for Diffraction Data (ICDD) databases to identify phases. Table 3.1 contains the mineral names, compositions, and ICDD reference codes of the phase identified in this Chapter. The majority of referenced patterns of the major phases (>10% mass) and minor phases (2-10%) showed strong alignment of peak locations and intensities with data presented. Tobermorites 9Å, 12.5Å, 13Å were the exceptions; the best alignment was with their highest intensity, basal plane peaks. The secondary and tertiary peaks occasionally showed lower alignment or matched better with a different spacing tobermorites.

Table 3.1. A list of mineral names, chemical formulae, and ICDD reference codes for the phases identified in this work. Major phases over an estimated 10% mass are indicated by (+), minor phases from 2-10% mass by (-), and trace phases under 2% by (t).

Mineral Name	**Chemical formula**	**ICDD reference code**
Calcite (+)	$CaCO_3$	04-008-0198
Vaterite (-)	$CaCO_3$	00-025-0127
Bütschliite (t)	$K_2Ca(CO3)_2$	04-010-1207
Portlandite (t)	$Ca(OH)_2$	04-014-7726
α-Al_2O_3 (t)	Al_2O_3	00-005-0712
Tobermorite – 9Å (-)	$Ca_4Si_6O_{16}(OH)_2 \bullet 2H_2O$	00-010-0374
Tobermorite (+)	$Ca_4Si_6O_{16}(OH)_2 \bullet 4H_2O$	00-019-1364
Tobermorite – 12.5Å (-)	$Ca_{7.76}\ Si_{6.76}O_{18.8}(OH)_{4.88}(H_2O)_{7.84}$	01-081-9792
Tobermorite – 13Å (-)	$Ca_{16}(Si_8O_{28})(H_2O)_{13}$	01-081-9793
Gyrolite (+)	$Ca_4(Si_6O_{15})(OH)_2 \cdot 3H_2O$	00-005-0712
Unnamed CCSH (-)	$Ca_9(Si_{16}O_{34}(OH)_{14})(H_2O)_8$	01-074-7587
Unnamed CCASH (+)	$CaAl_2Si_7O_{18} \bullet 1.7H_2O$, ICDD	00-021-0132
Gismondine-Na (-)	$Na_{3.6}Al_{3.6}Si_{12.4}O_{32} \bullet 14H_2O$	01-080-0699
Rhodesite reference	$KNaCa_2Si_8O_{19}(H_2O)_5$	04-016-9687

Select samples were further analyzed via thermogravimetric analysis (TGA, Netzsch STA-449 F1, Bayern, Germany) to measure the amount of hydration and carbonation. For this characterization, 20 mg of powder was placed in a Pt-Rh crucible and heated at a rate of 10 °C/min to 1000 °C. The data were collected and compared to the literature.[37, 39, 44]

Select supernatants from the synthesis experiments were analyzed via inductively coupled plasma – optical emission spectroscopy (ICP-OES, Thermofisher ICAP 6200). For digestion, 1 mL of supernatant was added to 9 mL of a 1 M HF and 1 M HNO_3 solution. The solutions were then diluted to 300x with DI water. The Al, B, Ca, Na, and Si concentrations were measured in triplicate. The supernatants of the powderless glass experiments were diluted 2000x in DI water, then measured for Al, B, Ca, K, Na, and Si.

3.3 Results

The CaO experiments reacted differently with NaOH when cured in Teflon or borosilicate glass for 3 days, shown in the XRD results of the precipitate in Figure 3.2. The bottom two spectra show the reaction in DI water, where in glass a small amount of tobermorite – 9Å formed, compared to the Teflon where tobermorite formed at a higher crystallinity consistent with the literature.[19, 20] The glass experiment in 0.56M NaOH produced a suggested Na-CCSH phase with the closest pattern found being a potassium sodium CCSH phase ($KNaCa_2Si_8O_{19}(H_2O)_5$, ICDD 04-016-9687) in the rhodesite family, shown below Figure 3.2. The suggested Na-CCSH shows a basal plane peak at 7.32 °2θ that aligns better with rhodesite rather than the 7.8 °2θ of the tobermorite basal plane. The 0.56 M NaOH glass experiment also shows an alumina rich zeolite, referred to in this work as gismondine-Na. No Al_2O_3 was added to this sample, so gismondine-Na is expected to have formed hydrothermally from borosilicate glass. Comparatively, the 0.56 M Teflon precipitates produced tobermorite with a lower intensity than the Teflon DI water precipitates, as described by literature.[21] In summary, the Teflon experiments show decreased crystallinity of tobermorite with NaOH, while glass experiments show improved crystallinity of the Na-CCSH phase with NaOH. Glass precipitates also show an increase in $CaCO_3$, in the form of calcite and vaterite, as compared to their Teflon counterparts.

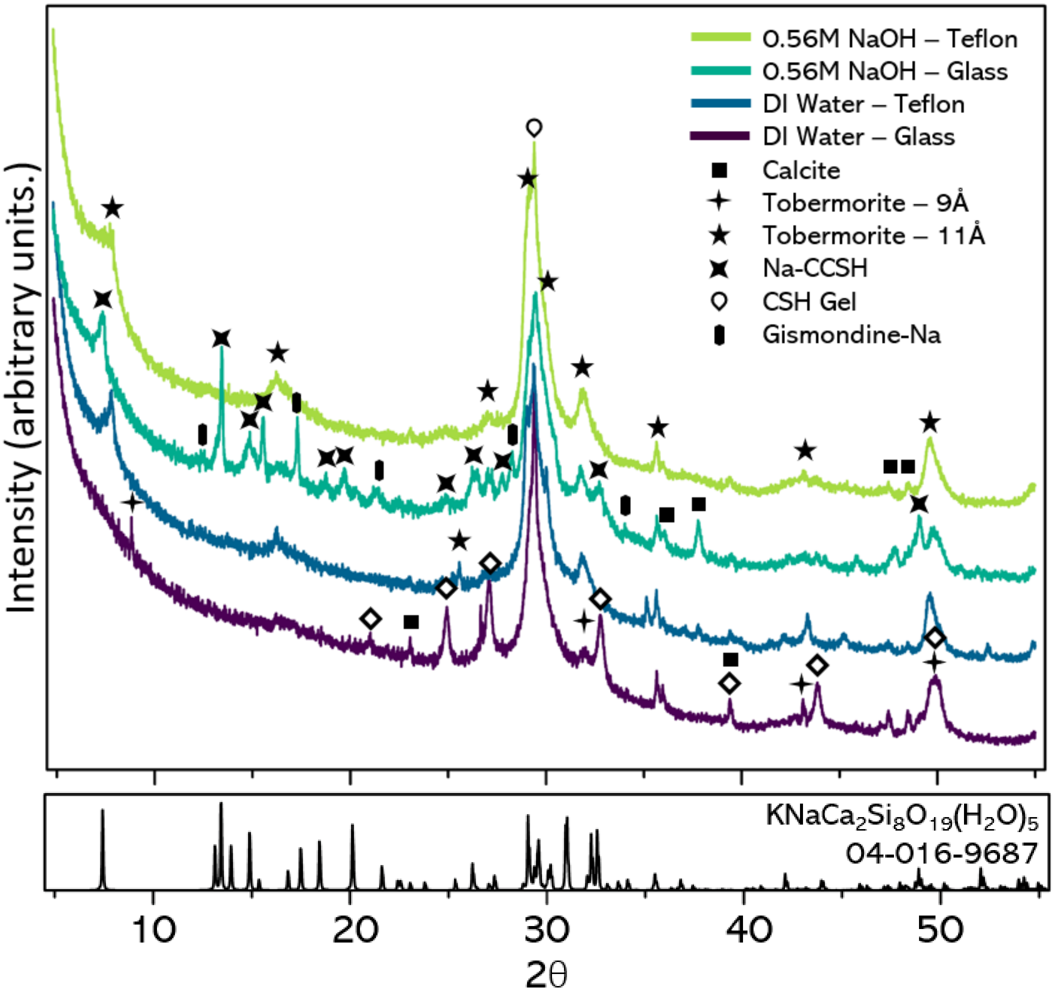

Figure 3.2. XRD spectra comparing CaO experiments cured in glass or Teflon with DI water or NaOH. Note the shift in the low 2θ peaks across conditions.

The $CaCO_3$ experimental data show more consistent reaction products when cured in Teflon or glass compared to the CaO experiments. Only the 0.56M NaOH $CaCO_3$ experiments are shown in Figure 3.3 as DI water experiments did not react. The XRD results in Figure 3.3a show the proposed Na-CCSH phase more clearly, with the major peaks aligning with what was seen in Figure 3.2. The $CaCO_3$ + Al_2O_3 precipitates in Teflon showed the highest intensity of the Na-CCSH phase, and the pure $CaCO_3$ in Teflon showed the lowest intensity. Only minor peaks are seen in the glass experiments that are not present in the Teflon. The minor peaks match better with the referenced rhodesite phase and are labeled as (K, Na)-CCASH, with K and Al sourced from glass dissolution. Gismondine-Na is also present in the glass precipitates and not seen in the Teflon precipitates like the CaO experiments in Figure 3.2, indicating again that the dissolved borosilicate test tube may be adding Al to the precipitates. DTG data in Figure 3.3b show similar trends, with the pure $CaCO_3$ in Teflon showing the least amount of CCSH dehydration and the most unreacted $CaCO_3$. Conversely, the precipitates from $CaCO_3$ + Al_2O_3 in Teflon produced the most hydrates. While the Teflon sample varied noticeably, the glass experiments with and without Al_2O_3 showed comparable hydration and remaining $CaCO_3$. Overall, Figure 3.3 shows that $CaCO_3$ samples required NaOH to precipitate the Na-CCSH phase, with Al_2O_3 improving crystallinity and hydration. Synthesis in the borosilicate glass test tube minimized the effect of Al_2O_3 on crystallinity and hydration, likely by the glass acting as a source of Al_2O_3.

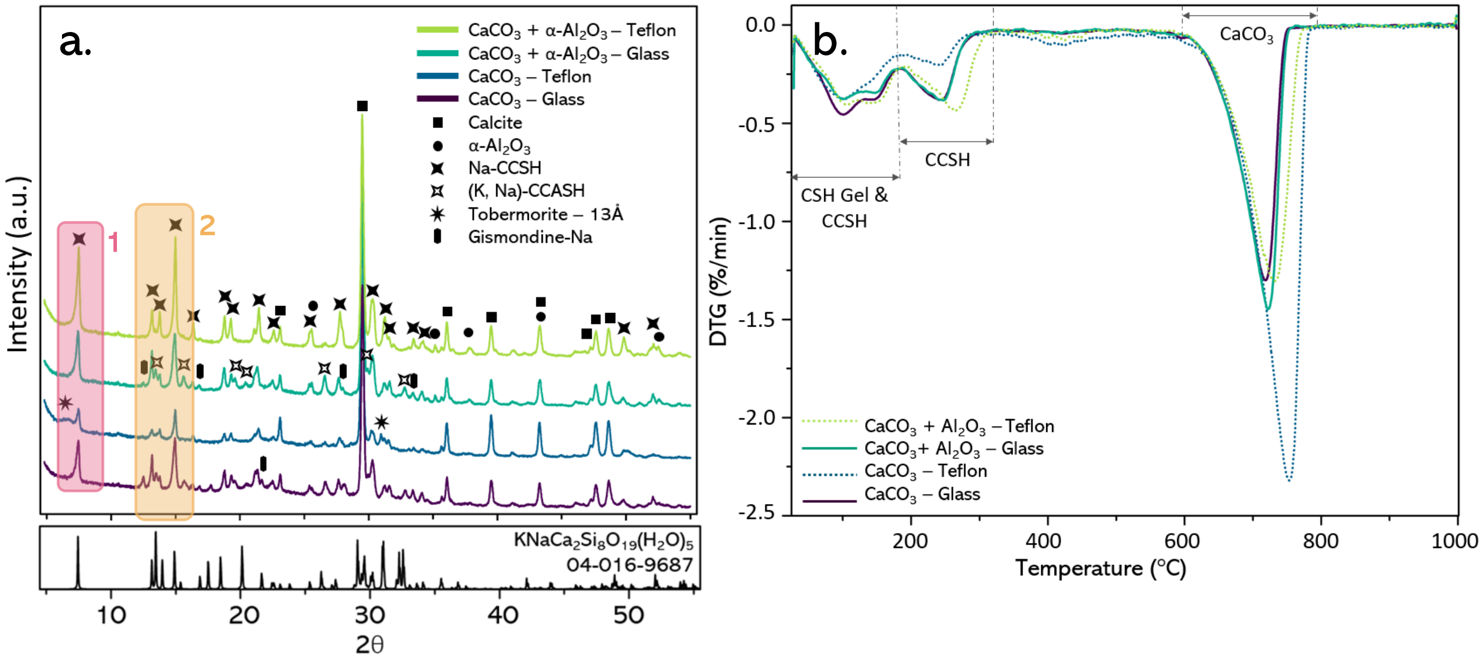

Figure 3.3. $CaCO_3$ experiments cured in glass or Teflon vessels for 3 days in 0.56M NaOH a. DTG plot, b. XRD spectra. Note the changes in intensity in highlighted region 1 of 3.3a, and the additional peaks seen in glass experiments in highlighted Region 2.

ICP-OES analysis of the powderless glass experiments is presented in Figure 3.4, showing that B, K, Na, and Si are all added to the supernatants as NaOH dissolves the glass. All four elements show an increase in concentration with time. The [Na$^+$] and [Si] show similar concentrations at each timestep and across NaOH concentrations, about 10,000 ppm for 0.28 M NaOH, and 20,000 ppm for 0.56 M NaOH. The matching concentrations indicate that Na increases Si solubility, likely forming colloidal silica. The starting [Na$^+$] for 0.28 M NaOH is 11,200 ppm and 0.56M NaOH is 22,400 ppm. Here, Al and Ca are not shown, as their concentrations remained at 0 ppm across all timesteps. The black or grey error bars on the symbols show one standard of deviation from the measurements, and very little uncertainty is seen. Additionally, no DI water experiments are shown because there were no measurable amounts of ions in solution.

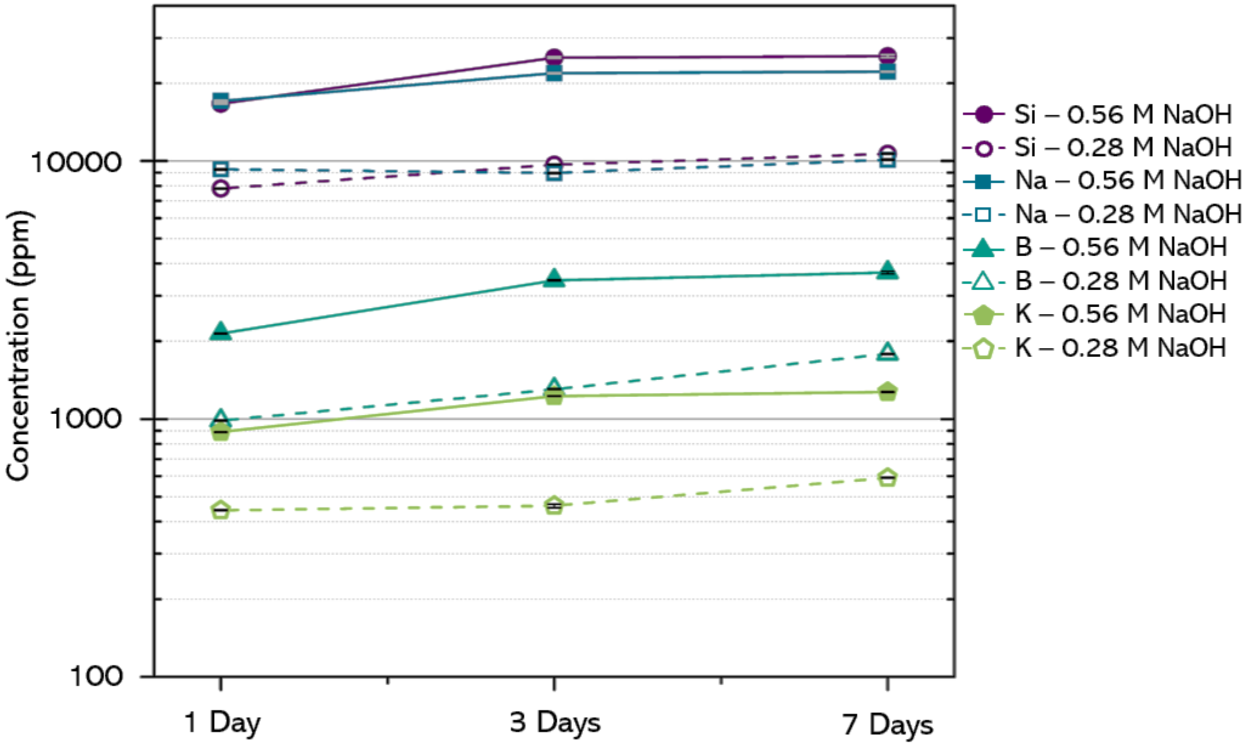

Figure 3.4. A logarithmic plot of the elemental concentrations of the borosilicate glass tubes supernatant in 0.28 M NaOH or 0.56 M NaOH measured via ICP-OES. The error bars are 1 standard of deviation.

ICP-OES data of both supernatants and digested precipitates from the 7-day $CaCO_3$ experiments confirm that dissolved glass introduced Al, B, K, Na, and Si into the reaction products, as seen in Figure 3.5. The 0.56 M NaOH synthesis supernatants show significant drops in B, K, Na, and Si compared to the dissolved glass data at the same concentration in Figure 3.4. Additionally, the synthesis supernatants do not show the same element concentration trends as the dissolved glass experiments, indicating certain aqueous species precipitated more often. The most notable example is that the [Si] in solution dropped to 0.25 times that of [Na^+] compared to the near equal concentrations seen in the dissolved glass solutions. It is expected that significant amounts of aqueous Si were consumed to form the precipitates, as seen in the shifted Ca:Si molar ratio of 5:13 from the 5:6 of the original powders. A similar trend can be seen when comparing the [B^{3+}] and [K^+] in Figure 3.5, where [K^+] is an order of magnitude less in the synthesis supernatant, but of comparable concentration in the precipitates. Both [Ca^{2+}] and [Al^{3+}] were not measurable in the supernatant, as seen in the dissolved glass data, but were measured in the powder. Both Ca and Al are expected to react readily with aqueous Si and precipitate out of solution. The Al concentration found in the precipitates of the pure $CaCO_3$ experiment was about half that of the Al concentration in the $CaCO_3$ + Al_2O_3 precipitates, indicating that Al was likely pulled from the glass.

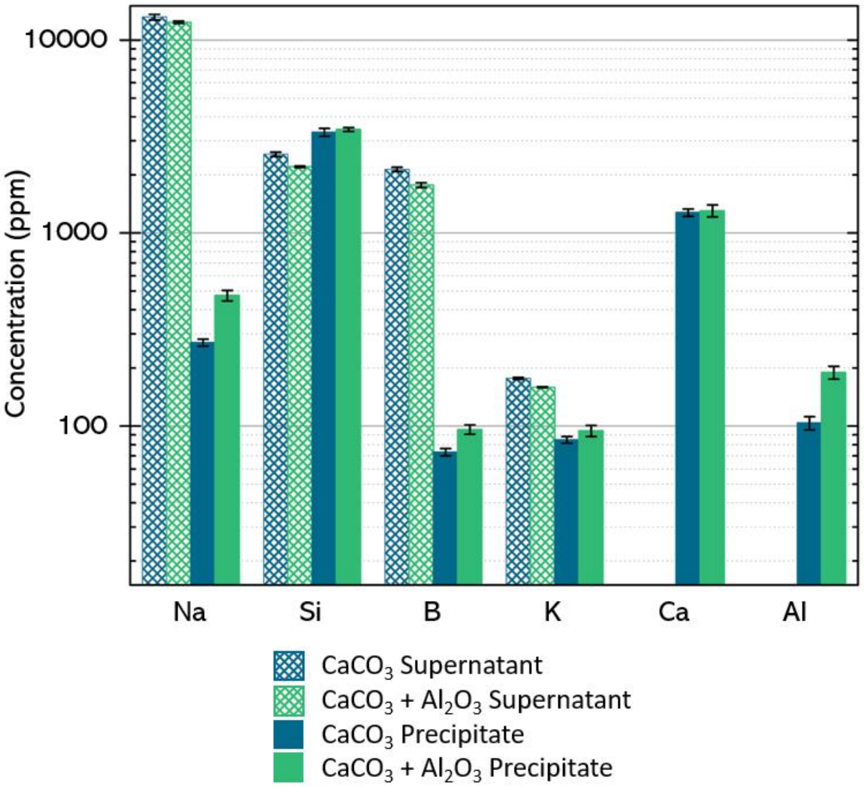

Figure 3.5. A logarithmic plot of the elemental concentrations of supernatant and digested precipitates from 7-day, 0.56 M $CaCO_3$ experiments. Note the addition of Al to the powder to the pure $CaCO_3$ experiment from the glass.

Subsequent glass experiments demonstrated that the higher NaOH concentration showed drastically increased crystallinity, as seen in Figure 3.6 where 7-day XRD spectra are presented for both 0.28 M NaOH (top row) and 0.56 M NaOH (bottom row). At the 0.28 M NaOH in Figures 3.6a and 3.6b, both CaO and $CaCO_3$ precipitated tobermorites, whereas the Na-CCSH phase was preferred at 0.56 M NaOH in Figures 3.6c and 3.6d. Adding Al_2O_3 did not show much effect in the 0.28 M NaOH data, but major changes in peak intensities are observed in the 0.56 M NaOH data. The XRD data of the 0.56 M NaOH experiments in Figure 3.6 also show that the crystallinity of the Na-CCSH phase in the $CaCO_3$ experiments is higher than their CaO counterparts which is most obvious when comparing the peak intensities to the noise in the data. Figure 3.6c shows that the addition of Al_2O_3 to the CaO experiments produced both basal spacings for tobermorite and the Na-CCSH phase around 7 °2θ, with the Na-CCSH phase at a much lower intensity compared to pure CaO. In Figure 3.6d, the Al_2O_3 + $CaCO_3$ precipitates show different peaks than the pure CaO precipitates, most notably around 16, 19, 27, and 30 °2θ, which are again distinguished as (K, Na)-CCASH. To summarize, all samples at higher NaOH produced higher intensities of CCSH phases and showed variance in the phases formed when Al_2O_3 was present.

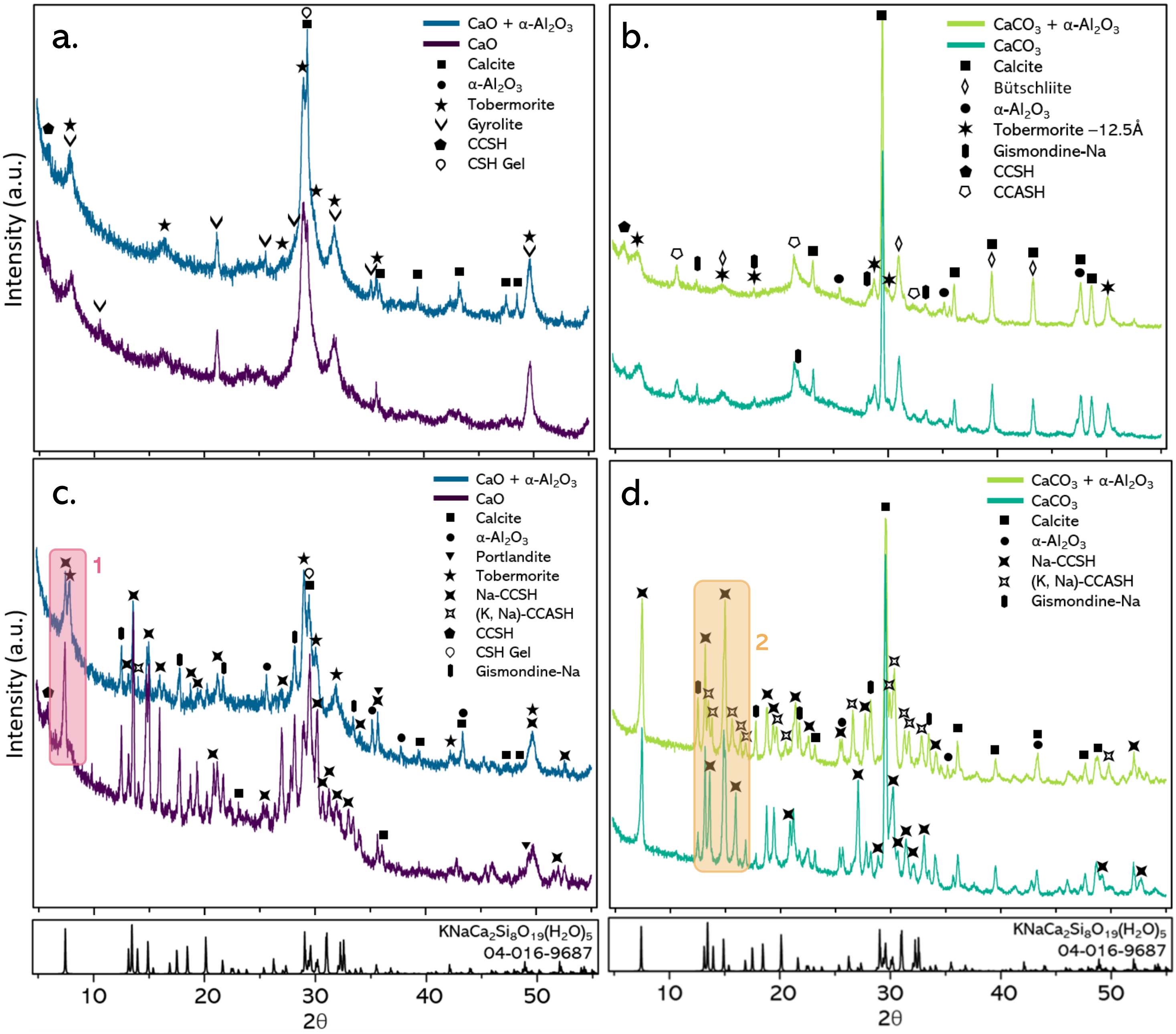

Figure 3.6. XRD spectra of 7-day experiments, ***a.*** *CaO - 0.28 M NaOH,* ***b.*** *$CaCO_3$ – 0.28 M NaOH,* ***c.*** *CaO – 0.56 M NaOH,* ***d.*** *$CaCO_3$ – 0.56 M NaOH. In Figure 3.6c, note how the CaO + Al_2O_3 precipitates show peaks for both tobermorite and the Na-CCSH phase in highlighted region 1. In Figure 3.6d, note the change in peaks with the addition of Al_2O_3 in highlighted region 2.*

The TGA data in Figure 3.7 show clear differences in the mass loss derivative (DTG) plots after 7 days for CaO (left column) and $CaCO_3$ (right column) experiments. The CaO precipitates in Figures 3.7a dehydrated about 10% more than the $CaCO_3$ in Figures 3.7b at 0.28 M NaOH and

6% more in Figure 3.7c compared to Figure 3.7d at 0.56 M NaOH. The majority of the hydration difference is attributed to the water loss of amorphous and semicrystalline CSH gel and hydrated silica gel because the DTG peaks are below 100 °C.[23, 39] The higher NaOH concentration also greatly affected both the CaO and $CaCO_3$ experiments by increasing total hydration and CCSH dehydration, seen in the peaks located between ~175-300 °C.[23, 38, 40] The CaO data in Figures 3.7a and 3.7c show much stronger effects with the Al_2O_3 addition compared to the $CaCO_3$ data in Figures 3.7b and 3.7d.TGA data indicated that the pure CaO precipitates hydrated 1.6 times more with the increase in NaOH, though CaO + Al_2O_3 precipitates only increased in hydration by a factor of 1.04 times. Both sets of $CaCO_3$ reaction products produced over twice the amount of CSH gel and CCSH compared with 0.56 M NaOH to those at 0.28 M and consumed more $CaCO_3$. The Al_2O_3 added to the 0.56 M NaOH $CaCO_3$ caused precipitates to dehydrate slightly less and retain more calcite than the pure $CaCO_3$ precipitates. Additionally, the 0.56 M NaOH $CaCO_3$ data in Figure 3.7d show much more pronounced dehydration in CCSH than their CaO counterparts in Figure 3.7c. This trend was also observed in Na-CCSH intensity with XRD data in Figures 3.6c and 3.6d. In summary, the CaO precipitates show overall greater hydration and variability with Al_2O_3, while the $CaCO_3$ precipitates show greater increase in CCSH phases at the higher NaOH concentration.

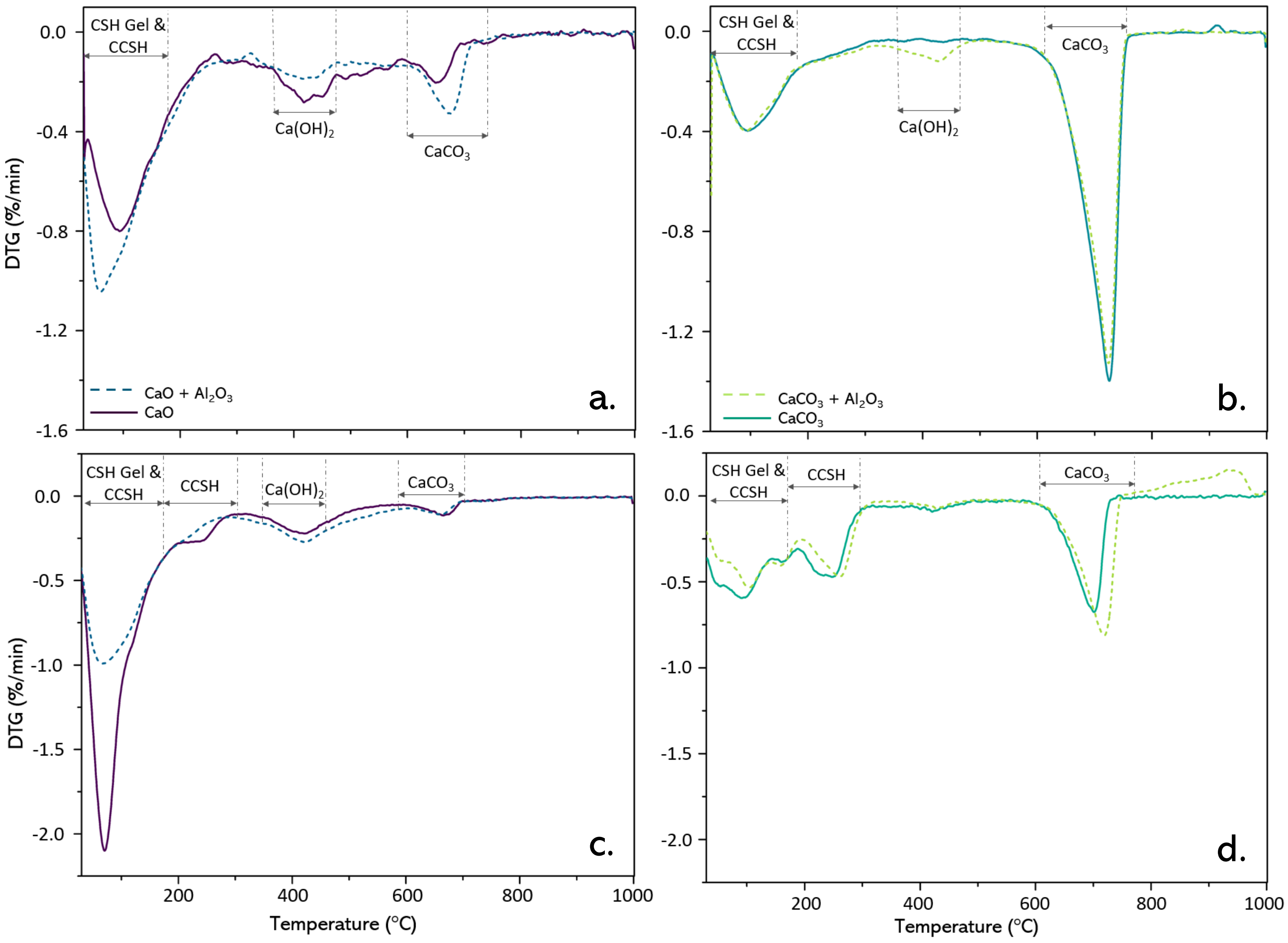

Figure 3.7. DTG data of all 7-day experiments. ***a.*** *CaO - 0.28 M NaOH,* ***b.*** *$CaCO_3$ – 0.28 M NaOH,* ***c.*** *CaO – 0.56 M NaOH,* ***d.*** *$CaCO_3$ – 0.56 M NaOH. Note how the CaO precipitates are dominated by CSH gel dehydration at both NaOH concentrations while the $CaCO_3$ precipitates show an increase in CCSH dehydration.*

SEM images of the 7-day $CaCO_3$ reaction products are shown below in Figure 3.8. Figure 3.8a shows the 0.28 M NaOH experiments where both flower petal like platelets and needles can be seen. The platelets were found across the powder in random orientations while the needles were usually found bundled together indicating growth from a central point. Elemental compositions measured via energy dispersive spectroscopy (EDS) of the crystals imaged did not match with the phases identified in the XRD data in Figure 3.6. Figure 3.8b shows what is expected to be a fractured shard of glass based on the EDS data matching the borosilicate composition and the smooth surface. The glass porosity and crystals growing from the surface indicate that material was leached from the glass and crystallized. Similar morphologies were seen with and without Al_2O_3 at both NaOH concentrations.

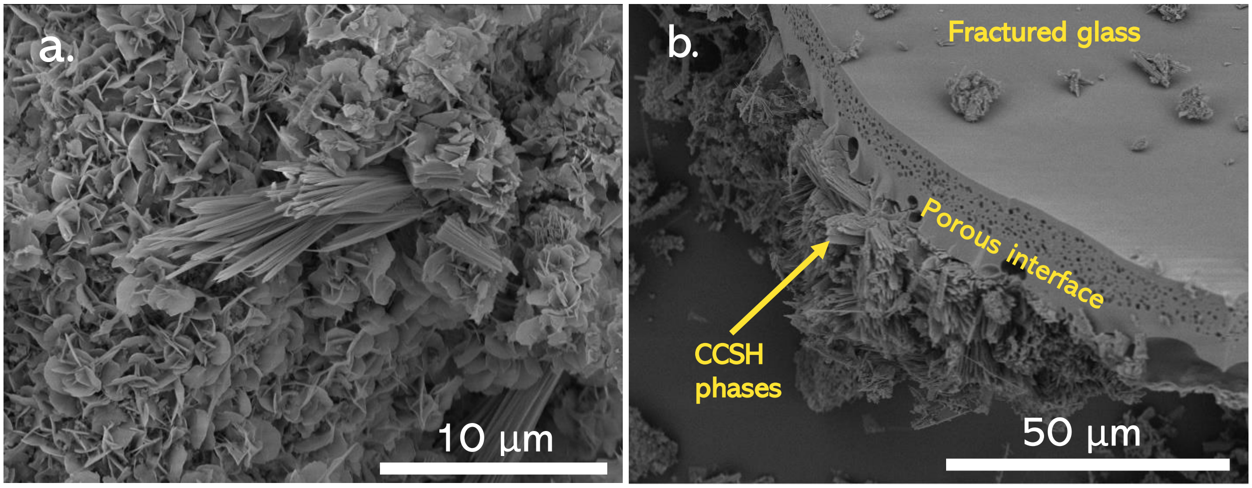

Figure 3.8. SEM images of the 7-day $CaCO_3$ precipitates at a. 0.28 M NaOH with flower petal and needle like crystals, b. 0.56M NaOH showing needle like crystals growing from a fractured piece of borosilicate glass. Note the change in scale.

3.4 Discussion

Three major findings are reported in this chapter: (1) the precipitation mechanisms and CCSH phases formed are affected by the dissolution of borosilicate glass test tubes when compared to Teflon liners; (2) the higher NaOH concentration increases the direct precipitation of CCHS phases from both CaO and $CaCO_3$; and (3) the 0.56 M NaOH experiments allow for the direct precipitation of a previously undocumented Na-CCSH phase.

3.4.1 CaO experiments

The CaO experiments show a direct increase in CCSH precipitation with NaOH when cured in the borosilicate test tubes, similar to the results seen in Chapter 2. Previously, we hypothesized that the NaOH added in Chapter 2 promoted the dissolution of unreacted micro silica and formed colloidal silica to allow for direct precipitation of tobermorite. However, the lack of portlandite in the CaO experiments of this chapter indicates that the finer ground micro silica used reacted to completion with CaO and water to form CSH gel. The borosilicate glass was instead the source of colloidal silica, as borosilicate glass has been shown to dissolve with exposure to NaOH solutions, increasing exponentially with temperature.[45,46] Equation 3.1 restates the notional colloidal silica reaction for convenience.

$$xSiO_{2(am)} + H_2O_{(l)} + OH^- \overset{Na^+}{\longleftrightarrow} Si_xO_y(OH)^{\delta}_{(aq)} \tag{3.1}$$

Literature on the alkaline formation of silica colloids in the presence of alkali metals indicates that Na^+ performs the best at stablizing surface charges, with NaOH specifically producing stable, adsorbed complexes.[41] Additionally, increasing NaOH concentrations have been shown to promote charge-induced crystallization of silica colloids.[47] Figure 3.4 shows the elemental concentrations of the dissolved glass solutions at 0.28 M and 0.56 M NaOH, and a similar plot for the 0.1 M NaOH experiments in Chapter 2 can be found in Figure A.2 of the Appendix.

The direct precipitation of CCSH from CaO and micro silica requires a source of Ca^{2+} to react with to form CCSH. Here, Ca^{2+} ions are supplied from the CSH gel itself, as CSH gel has been shown to emit Ca^{2+} in NaOH solutions over time.[48] In the time it takes for significant quantities of Ca^{2+} ions to enter the solution, the silica colloids likely polymerize into a semi-ordered form due to the aforementioned charge induced crystallization in the presence of

NaOH.[47] The recontextualized direct precipitation can still be described by the reaction pathway in Chapter 2, which is restated in Equation 3.2.

$$Si_xO_y(OH)^{\delta}_{(aq)} + mCa^{2+} + H_2O_{(l)} \xleftrightarrow{Na^+,time,temp} Ca_mSi_x(OH)_y \cdot zH_2O_{(s)} \tag{3.2}$$

The differences in phases seen across sodium levels is expected to be due to the mobility and concentration of Ca, silica, and water. In traditional tobermorite synthesis using CaO, like the Teflon and DI water experiment in Figure 3.2, crystallization occurs through ordering of the CSH gel; the formation of a crystal lattice is expected to depend on the kinetics of Ca, silica, and water moving through the gel matrix. Adding Na^+ ions to the gel from NaOH likely impedes Ca, silica, and water moving through the matrix and slows the kinetics for crystallization. However, the mobility of Ca, silica, and water would be much higher in solution, and direct precipitation of CCSH phases is expected to have faster kinetics than gel crystallization.

The nuclei formed in solution from direct precipitation are hypothesized to promote the CSH gel to order. At 0.28 M NaOH, the XRD spectra in Figure 3.6a show that tobermorite and gyrolite precipitated, though it is unclear if crystallization of CSH gel or direct precipitation was the dominant mechanism. The 0.28 M NaOH precipitates also show only minor differences in the phases formed with and without Al_2O_3, similar to Chapter 2 results. At 0.56 M NaOH, the Na-CCSH phase shown in Figure 3.6c was expected to form via direct precipitation. Interestingly, the presence of Al_2O_3 decreased both the crystallinity of CCHS phases and the total hydration, seen in Figures 3.6c and 3.7c respectively. Here, Al_2O_3 likely forms calcium aluminum silicate hydrate (CASH) gel, which is more stable than the CSH counterpart.[9] Al-tobermorite is expected to have crystallized from the CASH gel alongside the Na-CCSH phase precipitating from solution. This double precipitation between Al-tobermorite and the Na-CCSH phase may have been in competition for unstructured CSH gel, explaining why the CaO + Al_2O_3 does not show a large increase in hydration with NaOH like the other 7-day experiments.

3.4.2 $CaCO_3$ experiments

The $CaCO_3$ precipitates show an even greater increase in CCSH precipitation with NaOH concentration than the CaO precipitates in Figures 3.6 and 3.7. Direct precipitation is expected to be the dominant reaction pathway because $CaCO_3$ has a much lower dissolution rate than CaO and does not immediately form CSH gel. Calcite requires either acidic conditions or a $CaCO_3$:NaOH molar ratio of 2 or more to dissolve rapidly and thus is only slightly soluble in the NaOH solutions used.[49] $CaCO_3$ is expected to dissolve slowly and form carbonate and bicarbonate, following the reactions described in Equations 3.3 and 3.4, respectively.

$$CaCO_{3(s)} + 2NaOH_{(aq)} \leftrightarrow Ca^{2+}_{(aq)} + 2Na^{+} + CO^{2-}_{3(aq)} + 2OH^{-} \tag{3.3}$$

$$CO^{2-}_{3(aq)} + 2H_2O_{(l)} \leftrightarrow HCO^{-}_{3(aq)} + OH^{-}_{(aq)} + H_2O_{(l)} \leftrightarrow \ldots$$

$$\ldots H_2CO_{3(aq)} + 2OH^{-}_{(aq)} \leftrightarrow CO_{2(g)} + H_2O_{(l)} + 2OH^{-}_{(aq)} \tag{3.4}$$

The bicarbonate buffer reaction in Equation 3.4 produces CO_2 that is largely insoluble at 150 °C and will escape into the headspace of the vessel. It is expected that the reaction favors forming gaseous CO_2 and continuously dissolving more $CaCO_3$, as the head space is relatively understaturated in CO_2 compared to the solutions.

Colloidal silica is expected to form from both the borosilicate test tubes and the micro silica used as a reactant. Without a reactive source of Ca to form CSH gel, the microsilica dissolves in the NaOH solution and the resulting colloids polymerize. The direct precipitation occurs when enough $CaCO_3$ dissolves and reacts with the collidal silica. In Chapter 2, tobermorite precipitation was shown to increase with CO_2 at 3 days, peaking at the AC condition. With the additional information in this chapter, it is clear that the CaO that did not react with microsilica to form CSH gel was driven by CO_2 to form calcite instead of portlandite. The $CaCO_3$ dissolved in the 0.1 M NaOH and is hypothesized to provide more Ca^{2+} for colloidal silica to react with than both portlandite and CSH gel. $CaCO_3$ dissolution also explains why the Chapter 2 precipitates from different P_{CO_2} did not show drastic differences in carbonation. Beyond the formation of calcite, it is unclear if CO_2 directly impacted the solution chemistry or precipitation of CCSH phases.

The Na-CCSH phase is expected to be sensitive to both added Al_2O_3 and the elements from the glass dissolution. The precipitates from pure $CaCO_3$ in Teflon show less hydration possibly due to competitive nucleation between the Na-CCSH phase and tobermorite – 13Å, as demonstrated in Figure 3.4a. The addition of Al_2O_3 improved the crystallinity of the Na-CCSH phase in the Teflon experiments. The test tube $CaCO_3$ experiments showed similar hydration and crystallinity of Na-CCSH likely due to the Al leached from the dissolving glass. The Al, B, and K added from the glass are expected to have caused the shifts seen in in the XRD spectra of Figure 3.4b, as the (K,Na)-CCASH phase is more similar to the referenced rhodesite variation than the Na-CCSH phase. Al_2O_3 added to the 7-day $CaCO_3$ experiments conducted in borosilicate test tubes shows little effect on overall hydration at 0.28M NaOH, and slightly decreases overall hydration at 0.56 M NaOH, shown in Figures 3.6b and 3.6d, respectively.

Data from other work using slags or volcanic minerals rich in calcium silicates can be reinterpreted to support the direct precipitaiton hypothesis.[22–24, 50] Similar [Na^+], sourced from NaOH, Na_2CO_3, or $HNaCO_3$, are used in these studies to hydrothermally cure different reactants and produce tobermorite and other CCSHs. The rate-limiting dissolution of the mineral surfaces allows enough time for the collidal silica to undergo polymerization in solution and form CCSHs directly from solution instead of via crystalization of CSH gel. The aqueous reaction described is also supported by studies of ancient Roman concretes, where the dissolution of volcanic glasses over time in sea water promoted growth of Al-tobermorite.[13–16]

3.5 Conclusions

The effects of NaOH concentration and aqueous silica mobility on precipitation of tobermorite were studied using X-ray diffraction, thermogravimetric analysis, and inductively coupled plasma – optical emission spectroscopy. This work demonstrates that direct precipitation of CCSH phases from solution can be achieved by increasing NaOH concentrations and slowing dissolution of Ca and Si sources to minimize CSH gelation. When silica is not confined to CSH gel, the NaOH is hypothesized to increase colloidal silica polymerization. Over time, the speculated, semi-ordered silica structures react in solution with Ca^{2+} ions to produce new phases, like the Na-CCSH phase. $CaCO_3$ was shown to produce more CCSH phases than CaO at similar times and NaOH concentrations.

A graphical summary of the proposed mechanism is presented in Figure 3.9 with four reaction pathways illustrated. Reaction 1 shows a. CaO + micro silica in DI water, cured in Teflon, b. the formation of CSH gel, and c. the CSH gel crystallizing into tobermorite. Reaction 2 shows CaO + micro silica in 0.56 M NaOH solution, cured in Teflon, b. the formation of CSH gel with Na^{+} ions interspersed, and c. the crystallization of CSH gel into tobermorite partially interrupted by Na^{+} ions. Reaction 3 shows CaO + micro silica in 0.56 M NaOH solution, cured in glass, b. the formation of CSH gel with Na^{+} ions interspersed and glass dissolution forming colloidal silica, c. the ordering of colloidal silica and the NaOH removing Ca^{2+} ions from the CSH gel, d. the formation of the Na-CCSH phase, depicted based on the crystal structure of rhodesite. Reaction 4 shows a. $CaCO_3$ + micro silica in 0.56 M NaOH solution, cured in either glass or Teflon, b. NaOH dissolving the $CaCO_3$ into CO_3^- and Ca^{2+} and the micro silica (and glass) producing colloidal silica, c. the CO_2 escaping solution and the colloids ordering, d. the formation of the Na-CCSH phase.

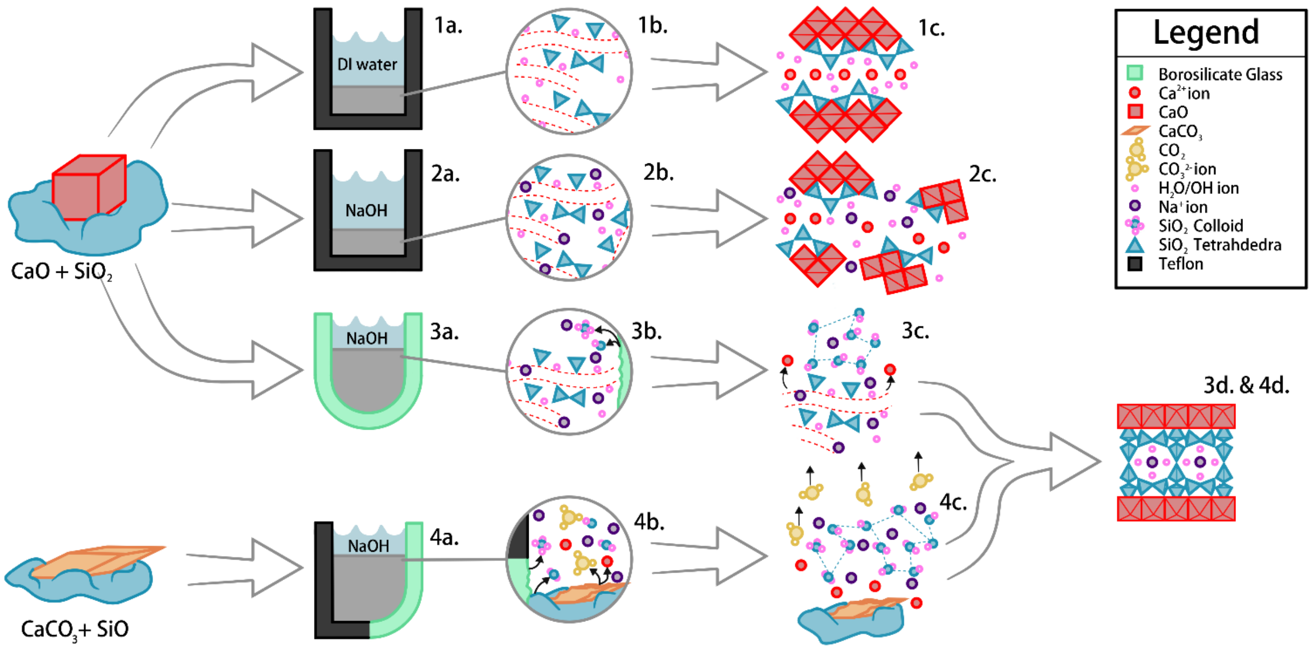

Figure 3.9. A notional depiction of the precipitation pathways to form CCHS phases. The abbreviated reaction pathways are: 1. CaO + micro silica in Teflon and DI water producing tobermorite; 2. CaO + micro silica in Teflon and 0.56M NaOH, with Na^+ ions impeding tobermorite crystallization; 3. CaO + micro silica in glass and 0.56M NaOH producing the Na-CCSH phase (based on rhodesite) from glass dissolution products; and 4. The $CaCO_3$ + micro silica in glass and 0.56M NaOH producing the Na-CCSH phase.

Decoupling CCSH synthesis from the crystallization of CSH gels may allow for novel synthesis approaches in researching new cements or curing methods. The extensive literature on sol-gel processing of ceramics could provide useful references for tailoring the stoichiometry of CCSH phases and illuminate new chemical pathways. The increase in precipitation with NaOH points to potential uses for high [Na^+] solutions from desalinization brines or seawater in combination with recycled glass for new cementitious materials.

i. *Why were CaO and micro silica experiments dependent on NaOH to precipitate tobermorite in Chapter 2 when the literature suggests otherwise?*

    a. The NaOH dissolved the borosilicate glass test tubes and added colloidal silica to solution that allowed tobermorite to directly precipitate.

ii. *How does CCSH precipitation vary in borosilicate glass test tubes versus Teflon vessels?*

    a. CaO experiments precipitated tobermorite in Teflon while precipitating the suggested Na-CCSH phase from the test tubes. $CaCO_3$ experiments precipitated primarily the Na-CCSH phase in both glass and Teflon, although Al, added from Al_2O_3 or the glass dissolution, improved the crystallinity and hydration at 3 days. Glass dissolution species also impacted precipitates from $CaCO_3$ by changing minor peaks in XRD to better match rhodesite.

iii. *How does CCSH precipitation from $CaCO_3$ differ compared to CaO?*

    a. $CaCO_3$ is hypothesized to directly precipitate CCSH phases from solution. CaO undergoes ordering of crystalline gel unless enough colloidal silica and NaOH are in solution, allowing both precipitation mechanism are expected.

3.6 Future work

Identifying the Na-CCSH and (K,Na)-CCASH phases is a priority for future work, as their crystal structure could illuminate how the colloidal silica orders in solution. Future experiments could explore how glass dissolution elements affect colloidal silica polymerization and bonding via heated NMR, FTIR, or Raman spectroscopy, with comparison to pure colloidal silica solutions. Implementing heated sodium silicate solutions to mortar or concrete curing could provide new techniques to produce CCSH phases.

4. CCSH precipitation from pseudowollastonite in carbonated environments

4.0 Background

Chapters 2 and 3 demonstrated how tobermorites and other CCSH phases were precipitated either from gel crystallization or directly from solution. This chapter will explore precipitation of CCSH phases and $CaCO_3$ from a model calcium silicate pseudowollastonite (pwol) to better design cements with high strengths and high carbon sequestration. The effects of NaOH concentrations, Al_2O_3 additions, and gaseous CO_2 at various partial pressures (P_{CO_2}) on CCSH precipitation were explored. Additionally, Na_2CO_3 was used as both a Na and CO_2 source to observe the differences between gaseous and salt bound CO_2. NaOH was found to precipitate tobermorite – 13Å and other CCSH phases. Al_2O_3 was often found to increase the crystallinity of CCSH phases days. CCSH precipitation was observed to decrease with P_{CO_2} while $CaCO_3$ precipitation showed an increase with P_{CO_2}. Na_2CO_3 experiments showed significant CCSH and $CaCO_3$ precipitation.

4.1 Research questions

i. Is the precipitation mechanism of CCSH phases from pwol different from the pure reactants used in Chapters 2 and 3?

ii. Is there a combination of NaOH concentration and P_{CO_2} that allows for both CCSH phases and $CaCO_3$ to precipitate?

iii. How does gaseous vs solid (salt) CO_2 affect the precipitation of CCSH phases and $CaCO_3$?

4.2 Methods

4.2.1 Synthesizing pwol

Pwol was synthesized from a 0.95:1 molar ratio of $CaCO_3$ (Huber, 97% pure) and Elkem micro silica 965 (95% pure), respectively. The powders were combined, then ball milled for 1 hour. The powder was then placed into a bowl and weighed. A 1.25 M NaOH (Fisher, 97% pure) solution with a mass of 25% that of the combined powder mass was mixed in using a KitchenAid Classic 4.5 L mixer. The slurry was baked at 80 °C for 24 hours. The dried chunk was fired to 1250°C and held at temperature for 9 hours in an Evenheat 1818 HF II pottery kiln. A section of the fired material was broken off and ground for X-ray powder diffraction (XRD, Malvern-Panalytical Empyrean, Worcestershire, UK). When confirmed to be pwol, the fired material was broken with hammer and chisel, and ground to a coarse powder via a hand mill. The powder was then ball milled using ZrO_2 media for 24 hours and filtered through a #200 sieve (75 µm). The separated powder was ball milled again for 24 hours before being stored in a sealed container. Figure 4.1 shows the XRD spectra of the synthesized pwol. Wollastonite (wol), the lower temperature polymorph of $CaSiO_3$, is present due to the limited heating capabilities of the kiln, and the zirconia is from the milling media. Rietveld analysis using GSAS-II indicates that about 70% by mass was pwol (estimated standard of deviation = 0.715%), up to 20% was wol (ESD = 0.836%), and ZrO_2, rankinite ($Ca_3Si_2O_7$, ESD = 0.169%), and calcio-olivine (Ca_2SiO_4, ESD = 0.598%) all ≤ 3%. The plotted fit of the refinement can be found in Figure A.3 in the Appendix.

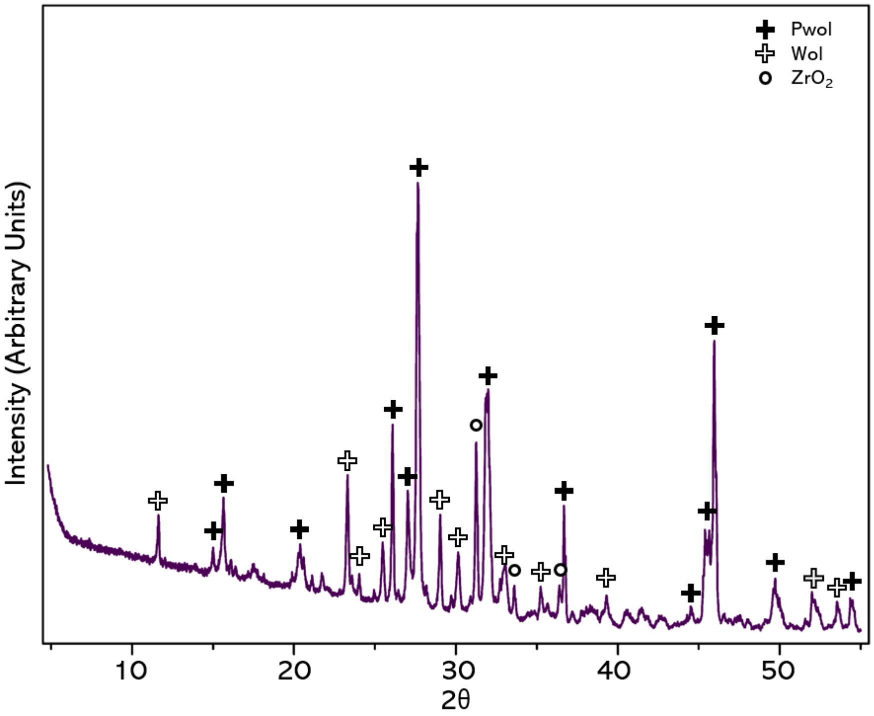

Figure 4.1. XRD spectrum of the synthesized pwol

4.2.2 Hydrothermal experiments

Two sets of preliminary experiments were conducted. In the first experiment, 1.046 g pwol and 0.954 g Na_2CO_3 (Sigma Aldrich, 99.5% pure) were mixed in borosilicate test tubes, following the respective 1:1 molar ratio used by Guillot et al.[23] Twenty milliliters of DI water or 0.1 M NaOH solution were added. In the second experiment, 2 g of pwol in a test tube was mixed with 20 mL of 0.1 M acetic acid, with or without the addition of 0.1 M NaOH. Both sets of experiments were cured concurrently with the pure reactant experiments from Chapter 2 for 1, 6, 24, 72, or 168 hours.

A significant amount of CO_2 escaped from the preliminary Na_2CO_3 pwol experiments into the headspace of the large pressure vessel, contaminating pure reactant experiments in Chapter 2. Two repeat experiments were run to confirm the effect of the CO_2 partial pressure on the reaction by curing samples for 3 days in an isolated 75 mL vessel (Parr Series 4740 High Pressure)

150°C, referred to as the Isolated condition. The first experiment contained pwol, Na_2CO_3, and 20 mL of 0.1 M NaOH in a test tube. The second isolated experiment contained pwol and 1 M NaOH, which is the same concentration $[Na^+]$ in prior experiments. The P_{CO_2} was set to 92 psi for 1 hour before curing, which was estimated via the ideal gas law to match the molar CO_2 concentration added from Na_2CO_3. The pressure vessels used are displayed in Figure 4.2.

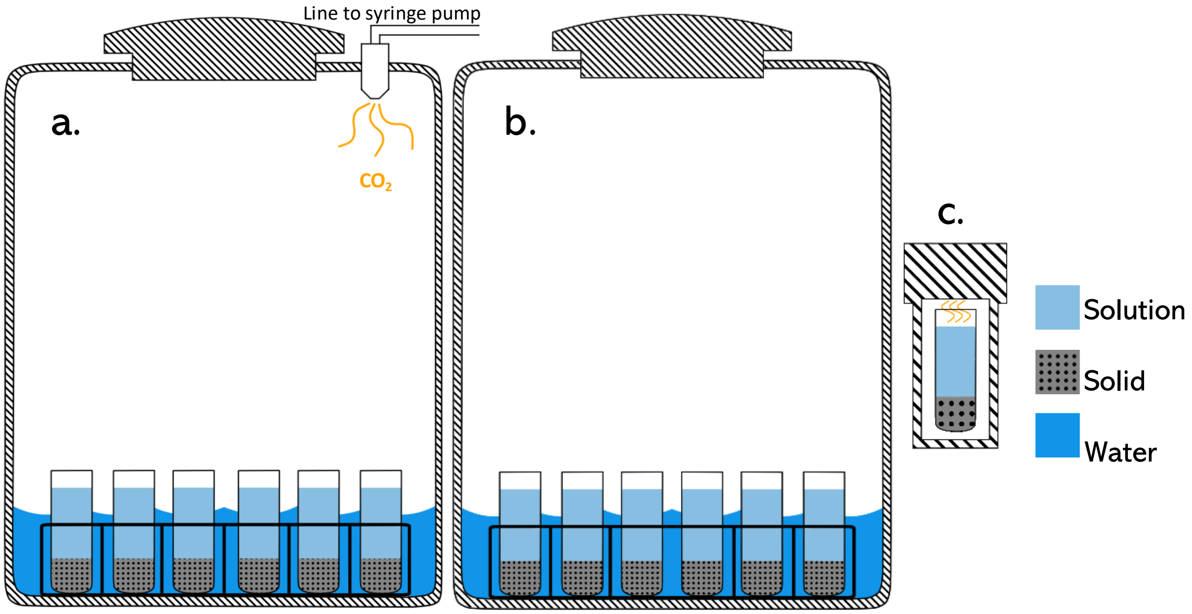

Figure 4.2. The experimental set up where samples were cured at 150 °C in a pressure vessel a. with gaseous CO_2, b. without gaseous CO_2, c. in the isolated batch reactor.

The majority of experiments in the chapter consisted of either 2 g of pwol or 1.9 g pwol + 0.1 g α-Al_2O_3 (Fisher, 99.9% pure) placed into a borosilicate test tube (Fisher). The powders were mixed with 20 mL of either DI water, 1 M, or 2 M NaOH solution. The test tubes were placed into a rack and sealed in a 10 L pressure vessel with 2 L of water in the basin, shown in Figure 4.2a. CO_2 was injected via a syringe pump (Teledyne ISCO 500D, Lincoln, NE, US) and allowed to equilibrate for 1 hour to attain a P_{CO_2} of 3 psi, 6 psi, 15 psi, or 30 psi at 150 °C. The syringe pump had an accuracy of ±1 psi. Note that the P_{CO_2} of 6 psi was calculated to match the pwol:CO_2 molar ratio of 1:1 in the preliminary isolated experiments. The vessels were then heated in an oven at 150 °C[23, 29, 33] (± 3 °C) for 1 day, 3 days, or 7 days of curing. Experiments without gaseous CO_2 were conducted in a completely isolated pressure vessel, seen in Figure 4.2b. Experiments using Na_2CO_3 (Fisher, 99.5% pure) were also conducted with Na^+ concentrations matching the 1 M or 2 M NaOH experiments. The Na_2CO_3 experiments cured without gaseous CO_2 at the prior mentioned curing conditions. The vessels were removed from the oven, and the test tubes were naturally cooled to room temperature after the desired cure time. The precipitates were filtered from solution using 25 µm filter paper (Whatman), acidified with 0.1 M acetic acid (Fisher, glacial), and then dried at 50 °C for 24 hours and stored. Additional borosilicate test tubes were run without powder under the same hydrothermal conditions and times filled with 20 mL of DI water, 1 M NaOH, or 2 M NaOH to establish baseline information on the test tube solubility.

4.2.3 Characterization

X-ray powder diffraction (XRD, Malvern-Panalytical Empyrean, Worcestershire, UK) of the dried precipitates was conducted at the following parameters: Cu Kα-radiation (λ =1.5405 Å); current = 40 mA; tension = 45 kV, GaliPIX Detector scanning 501 steps at a time; measurement range = 4.8–55 °2θ; time per step = 90 s; and step size = 0.0143 °2θ. The sample stage was spun during the scans to minimize the effects of orientation. The data were analyzed with Highscore Plus (Version 4.9), using the International Centre for Diffraction Data (ICDD) databases to identify phases. Table 4.1 contains the mineral names, compositions, and ICDD reference codes of the phase identified in this work. All referenced patterns of the major phases (>10% mass) and minor phases (2-10%) identified aligned with of peak locations and intensities with data presented.

Table 4.1. A list of mineral names, chemical formulae, and ICDD reference codes for the phases identified in this work. Major phases over an estimated 10% mass are indicated by (+), minor phases from 2-10% mass by (-), and trace phases under 2% by (t).

Mineral Name	Chemical formula	ICDD reference code
Pwol (+)	$CaSiO_3$	01-080-9543
Wol (+)	$CaSiO_3$	02-027-1064
Aragonite (-)	$CaCO_3$	04-013-9616
Calcite (-)	$CaCO_3$	04-008-0198
α-Al_2O_3 (-)	Al_2O_3	00-005-0712
Zirconia (t)	ZrO_2	04-013-4749
Tobermorite – 13Å (+)	$Ca_{16}(Si_8O_{28})(H_2O)_{13}$	01-081-9793
Pectolite (-)	$NaCa_2Si_3(OH)$	01-076-0951
Rhodesite (+)	$(Ca,K,Na)_8Si_{16}O_{40}\bullet 11H_2O$	00-022-1253
Unnamed CCSH (-)	$Ca_9(Si_{16}O_{34}(OH)_{14})(H_2O)_8$	01-074-7587
Gismondine-Na (-)	$Na_{3.6}Al_{3.6}Si_{12.4}O_{32}\bullet 14H_2O$	01-080-0699
Analcime (-)	$K_{0.19}Na_{7.69}Ca_{0.06}Al_8Si_{16}O_{48}(H_2O)_8$	04-024-8347
Mordenite (-)	$Ca_{2.5}Na_2Al_7Si_{41}O_{96}\bullet 24H_2O$	00-060-0846

Select samples were further analyzed via thermogravimetric analysis (TG, Netzsch STA-449 F1, Bayern, Germany) to measure the amount of hydration and carbonation. For this characterization, 20 mg of powder was placed in a Pt-Rh crucible and heated at a rate of 10 °C/min to 1000 °C. The data were collected and compared to the literature.[37, 39, 44]

Supernatants from the powderless glass experiments were analyzed via inductively coupled plasma – optical emission spectroscopy (ICP-OES, Thermofisher ICAP 6200, Waltham, Massachusetts, US). The supernatants were diluted to 2000x with DI water. The Al, B, Ca, K, Na, and Si concentrations were measured in triplicate.

4.3 Results

4.3.1 Preliminary experiments

An initial set of experiments was conducted using Na_2CO_3 and 0.1M NaOH to confirm CCSH phases could be precipitated from pwol.[23] Only when the preliminary experiments were isolated in the batch reactor were CCSH phases found in the precipitates, as seen in Figure 4.3. The isolated precipitates contained tobermorite – 13Å, rhodesite, and pectolite, where rhodesite is expected to form from the addition of K from the glass dissolution. In addition, aragonite and gismondine-Na were found in the isolated precipitates, also seen in the addition carbonation and standard conditions. The additional carbonation condition again refers to the experiments conducted under an unknown P_{CO_2}, as described in Chapter 2. In the additional carbonation and standard conditions, the loss of CO_2 to the head space and interacting with other samples in the pressure vessel appears to have prevented CCSH precipitation.

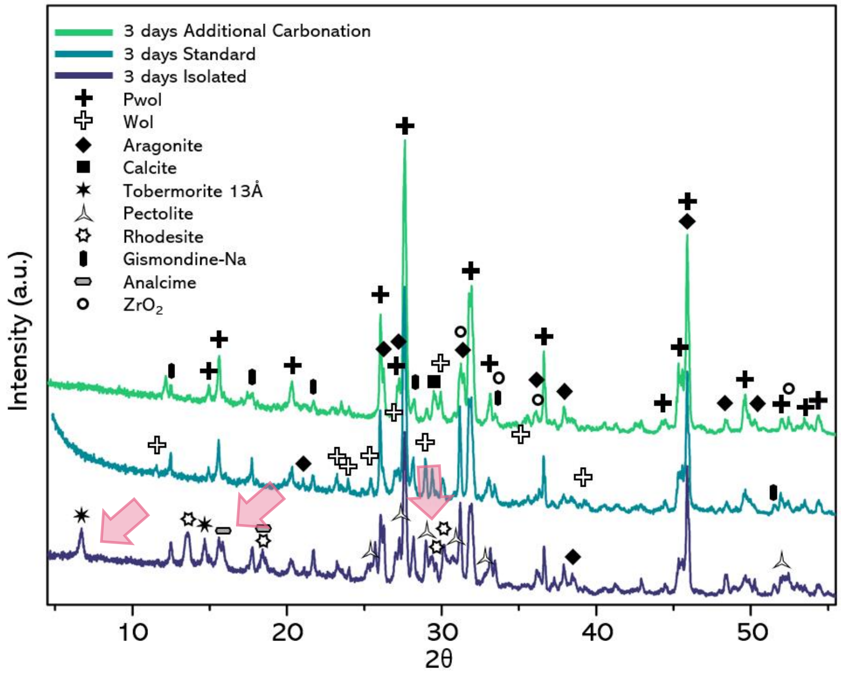

Figure 4.3. XRD data of pwol and Na_2CO_3 precipitates cured for 3 days showing how CO_2 can affect precipitation of CCSH phases. Note how the isolated condition in the batch reactor produced CCSH phases, indicated by arrows, that were not seen in the additional carbonation and standard conditions.

An additional isolated experiment was run to compare gaseous CO_2 versus Na_2CO_3 at the same $[Na^+]$ and $[CO_2]$, shown in the XRD data of Figure 4.4. Both experiments precipitated CCSH phases and aragonite, though obvious differences in intensity of CCSH and $CaCO_3$ phases can be seen. The gaseous CO_2 precipitates show a lower intensity for the tobermorite – 13Å peaks than the Na_2CO_3 precipitates. A second low 2θ peak after tobermorite – 13Å that corresponds to rhodesite is also present in the gaseous CO_2 precipitates that is not seen in the Na_2CO_3 precipitates. Pectolite and analcime, a sodium aluminum silicate hydrate, were not matched in the gaseous CO_2 precipitates where they were in the Na_2CO_3 precipitates, most obvious between 25-35 ˚2θ. Finally, the gaseous CO_2 precipitates show a much higher intensity for aragonite than the Na_2CO_3 precipitates, indicating more carbonation occurred.

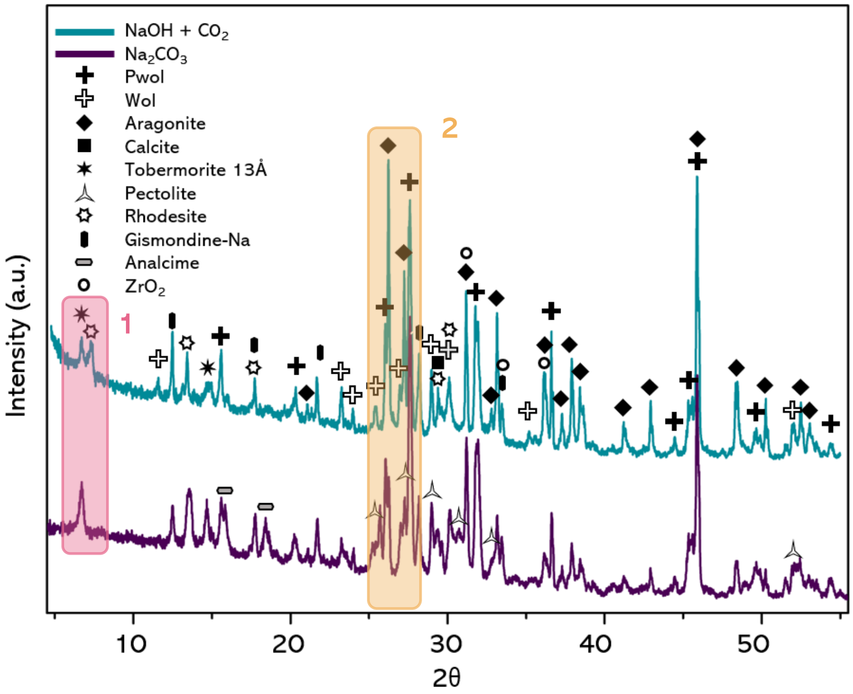

Figure 4.4. XRD data comparing the precipitates of isolated experiments using gaseous CO_2 versus Na_2CO_3 at the same $[Na^+]$ and $[CO_2]$. Not the differences in the data for tobermorite – 13Å and rhodesite peaks in the highlighted region 1, and aragonite and pectolite in the region 2.

4.3.2 No carbonation baseline experiments

The precipitation of CCSH phases from pwol increased with time in 2 M NaOH, as seen in the XRD spectra in Figure 4.5. A similar increase was observed with NaOH concentration, shown in Figure A.4 in the Appendix. However, the majority of data presented in this Chapter will focus on the 2 M NaOH experiments because the trends are the clearest in these data. Figures 4.5a and 4.5b show the intensities of tobermorite – 13Å, pectolite, and rhodesite are the highest at 7 days, along with gismondine-Na for reaction products both with and without Al_2O_3. Both pwol and wol decline in intensity with time and the formation of CCSH phases in the experiments with and without Al_2O_3, though the pwol + Al_2O_3 precipitates show greater reduction of wol. The pwol + Al_2O_3 precipitates in Figure 4.5b also show higher intensities for tobermorite – 13Å, rhodesite, and pectolite at 3 days, but the differences are nearly equalized at 7 days. Finally, the pwol + Al_2O_3 precipitates show lower intensity for Gismondine-Na than the pure pwol precipitates at 7 days. TG data are shown in Figures 4.5c and 4.5d where DTG is the derivative of the TG data. At 1 day, the XRD data indicate that primarily CSH gel formed, corresponding to the DTG peak at about 90 °C seen in Figures 4.5c and 4.5d.[39] In the 3 day samples where CCSH phases formed, tobermorite – 13Å is expected to dehydrate into tobermorite – 11Å in the same temperature range as CHS gel dehydration,[40] increasing the peak at 90 °C. The peak found at 175 °C corresponds to tobermorite – 11Å dehydrating,[40] while the peak at 250 °C is expected to be rhodesite and gismondine-Na dehydration. The TG data indicate that the experiments with and without Al_2O_3 show very close total dehydration from 30-400 °C, with the Al_2O_3 experiments dehydrating slightly more at every timestep. After 7 days, the pure pwol sample lost 10.72% mass to water vapor and the pwol + Al_2O_3 lost 10.91%.

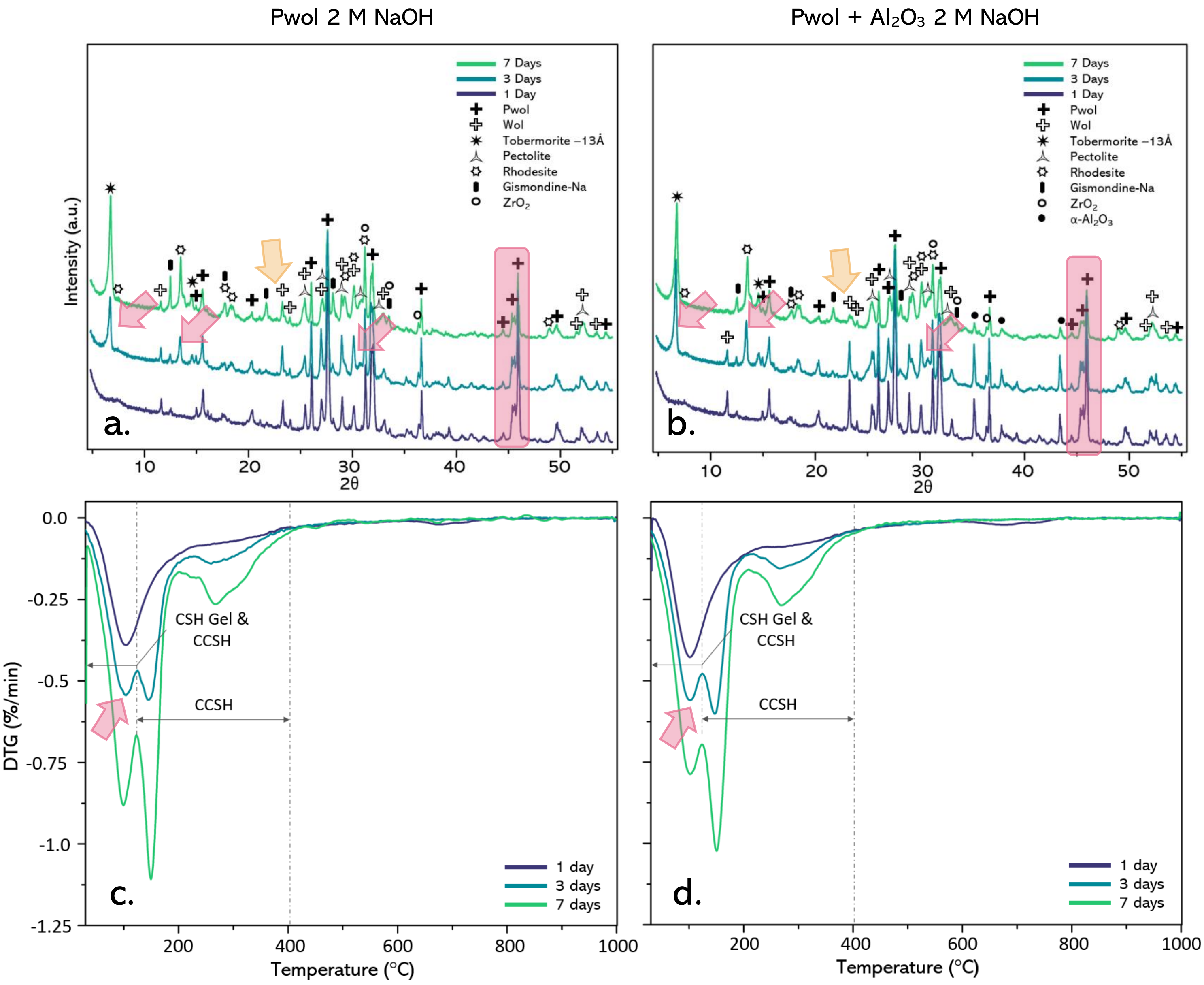

Figure 4.5. 2 M NaOH experiments at all times a. XRD of pure pwol, b. XRD of pwol + Al_2O_3, c. DTG of pure pwol, d. DTG of pwol + Al_2O_3. Note how, in a. and b. data, the pwol + Al_2O_3 precipitates show higher intensities for CCSH phases, supported by the stronger DTG peaks in c. and d. (pink arrows). Additionally, note how the pwol + Al_2O_3 precipitates show higher consumption of wol in b. than pure pwol in a. (yellow arrows). Finally, note the consumption of pwol seen in the reduce peak intensities in the highlighted region.

The glass dissolution data shown in Figure 4.6 has similar concentration trends and ratios of species in solution to the data presented in Chapter 3; Na and Si show near equal concentrations, and all elements show concentration increase with time. The starting concentration for 1 M NaOH is 40,000 ppm and 0.56M NaOH is 80,000 ppm. The black or grey error bars indicate one standard of variation and that very little uncertainty was seen for the data collected. The DI water experiments did not have any measurable concentrations of the elements tested and are not included.

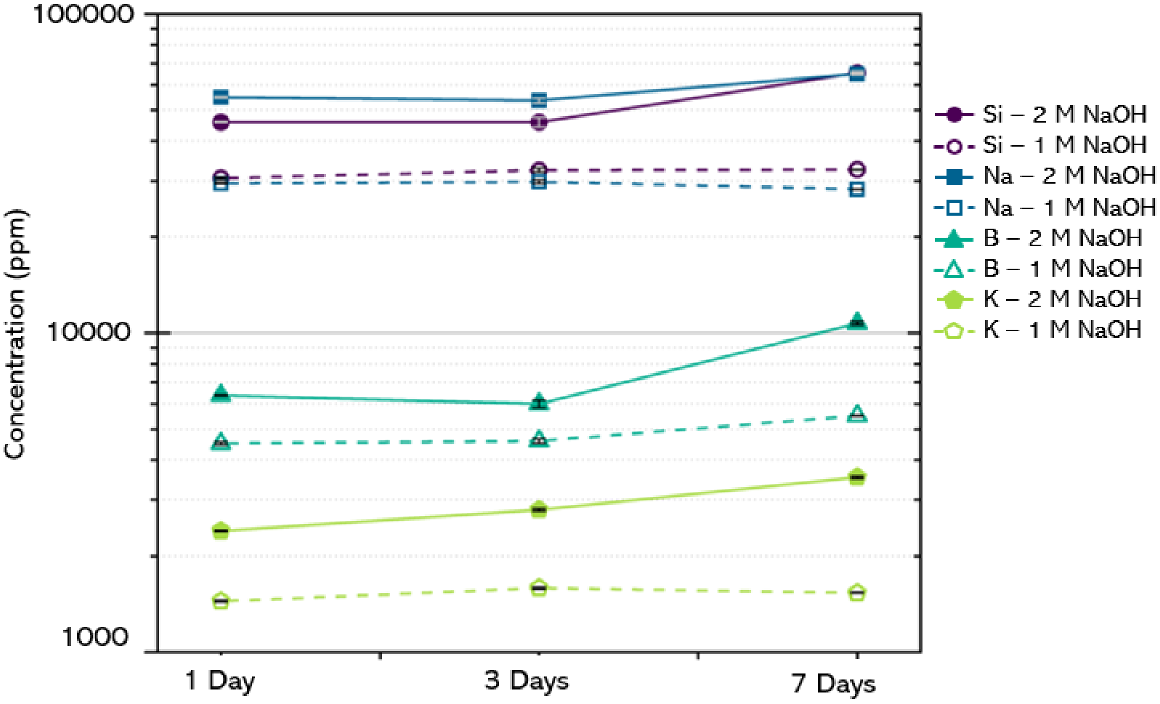

Figure 4.6. A logarithmic plot of elemental concentrations from the powderless glass experiment supernatants measured via ICP-OES. The black or grey error bars indicate one standard of variation.

4.3.3 Variable P_{CO_2} experiments

The addition of CO_2 drove the system to form the calcium carbonates aragonite and calcite at the expense of CCSH phases across all P_{CO_2} conditions, as seen in the 7-day, 2 M NaOH data presented in Figure 4.7. Pwol is consumed to form primarily aragonite, with calcite increasing with P_{CO_2}. Calcium carbonate formation also increased with NaOH concentration (not shown). Wol, however, does not decrease with the P_{CO_2}, indicating that CO_2 may preferentially react with pwol. At 3 psi P_{CO_2}, reaction products with and without Al_2O_3 produced small amounts of CCSH. The pure pwol precipitates in Figure 4.7a produced tobermorite – 13Å and rhodesite, while the pwol + Al_2O_3 precipitates in Figure 4.7b produced tobermorite – 13Å and an unnamed CCSH. Both the experiment with and without Al_2O_3 produced gismondine-Na. At 6 psi, the pure pwol experiments only produced mordenite, expected to be another zeolite formed from the borosilicate glass. The pwol + Al_2O_3 at 6 psi produced lower intensity tobermorite – 13Å and CCSH than the 3 psi, and no gismondine-Na was matched. Interestingly, 6 psi was calculated to match the pwol:CO_2 molar ratio of 1:1 in the preliminary isolated experiments in Figures 4.3 and 4.4. At 15 psi, only aragonite and calcite were found, both increasing at 30 psi (not shown). When CCSH phases were not formed at higher P_{CO_2}, the supernatants were supersaturated with amorphous silica. The broad peak found centered around 21 °2θ corresponds to the amorphous silica found in the powder.

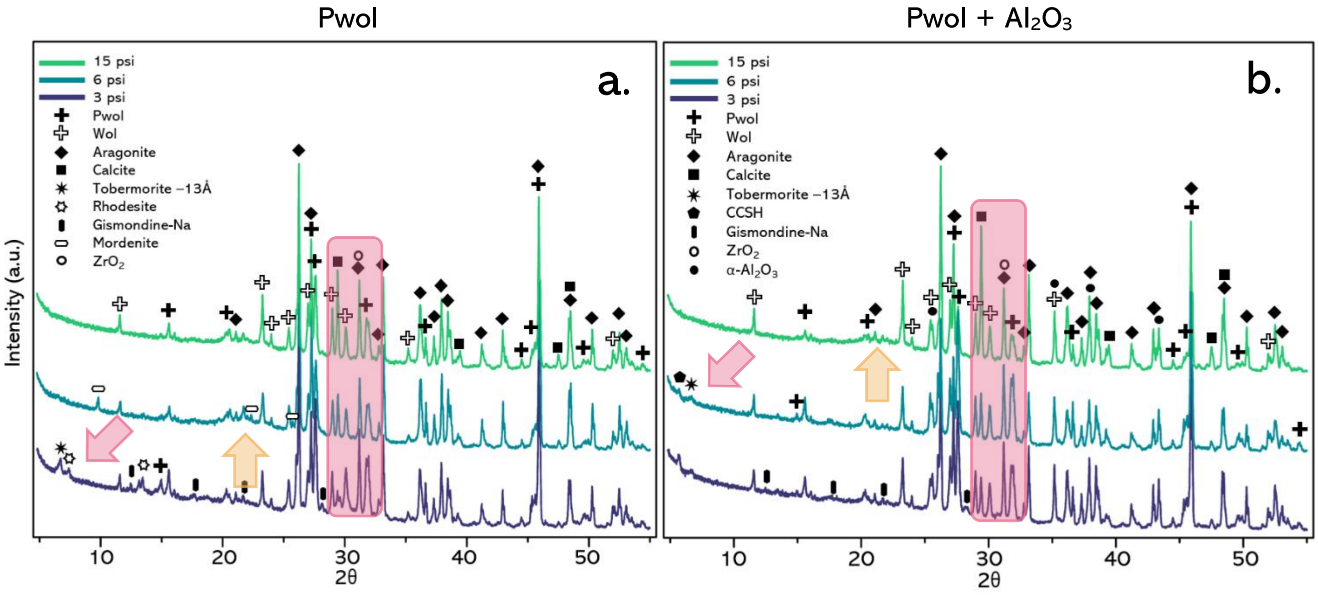

Figure 4.7. 2 M NaOH experiments at 7 days for 3 psi, 6 psi and 15 psi P_{CO_2} a. XRD of pure pwol, b. XRD of pwol + Al_2O_3. Note the differences in the CCSH phase and at what P_{CO_2} they precipitated, indicated by the pink arrows. Also note the broad peak at 21 °2θ amorphous silica, indicated by yellow

arrows. Finally note increase in calcite intensity and decrease in pwol intensity over time in the highlighted region.

4.3.4 Na_2CO_3 experiments

CCSH phases and calcium carbonates were both found across all concentrations when using Na_2CO_3 as both a Na and CO_2 source. Here the total CO_2 added from Na_2CO_3 would equate to a P_{CO_2} of about 3.8 psi at 150 °C, assuming all CO_2 in solution escaped into the headspace of the pressure vessel. Tobermorite – 13Å, pectolite, rhodesite, and gismondine-Na are all found in the 1-day, 2 M Na concentration ($[Na^+]$) experiments in Figures 4.8a and 4.8b but were not seen in the NaOH baseline precipitates in Figure 4.5. In the 7-day reaction products, the rhodesite intensities are higher than the baseline NaOH experiments in Figure 4.5. The pure pwol experiments in Figure 8a show higher intensities for the CCSH phases at both 1 and 3 days than the pwol + Al_2O_3 experiments. After 7 days, the pwol + Al_2O_3 reaction products show the highest intensity for tobermorite – 13Å. Pwol is consumed in both experiments with and without Al_2O_3 to form the CCSH phases and carbonates. No decrease in wol intensity was observed in the Na_2CO_3 precipitates in Figure 4.8, aligning more with the variable P_{CO_2} experiments than the NaOH baseline experiments. Instead, there is a slight increase in wol intensity at 7 days, with a similar observation recorded by Guillot.[23] DTG data indicate that the pwol + Al_2O_3 experiments in Figure 4.8d have broader dehydration peaks centered around 90 °C. After 7 days, the pure pwol experiment in Figure 4.8c shows greater dehydration of tobermorite – 13Å and CSH gel at 110 °C, and slightly more dehydration for rhodesite and gismondine-Na than the pwol + Al_2O_3 precipitates at 250 °C. TG data indicate the pure pwol experiments show more total hydration. After 7 days, the pure pwol lost 9% mass to CSH gel and CCSH dehydration where the pwol + Al_2O_3 lost 8%. The DTG data in Figure 4.8c also show that the pure pwol experiment at 3 days produced the most calcium carbonates out of all the timesteps with or without Al_2O_3, with calcium carbonates accounting for about 11.6% of the total mass. This increase at 3 days was not seen in the pwol + Al_2O_3 precipitates in Figure 4.8d, where carbonation increased with time to a maximum of about 10.1% calcium carbonates by mass at 7 days as compared to 9.56% found in the pure pwol precipitates.

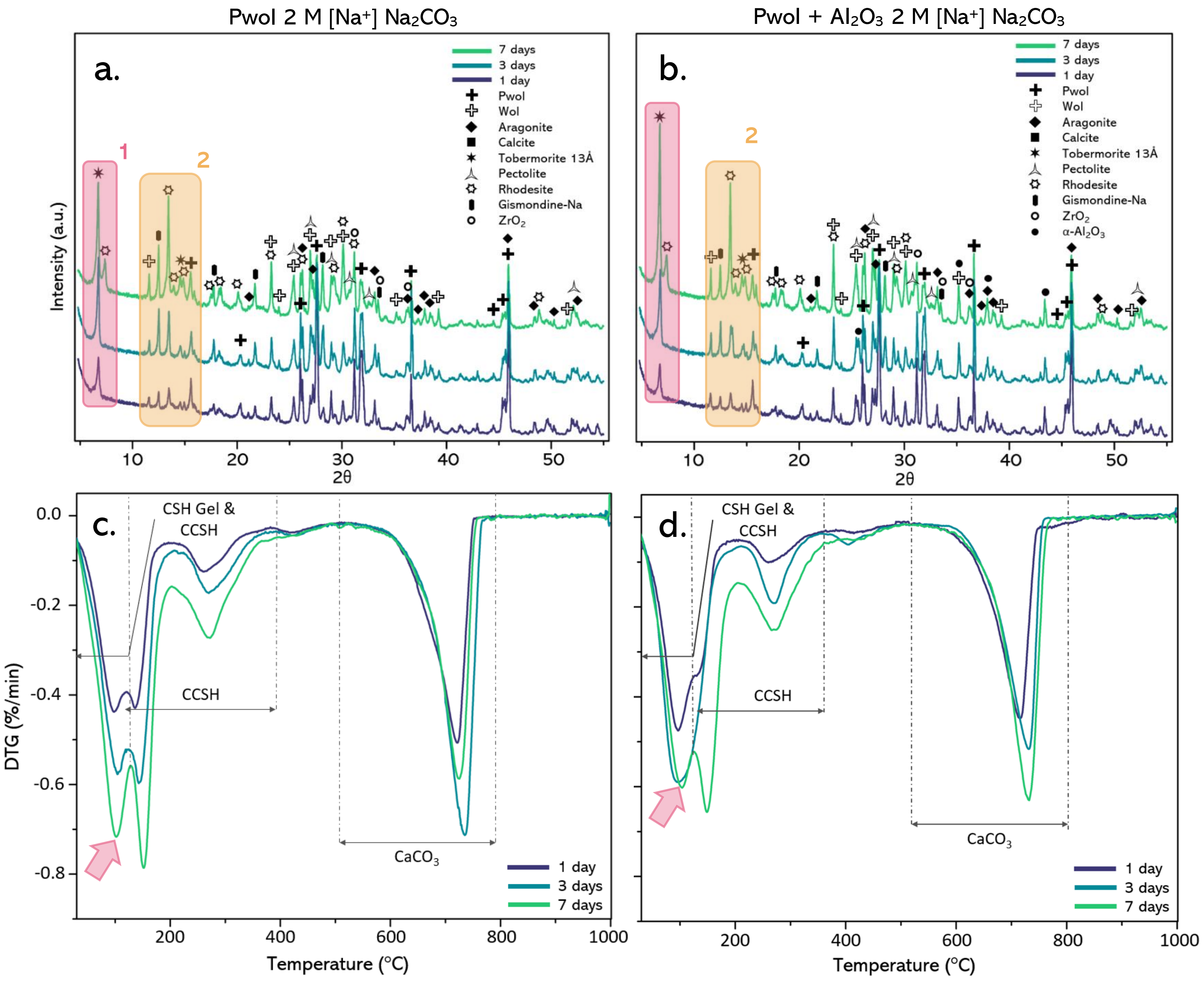

Figure 4.8. 2 M [Na$^+$] Na_2O_3 experiments a. XRD of pure pwol at all times, b. XRD of pwol + Al_2O_3 at all times, c. DTG of pure pwol at all times, d. DTG of pwol + Al_2O_3 at all times. In a. and b., note pwol precipitates in highlighted region 1 shows a higher tobermorite – 13Å peak than pwol + Al_2O_3 precipitates at 3 days, but pwol + Al_2O_3 precipitates show the higher tobermorite – 13Å peak at 7 days. Additionally, highlighted region 2 shows increases in wol intensity with time, and gismondine-Na is higher in the pwol precipitates than pwol + Al_2O_3 at every timestep. In c. and d. note the differences in DTG peak size and shapes.

The CCSH phases formed in the Na_2CO_3 precipitates at 1 M [Na$^+$] differ than 2 M [Na$^+$], unlike the 1 M and 2 M NaOH precipitates in Figure 4.5. Figures 4.9a and 4.9b show that for 1 M

[Na^+] the Na_2CO_3 experiments produced primarily rhodesite and gismondine-Na with tobermorite – 13Å matched only identified in the pwol + Al_2O_3 precipitates at 1 day. The XRD spectra show the low angle peak at 7.4 °2θ for rhodesite is the highest intensity peak, where prior spectra show the primary peak at 13.5 °2θ. After 7 days, the wol intensity increased significantly in experiments both with and without Al_2O_3. DTG data in Figures 4.9c and 4.9d show broad CSH gel peaks centered at 90 °C, similar to the 2 M [Na^+] pwol + Al_2O_3 experiments in Figure 4.8. The assumption that rhodesite has a dehydration peak at 250 °C is supported by the prominent peak found in Figures 4.9c and 4.9d. Similar to the 2 M [Na^+] Na_2CO_3 precipitates, the pure pwol reaction products lost more mass to dehydration at every timestep, with the 7-day pure pwol precipitates losing 5.13% mass to water vapor and the 7-day pwol + Al_2O_3 losing 3.72% mass. Calcium carbonate precipitation shows a similar trend to the 2 M [Na^+] Na_2CO_3 data, where the pwol + Al_2O_3 reaction products show greater carbonation at 1 and 3 days than pure pwol. After 7 days, the pwol precipitate consisted of 7.3% $CaCO_3$ by mass while the pwol + Al_2O_3 precipitates were 7.8% $CaCO_3$.

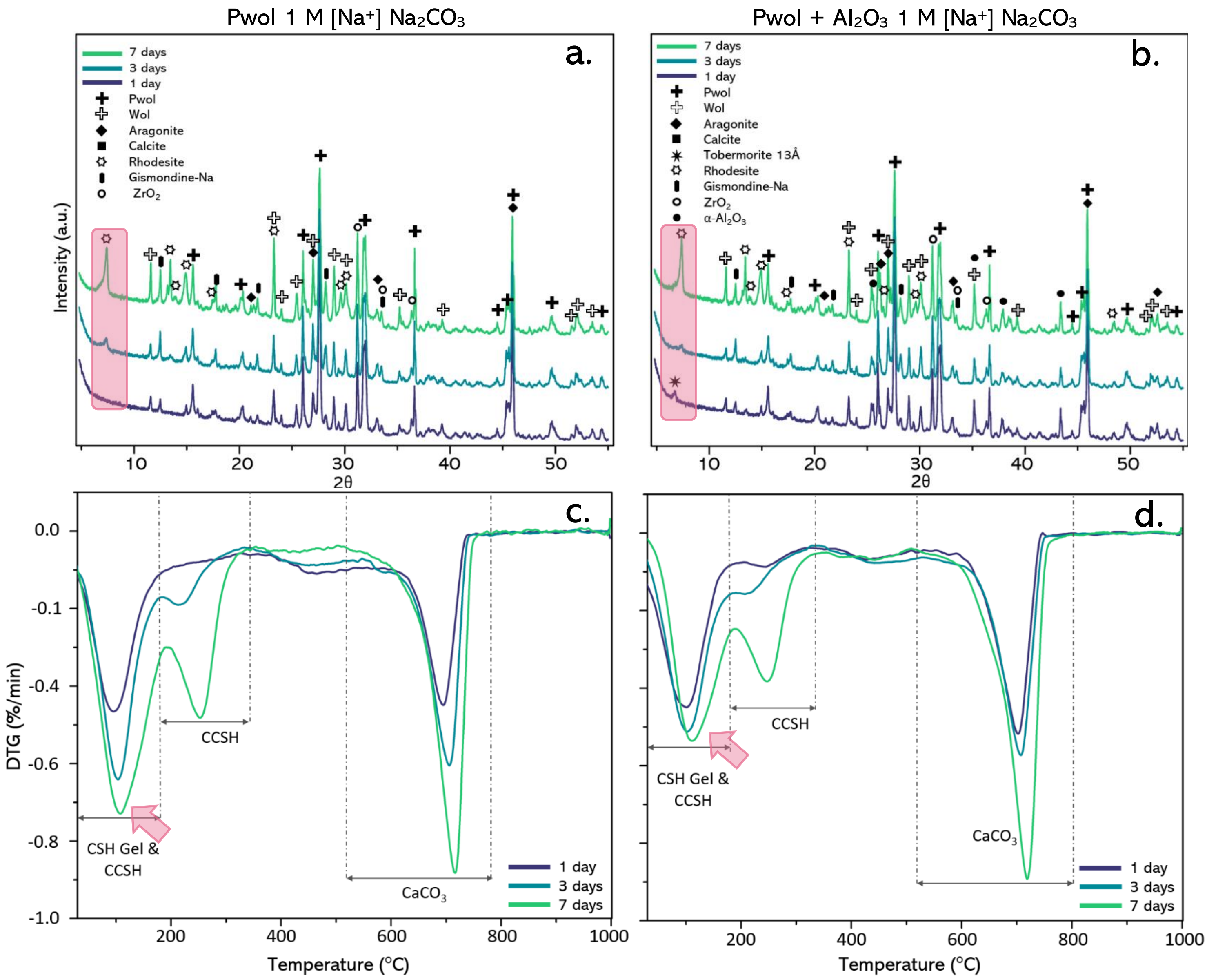

Figure 4.9. Data from the 1 M [Na^+] Na_2O_3 precipitates. A. XRD of pure pwol at all times, b. XRD of pwol + Al_2O_3 at all times, c. DTG of pure pwol at all times, d. DTG of pwol + Al_2O_3 at all times. Note how pwol + Al_2O_3 precipitates CCSH at one day. Also note the differences in hydration magnitude at each timestep between pwol and pwol + Al_2O_3 precipitates.

4.4 Discussion

The data presented in this work highlight four key findings: (1) the precipitation of CCHS phases and calcium carbonates increases with [Na^+]; (2) the presence of gaseous CO_2 drives the formation of calcium carbonates over CCSH phases; (3) the dissolution species from the borosilicate test tubes influence hydration species; and (4) the addition of Al_2O_3 aided the crystallinity of CCSH phases.

Precipitation of both CCSH phases and calcium carbonates was shown to increase with the [Na^+] under the conditions tested though different reasons are expected. For the CCSH phases, the increase in [Na^+] is hypothesized to boost the dissolution of both pwol and the borosilicate glass by slowly hydrolyzing silica along the exposed surfaces.[41, 45, 51] The silica then polymerizes and reacts with aqueous Ca to form the CCSH phases identified, following the previously hypothesized direct precipitation pathways of $CaCO_3$ experiments described in Chapter 3. For the calcium carbonates formed from gaseous CO_2, the increase in NaOH is expected to improve the gas solubility, described by the bicarbonate buffer reaction in Equation 4.1.

$$CO_{2(g)} + H_2O_{(aq)} \leftrightarrow H_2CO_{3(aq)} \leftrightarrow H^+_{(aq)} + HCO^-_{3(aq)} \leftrightarrow 2H^+_{(aq)} + CO^{2-}_{3(aq)} \tag{4.1}$$

The H^+ then dissolves the pwol into aqueous silica and Ca^{2+}, the latter of which readily reacts with the CO_3^{2-} in solution to form calcium carbonates.

The drive towards CO_2 equilibrium between the headspace and solutions is expected to have caused the differences in precipitates observed between gaseous CO_2 and Na_2CO_3 experiments even with similar molar [Na^+] and [CO_2]. In the P_{CO_2} experiments, CO_2 is saturated in the headspace and enters the solutions to equilibrate, driving Equation 4.1 to the right. H_2CO_3 is formed in solution, which attacks pwol and forms calcium carbonates. As CO_2 is precipitated out of solution, more gas from the headspace is able to enter solution and repeats the cycle to form more calcium carbonate. In the time that it takes for the aqueous SiO_2 to polymerize, calcium has already been consumed to form calcium carbonates, which prevents CCSH precipitation. Additionally, the aqueous carbonate species acted as acids to buffer the NaOH solution, as seen in Equation 4.1. The reduced pH could also lower the favorability of CCSH precipitation. The preliminary, isolated experiments in Figure 4.4 showed that using gaseous CO_2 instead of Na_2CO_3 drastically increased the aragonite intensity but still precipitated CCSH phases. The amount of CO_2 added to the batch reactor was lower than the amount added to the pressure vessels, reducing the drive to CO_2 equilibrium and the amount of carbonation. Similarly, the push towards calcium carbonates and pH changes are less intense at the lower P_{CO_2} experiments seen in Figure 4.7 at 3 psi, allowing for small amounts of CCSH to precipitate.

The Na_2CO_3 experiments precipitated both calcium carbonates and CCSH phases with similar molar concentrations of Na and CO_2 to some of the P_{CO_2} experiments. The inverse of Equation 4.1 occurs with Na_2CO_3 dissociation into Na^+ and CO_3^{2-}, described in Equations 4.2 and 4.3.

$$Na_2CO_{3(s)} \leftrightarrow 2Na^+_{(aq)} + CO^{2-}_{3(aq)} \tag{4.2}$$

$$CO^{2-}_{3(aq)} + 2H_2O_{(l)} \leftrightarrow HCO^-_{3(aq)} + OH^-_{(aq)} + H_2O_{(l)} \leftrightarrow \ldots$$

$$\ldots H_2CO_{3(aq)} + 2OH^-_{(aq)} \leftrightarrow CO_{2(g)} + H_2O_{(l)} + 2OH^-_{(aq)} \tag{4.3}$$

Equation 4.3 is driven to the right as large concentrations of CO_3^{2-} enter solution when the salt dissolves. While H_2CO_3 and HCO_3^- ions do form and attack the pwol to form calcium carbonates, the reaction is driven to produce CO_2. The CO_2 is largely insoluble at 150 °C and is expected to escape solution into the undersaturated headspace. The CO_2 does return, however, the water-CO_2 reaction to form H_2CO_3 in Equation 4.1 is expected to be the rate limiting step of the carbonate buffer reaction. Thus, the escaped gas will take time to reenter solution. Additionally, the aqueous carbonate species acted as a base, maintaining a favorable pH for

CCSH precipitation. With less CO_2 consuming Ca^{2+} and desirable pH levels, aqueous silica is hypothesized to order and react with Ca^{2+} to form CCSH phases.

The addition of Al_2O_3 was shown to improve crystallinity of CCSH phases after 3 days in NaOH solutions, as seen in Figure 4.5. While Al_2O_3 also improved crystallinity of CCSH phases in the Na_2CO_3 experiments, it decreased hydration in Figures 4.8 and 4.9. This observed difference in how Al_2O_3 affects hydration between NaOH and Na_2CO_3 is not well understood. The total hydration may have dropped due to Al_2O_3 improving carbonation after 7 days and reducing the Ca^{2+} available for CCSH phases, with a similar carbonation trend seen in the gaseous CO_2 data in Figure 4.7. The decreased hydration with Al_2O_3 could also be attributed to the decrease in precipitated gismondine-Na, however the NaOH experiments also show a decrease in gismondine-Na with Al_2O_3. Data in Chapter 3 show that Al_2O_3 decreased hydration in precipitates cured in glass at 0.56M NaOH.

4.5 Conclusions

The effect of NaOH concentration, partial pressures of CO_2, and the use of Na_2CO_3 as both an Na and CO_2 source on CCSH precipitation from pwol were explored using X-ray diffraction and thermogravimetric analysis. NaOH was found to improve both CCSH and calcium carbonate precipitation. The presence of gaseous CO_2 was found to drive the system to produce calcium carbonates, even at low P_{CO_2}. Na_2CO_3 was found to produce significant amounts of both CCSH phases and calcium carbonates. Utilizing Na_2CO_3 instead of gaseous CO_2 could produce mortars and concretes with improved strengths and decreased porosities. Na_2CO_3 could potentially simplify curing setups for carbon sequestration by eliminating the need for expensive pressure vessels, though the viability of Na_2CO_3 as a carbon source needs to be researched.

A graphical summary of the chemical pathways described is provided in Figure 4.10, with three reaction pathways. Reaction 1 shows a. pwol dissolving in NaOH solution, producing Ca^{2+} and colloidal silica, and the borosilicate glass producing colloidal silica, b. the ordering of colloidal silica in solution, and c. the precipitation of CCSH phases. Reaction 2 shows a. gaseous CO_2 forming carbonic acid that dissolves pwol in NaOH, producing Ca^{2+} and colloidal silica, b. Bicarbonate ion interacting with Ca^{2+} ions, and c. the precipitation of $CaCO_3$ phases and amorphous silica. Reaction 3 shows pwol dissolving in Na_2CO_3 solution, producing carbonate ions, Ca^{2+}, and colloidal silica, b. precipitation of $CaCO_3$ phases while CO_2 escapes solution and silica colloids order, and c. the precipitation of CCSH phases.

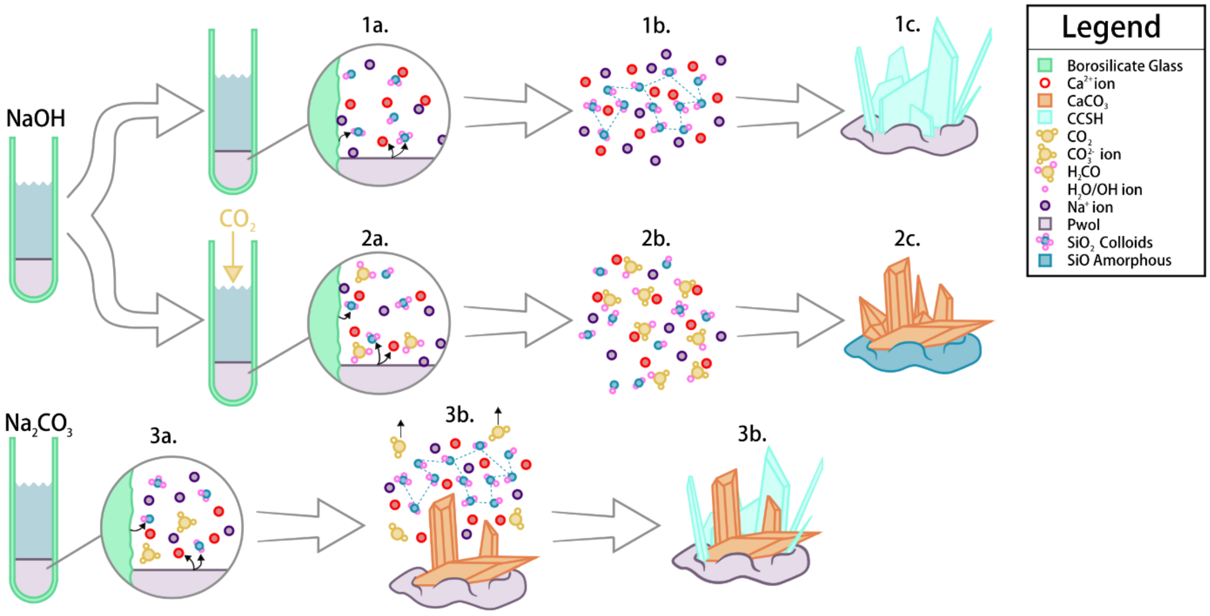

Figure 4.10. A notional diagram outlining the precipitation pathways of the various conditions explored in this work. The abbreviated reactions depicted are: 1. pwol dissolving in NaOH solution to precipitate CCSH phases; 2. pwol dissolving from carbonic acid produced from gaseous CO_2 *and precipitating* $CaCO_3$ *phases; and 3. Pwol dissolving in* Na_2CO_3 *solution and precipitating both* $CaCO_3$ *and CCSH phases.*

i. *Is the precipitation mechanism of CCSH phases from pwol different from the pure reactants used in Chapters 2 and 3?*
    a. Pwol precipitates CCSH phases through direct precipitation, similar to the $CaCO_3$ samples in Chapter 3.

ii. *Is there a combination of NaOH concentration and P_{CO_2} that allows for both CCSH phases and $CaCO_3$ to precipitate?*
    a. Preliminary batch reactor experiments showed small amounts of CCSH precipitation at 92 psi, likely due to the limited concentration of CO_2. In the large pressure vessels, small quantities of CCSH phases were observed to precipitate from pwol in 1 or 2 M NaOH at a P_{CO_2} of 3 psi.

iii. *How does gaseous vs solid (salt) CO_2 affect the precipitation of CCSH phases and $CaCO_3$?*
    a. Gaseous CO_2 drives the system to precipitate $CaCO_3$ phases due to aqueous CO_2 species acting as an acid, while Na_2CO_3 precipitated CCSH and $CaCO_3$ phases because aqueous CO_2 species acted as a base.

4.6 Future Work

Future experiments should test how $HnaCO_3$ affects CCSH precipitation. Work should also explore and optimize pwol mortar and concrete curing techniques utilizing Na_2CO_3 solutions with the goal of minimizing CO_2 loss from the salt. Curing experimentation could also include adding sodium silicate and/or seawater solutions as a Na^+ source. Crushed or powdered glasses, like borosilicate glass and soda glass, should be in incorporated into pwol mortar and concrete mix designs as an additive, to test the viability of recycled glass as an alternative to the volcanic glasses used by Romans.

5. CCSH precipitation from waste products

5.0 Background

Industrial waste storage and management is a large environmental problem. For example, coal ash from energy production is the second most abundant waste material in the US with 890 million tons produced annually, about half of which ends up impounded in landfills.[52] While new initiatives in greener energy production are being introduced, there is still decades worth of material impounded across the US. Similarly, mining and ore refining processes produce millions of tons of slags that are sent to landfills, with records showing about 17 million tons of ferrous slags used annually.[53] Ashes and slags have been used as pozzolans to improve OPC, however the vast majority produced remain unutilized. Using the chemical mechanism proposed in earlier Chapters, it is hypothesized that these wastes could be used as cheap, low carbon impact feedstock to produce durable, high strength cementitious materials.

The following exploration of waste product combinations was conducted by Rachel McNamara for her undergraduate capstone project in 2022 under my mentorship. She completed the initial characterization of the materials, the experiments, and the data collection, excluding ICP-OES. I provided the analysis and interpretation of the XRD and TGA data.

5.1 Research Questions

i. How does CCSH precipitation differ across combinations of waste products?
ii. How do additional elements from the waste products like Mg, Fe, and S affect the CCSH precipitation mechanism hypothesized?
iii. Can the CCSH phases found in prior sections be precipitated from waste products?

5.2 Methods

5.2.1 Waste product identification

Three calcia-rich slags were utilized: lime kiln dust named Code L(Mississippi Lime Co); basic oxygen furnace slag named Slag 4 Greig (S4G); and slag cement (SC, St. Mary's Cement, grade 100 ground granulated blast furnace slag). Additionally, three silica-rich waste products were utilized, identified as Wacker silica fume (WSF), Panadyne silica fume (PSF), and Class F fly ash (Fly). Oxide compositions were measured using X-ray fluorescence (XRF, Panalyitcal Benchtop Epsilon 3x, Worcestershire, UK), shown below in Table 5.1. The Epsilon XRF machine has a reported sensitivity of < 1 ppm by mass, but the accuracy of the data is expected to be ±5% mass because of the carbon and water present in various samples.

Table 5.1 The oxide percentages of the waste products from XRF data. Note that all elements do not sum up to 100 due to the many trace elements.

Waste products	Al_2O_3	**CaO**	Fe_2O_3	K_2O	MgO	MnO	P_2O_5	SO_3	**SiO_2**	SrO	TiO_2
Code L	1.6	**86.3**	1.7	0.8	--	--	--	6.0	**2.718**	--	0.2
S4G	8.2	**47.3**	2.8	0.6	3.7	1.9	0.3	7.9	**25.2**	0.2	1.2
SC	7.3	**46.3**	0.8	0.6	8.8	0.5	0.3	2.8	**32.1**	--	0.4
Fly	--	**0.1**	0.2	0.9	0.4	--	0.3	--	**96.5**	--	--
PSF	0.7	**0.3**	1.6	0.5	0.3	0.1	0.3	0.7	**95.3**	--	--
WSF	0.6	**0.7**	--	--	--	--	0.2	--	**98.9**	--	--

Each waste product was ball-milled using zirconia milling media for 24 hours and sieved to 90 μm. The particle size was determined using the ImageJ Fiji software to analyze scanning electron microscopy (SEM) images of the powders. First, the scale was set within the program to correlate the length in pixels to the actual length. Then, a grid was overlaid on the image and each particle at an intersection point of the grid was measured along two major axes if possible. These measurements were exported, and particle size was computed according to Equation 5.1.

$$A=\pi ab \tag{5.1}$$

Here a and b represent the length of the major axes, and the particle is approximated as an ellipse. Particles at grid points that could not be quantified were skipped. The average particle size and standard deviation can be seen in Table 5.2. The Class F fly ash had the largest average particle size at 1575 μm^2, which is less than 20% of the maximum size allowed through the sieve, 8100 μm^2. Comparatively, the estimated particle size for the pure reactants used in Chapter 3 all average below ~300 μm^2. The Ca-rich wastes fall below 300 μm^2 and will likely react at similar rates to the pure CaO and $CaCO_3$ in Chapter 3 but the Si-rich wastes are likely to react slower than the ground micro silica.

Table 5.2 The average particle size and standard deviation of ball-milled waste products.

Waste product	**Average particle size (μm^2)**	**Standard deviation (μm^2)**
Code L	50.40	67.89
S4G	154.6	199.8
SC	146.4	181.0
Fly	1575	1373
PSF	1371	2431
WSF	505.3	1246

The XRD spectra of the waste products are shown in Figure 5.1, and the chemical formulae and ICDD reference codes are listed in Table 5.3. The Ca sources are shown in Figure 5.1a. The code L waste is primarily calcite, with some CaO and anhydrite. S4G is primarily a Fe-, Mg-containing variation of alumoakermanite with additional phases calcite, quartz, gypsum, ettringite, thaumasite, and harmunite. The SC waste was completely amorphous. The Si sources are shown In Figure 5.1b, all displaying a large and broad amorphous silica peak centered at 21 °2θ. Fly also contains quartz, and both Fly and PSF contain wüstite. It is not known what phase caused the second broad peak seen in the WSF spectra at 43 °2θ.

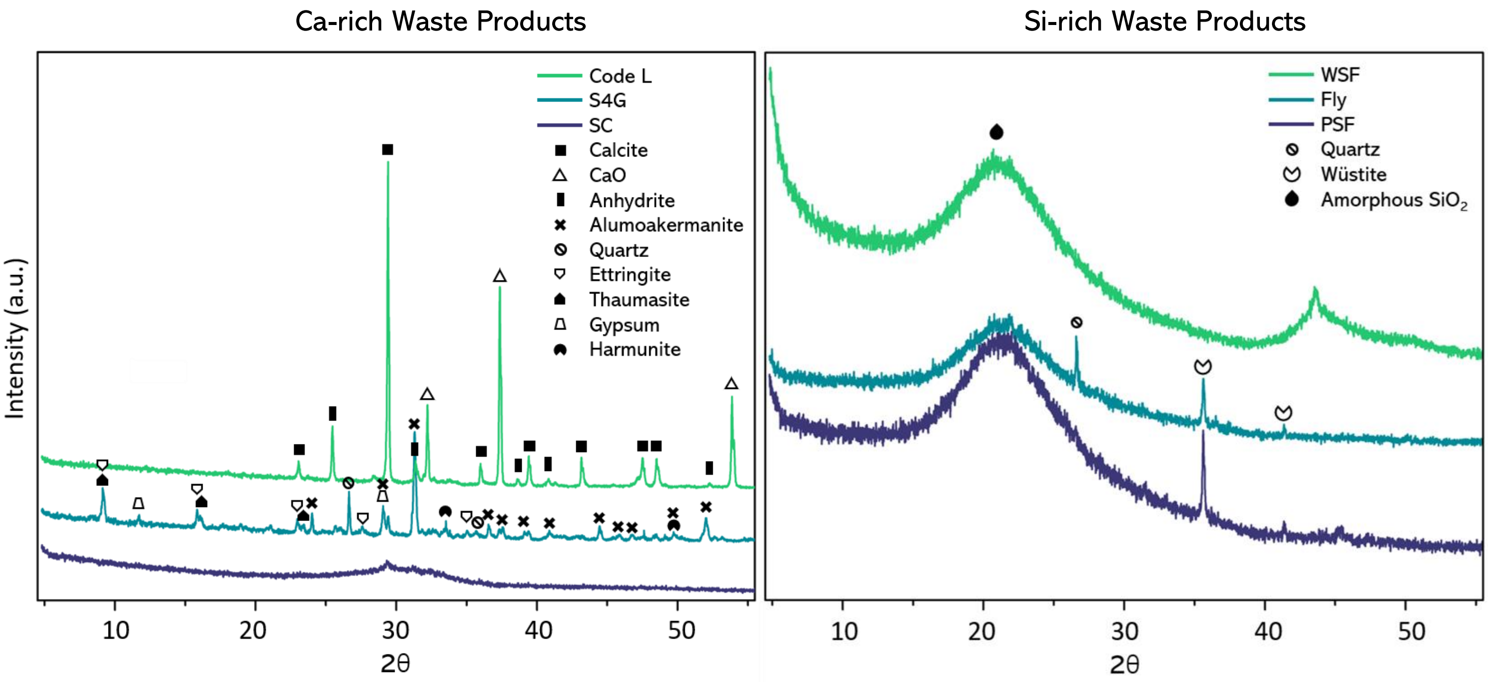

Figure 5.1 XRD spectra of the waste products. A. Ca-rich waste products, b. Si-rich waste products. Note how SC is an amorphous Ca source and that all the Si sources are amorphous.

Table 5.3. A list of mineral names, chemical formulae, and ICCD reference codes for the phases identified from reactants in this chapter.

Waste product	Mineral Name	Chemical formula	ICCD reference code
Code L	Calcite	$CaCO_3$	01-086-2334
	Calcia	CaO	04-003-7161
	Anhydrite	$CaSO_4$	04-007-6682
S4G	Alumoakermanite	$(Ca_{0.76}Na_{0.24})_2(Al_{0.5}Fe_{0.3}Mg_{0.2})(Si_2O_7)$	01-080-5267
	Gypsum	$CaSO_4 \bullet 2H_2O$	00-006-0046
	Ettringite	$Ca_6Al_2(SO_4)_3(OH)_{12}(H_2O)_{24}$	04-022-3982
	Thaumasite	$(Ca_3Si(OH)_6(H_2O)_{12})(SO_4)(CO_3)$	01-075-1688
	Harmunite	I_2O	00-032-0168
	Quartz	SiO_2	01-075-8320
Fly	Quartz	“ ”	“ ”
	Wüstite	FeO	04-008-2748
PSF	Wüstite	“ ”	“ ”

5.2.2 Hydrothermal experiments

A Ca-rich waste and Si-waste were combined to attain a Ca:Si molar ratio of 5:6 based on the XRF data. The mixtures are as follows: Mix 1 – Code L & WSF; Mix 2 – S4G & Fly; Mix 3 – SC & PSF, with the mass percentage of each shown in Table 5.4. Code L and WSF were combined because they had the highest mass percentages of Ca and Si respectively, while the other two pairs were chosen arbitrarily. The mixes were added to borosilicate test tubes at either 2g of waste mix + 20 mL of 0.1M NaOH, referred to as NaOH experiments, or 1.046g of waste mix + 0.954 g Na_2CO_3 + 20 mL of DI water,[23] referred to as Na_2CO_3 experiments. The test tubes were placed into a rack and sealed into a pressure vessel. The pressure vessels were then heated in an oven at 150 °C[23, 29, 33] (± 3 °C) for 1 day, 3 days, or 7 days of curing. The vessels were removed from the oven and the test tubes were naturally cooled to room temperature. The precipitates were filtered from solution, using 25 µm filter paper (Whatman) after curing, and the precipitates were acidified with 0.1 M acetic acid, filtered, and dried at 90 °C for 24 hours. The powders were then ground using a diamonite mortar and pestle (Fisher), sieved through a 45 µm mesh, and stored for future analysis.

Table 5.4 The mass percentages of the Ca-rich (top) and Si-rich (bottom) waste products in each mixture.

Mix 1		**Mix 2**		**Mix 3**	
Code L	53.21%	S4G	81.68%	SC	79.15%
WSF	46.80%	Fly	18.32%	PSF	20.86%

5.2.3 Characterization

XRD of the dried precipitates was conducted using the following parameters: Cu Kα-radiation (λ =1.5405 Å); current = 40 mA; tension = 45 kV, GaliPIX Detector; measurement range

= 4.8–55°2θ; time per step = 60 s; and step size =0.0143 °2θ. The sample stage was spun during the scans to minimize the effects of orientation. The scans were repeated 3 times and summed for analysis. The Empyrean has a detection limit of about 1% by mass. The data were analyzed with Highscore Plus (Version 4.9) using the International Centre for Diffraction Data (ICDD) database to identify phases. Table 5.5 contains the mineral names, compositions, and ICDD reference codes of the phase identified from the precipitates in this chapter. The majority of the reference patterns of the major phases (>10% mass) and minor phases (2-10%) identified showed strong alignment of peak locations and intensities with data presented. Gmelinite-Na was the exception, where the highest three intensity peaks aligned well but many of the lower intensity peaks misaligned.

Table 5.5. A list of mineral names, chemical formulae, and ICDD reference codes for the phases identified from precipitates in this chapter. Major phases over an estimated 10% mass are indicated by (+) and minor phases from 2-10% mass by (-).

Mineral Name	**Chemical formula**	**ICDD reference code**
Calcite (+)	$CaCO_3$	04-008-0198
Tobermorite – 13Å (-)	$Ca_{16}(Si_8O_{28})(H_2O)_{13}$	01-081-9793
Rhodesite (+)	$(Ca,K,Na)_8Si_{16}O_{40}\bullet 11H_2O$	00-022-1253
CCSH (-)	$Hca_2(SiO_4)(OH)$	04-016-0114
Gismondine-Na (+)	$Na_{3.6}Al_{3.6}Si_{12.4}O_{32}\bullet 14H_2O$	01-080-0699
Analcime (+)	$K_{0.19}Na_{7.69}Ca_{0.06}Al_8Si_{16}O_{48}(H_2O)_8$	04-024-8347
Gmelinite-Na (+)	$Na_{8.68}(H_2O)_{3.36}((Al_{7.42}Si_{16.58})O_{48}$	01-079-6686
Montmorillonite (+)	$(Ca,Na)_{0.3}Al_2(Si,Al)_4O_{10}(OH)_2\bullet xH_2O$	00-060-0320
Vishnevite (-)	$Na_8Al_6Si_6O_{24}(SO_4)\bullet 2H_2O$	00-046-1333

Select samples were further analyzed via TGA (Netzsch STA-449 F1, Bayern, Germany) to measure the amount of hydration and carbonation. For this characterization, 30 mg of powder was placed in a Pt-Rh crucible and heated at a rate of 10 °C/min to 1000 °C. The mass change data were collected and compared to the literature.[23, 36–38] The STA-449 F1 has a mass resolution of 0.025 μg.

5.3 Results

Both the NaOH and Na_2CO_3 experiments from all the waste products produced crystalline hydrates, but CCSH phases were not the dominant phases found unlike previous chapters. The Na_2CO_3 experiments across all mixes produced more crystalline hydrates, likely due to the increase in Na^+ concentration ($[Na^+]$) compared to the NaOH experiments.

The phases identified from the Mix 1 Na_2CO_3 experiments are shown in Figure 5.2a. At 1 day, the major phase was calcite, with some gismondine-Na also present. After 3 days, rhodesite was the major CCSH phase identified, with tobermorite – 13Å also matched after 7 days. A variety of crystalline sodium aluminum silicate hydrates (CNASH) phases were identified, including gismondine-Na, gmelinite-Na, analcime, and montmorillonite. The CNASH phases are partially expected to be products of glass dissolution. Interestingly, crystalline hydrate phases only formed when calcite dissolved after 1 day. In Figure 5.2b, the DTG shows the evolution of hydration and carbonation with time. The first peak centered at 110 °C is expected to be dehydration of various silicate hydrate gels containing Al, Ca, K, and Na,[39] the dehydration of tobermorite – 13Å into tobermorite – 11Å,[40] and the primary dehydration of montmorillonite.[38] The broad curve from 175-350 °C is expected to be the dehydration of rhodesite, tobermorite – 11Å,[40] and gismondine-Na. Analcime and gmelinite-Na, also dehydrate in this temperature range at 323 °C and 340 °C, respectively.[38] The sharp peak at 450 °C is expected to be the dehydration of amorphous calcium hydroxide (ACH), indicating that much of the Ca in the system was not precipitated into crystalline form. The peak at 800 °C for the 1-day sample was the decomposition of calcite into CaO and CO_2. The peak around 750 °C for 3 and 7 days is expected to be a combination of amorphous calcium carbonate (ACC) decomposition into CaO and CO_2 and the second dehydration peak of montmorillonite at 688 °C.[38]

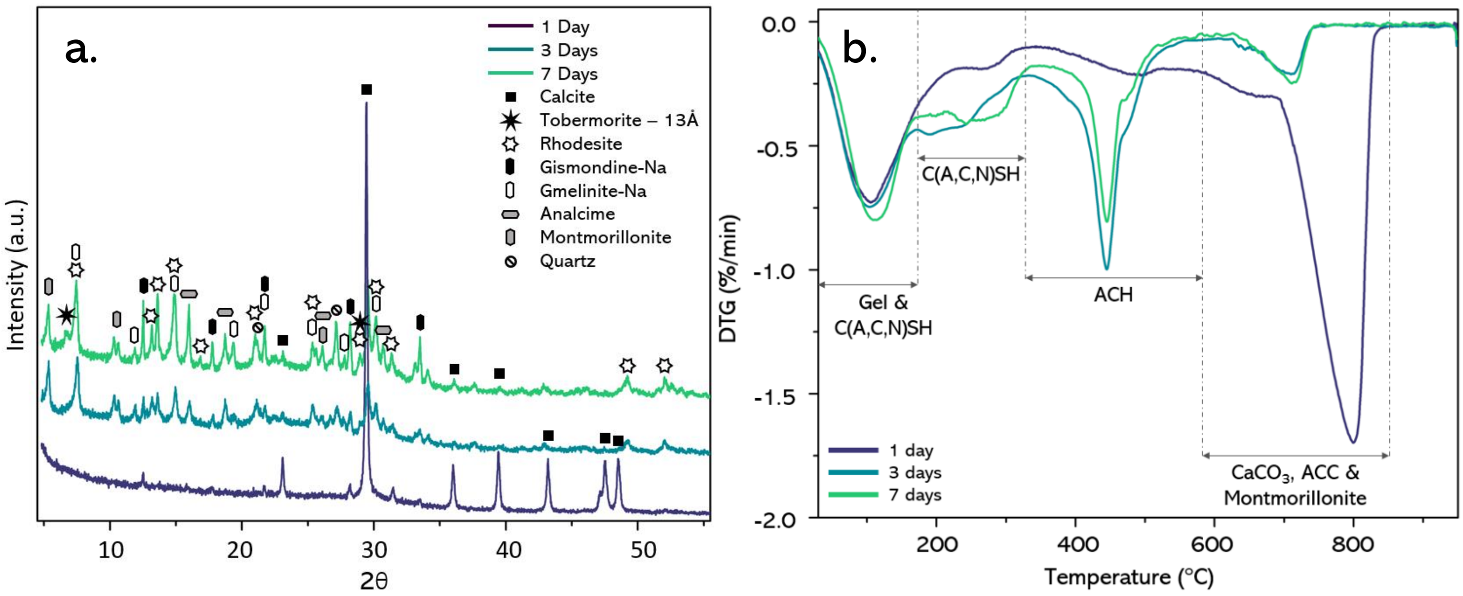

Figure 5.2 a. XRD spectra, b. DTG data of the Mix 1 Na_2CO_3 experiments at each timestep. ***C(A,C,N)SH*** *– Crystalline silicate hydrates containing a combination of Al, Ca, and/or Na;* ***ACH*** *– amorphous calcium hydroxide;* ***ACC*** *– Amorphous calcium carbonate*

The Mix 2 experiments produced a set of crystalline hydrates similar to those of Mix 1. Figure 5.3 shows that Mix 2 did not precipitate Tobermorite – 13Å and instead formed the sulphureous CNASH 82ishnevite. The intensity of gismodine-Na is also higher than that of Mix 1. Alumoakermanite decreased in intensity with time as the crystalline hydrates precipitated. The sulphate phases gypsum, ettringite, and thaumasite that were observed in the unreacted S4G were not identified. Similar to Mix 1, crystalline hydrates precipitated after calcite dissolved after 1 day. However, the unreacted S4G in Mix 2 in Figure 5.1 did show as high of a calcite intensity as the 1-day precipitates, indicating that the Na_2CO_3 first precipitated calcite from the dissolved waste.

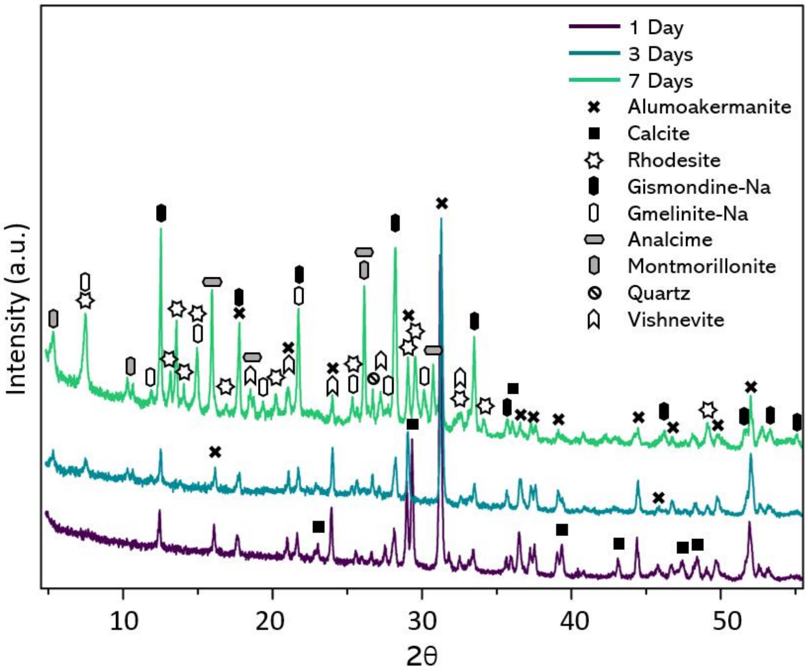

Figure 5.3 XRD spectra of the Mix 2 – Na_2CO_3 experiments at all timesteps.

The Mix 2 NaOH experiments are shown below in Figure 5.4. The majority of the phases present match the CNASH phases found in Figures 5.2a and 5.3. The only CCSH identified was an unnamed with a low intensity. DTG data in Figure 5.4b are consistent with the XRD data, showing no major changes in mass from 175-325 °C where CCSH phases are expected to dehydrate. The first peak centered at 110 °C is again expected to be Al-Ca-K-Na silicate hydrate gels and montmorillonite, and the second peak at 450 °C is expected to be ACH dehydrating. Here, the analcime and gmelinite-Na dehydration peaks are likely overshadowed by the dehydration of ACH. The peaks around 680 °C are expected to be both ACC decomposing into CaO and CO_2 and montmorillonite dehydration,[38] and the 7-day sample shows a final peak around 880 °C which is expected to be amorphous sodium carbonate (ANC) decomposing into Na_2O and CO_2.

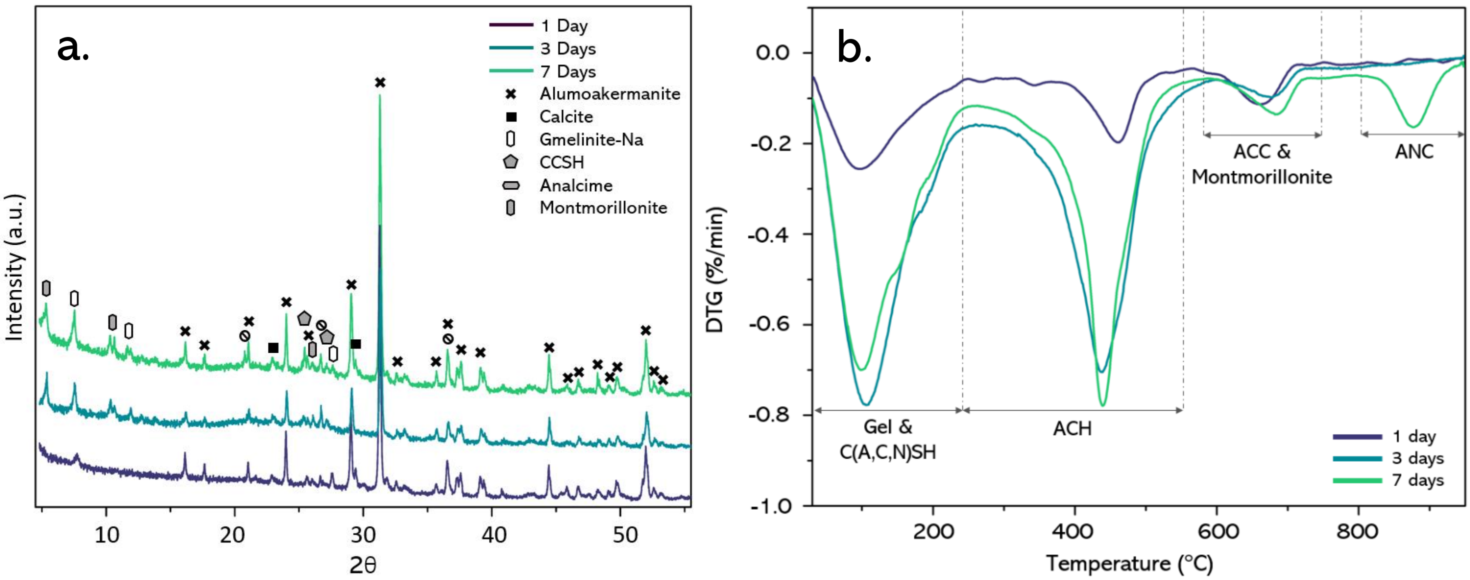

Figure 5.4 a. XRD spectra and b. DTG data of the Mix 2 NaOH experiments at all timesteps. ***C(A,C,N)SH*** *– Crystalline silicate hydrates containing a combination of Al, Ca, and/or Na;* ***ACH*** *– amorphous calcium hydroxide;* ***ACC*** *– Amorphous calcium carbonate;* ***ANC*** *– Amorphous sodium carbonate*

The Mix 3 experiments with NaOH and Na_2CO_3 only produced CNASH phases, as seen in Figure 5.5a. Due to data collection issues, only the 3 days samples are shown. The presence of gismondine-Na is the main difference between the two experiments, though gmelinite-Na, analcime, and montmorillonite all show increased intensities. At 7 days, the DTG data in Figure 5.5b show a clear increase in hydration in the Na_2CO_3 experiment compared to NaOH. The Na_2CO_3 precipitates show a much stronger first peak for Al-Ca-K-Na silicate hydrate gel and montmorillonite dehydration peak, which is also shifted closer to 110 °C than the NaOH experiment. The peak at 250 °C is expected to be gismondine-Na in the Na_2CO_3 experiment. The NaOH experiment shows much more dehydration of ACH at 450 °C than the Na_2CO_3 experiment, where the reverse is true for ACC at 680 °C.

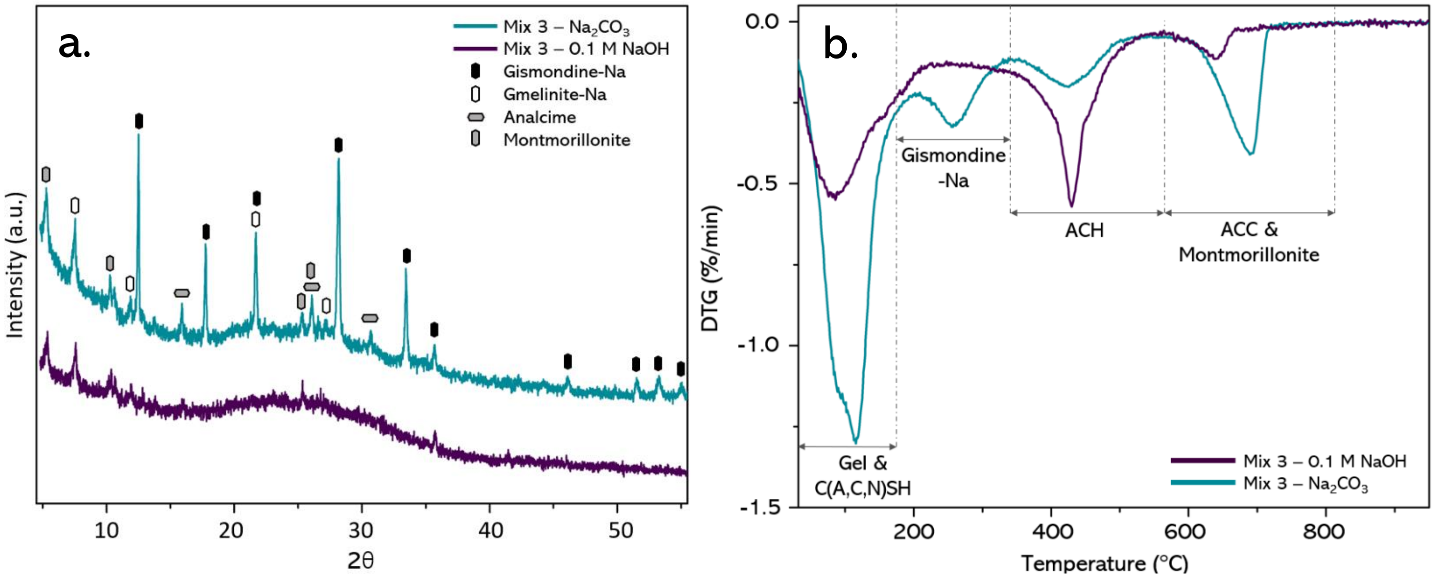

Figure 5.5 a. XRD spectra Mix 3 NaOH and NaCO$_3$ experiments at 3 days, and b. DTG data of the Mix 3 NaOH and NaCO$_3$ experiments at 7 days.

5.4 Discussion

The waste mix experiments produced more CNASH than CCSH phases as seen in the XRD spectra in Figures 5.2-5.5. CNASH phases were not desired, and it is unlikely that their precipitation would directly improve strength or durability like CCSH phase. Both analcime and montmorillonite have been used as pozzolans in OPC studies,[54, 55] indicating they react readily with portlandite and may not be chemically stable. Interestingly, these pozzolans formed in abundance despite considerable amounts of Ca in the unreacted materials. Comparing reactants and [Na$^+$] to Chapters 1 and 2, Mix 1 would be expected to form tobermorites in both NaOH and Na$_2$CO$_3$ at the concentrations used. However, the concentration of sulphates present in the Ca-rich wastes is suspected to impede CCSH precipitation. The DTG data in Figures 5.3, 5.4, and 5.5 show that instead of forming CCSH phases, Ca was likely found in ACH or ACC. In OPC research, additions of sulphate minerals have been shown to dissolve calcium containing phases.[56] OPC concretes were also shown to degrade in hydrothermal, aqueous environments, where aqueous S lowered the pH and destabilized CSH gel.[56] In this Chapter, the sulphates lowered the pH and made formation of CCSH phases, portlandite, or crystalline $CaCO_3$ less favorable. Without Ca available, the colloidal silica from both the glass and Si-rich waste dissolution reacted with Na and Al to form the CNASH phases identified.

Only in the Na_2CO_3 experiments were Mixes 1 and 2 able to produce the CCSH rhodesite, likely due to Na_2CO_3 buffering the solution to a higher pH and increased $[Na^+]$. The Mix 1 and 2 Na_2CO_3 samples also showed notable calcite concentrations at 1 day, that likely also buffered the solution as they dissolved. Interestingly, Mix 3 contained the lowest sulfur content in the XRF data of Table 5.1, yet did not produce any CCSH phases, as seen in Figure 5.5. It is hypothesized that because both wastes in Mix 3 are amorphous, the reactants immediately formed CSH gel, limiting the amount of Ca able to enter solution. The added Na and S are expected to have interfered with the crystallization of CSH gel, confining Ca to ACH or ACC and allowing colloidal silica to form CNASH.

5.5 Conclusions

The exploratory work in this chapter demonstrates the issues present in using untreated waste products to precipitate CCSH phases using the hydrothermal synthesis method outlined in this dissertation. Dissolved sulphate species are hypothesized to interfere with the crystallization of Ca containing phases, reducing both the crystallization of CSH gel and the direct precipitation of CCSH phase from colloidal silica. Colloidal silica largely reacted with Na and Al to form CNASH phases, which are not expected to directly aid strength or durability if precipitated in mortar or concrete. This chapter also demonstrates that buffering the solution pH with alkaline salts can partially overcome this issue. To utilize waste products via this synthesis method, CCSH phase precipitation will likely require highly alkaline solutions or removal of the sulphates present.

i. *How does CCSH precipitation differ across combinations of waste products?*
    a. The wastes that started as crystalline
ii. *How do additional elements from the waste products like Mg, Fe, and S affect the CCSH precipitation mechanism hypothesized?*
    a. S had the most prominent effect on CCSH precipitation by reducing the crystallization of Ca species.
iii. *Can the CCSH phases found in prior sections be precipitated from waste products*?
    a. Yes, but with less CCSH precipitation seen compared to prior experiments .

5.6 Future Work

Experiments should be repeated to complete this section of work. Firstly, ICP data of the Ca-rich wastes digested in 1 M HF and HNO_3 found differing Ca:Si molar ratios than the XRF data, shown in Figure A.5 of the appendix. The XRF ratios were found to be 1.18x higher than the ICP data in the Code L waste, 0.678x lower in S4G, and 0.673x lower in the SC. The ratios will need to be adjusted using the ICP data instead. Additionally, repeats in Teflon should be conducted to identify how much the glass dissolution aided CCSH precipitation.

Utilizing waste products to produce CCSH phases using the information gathered in this dissertation should be further pursued. The mechanism by which sulphates inhibit precipitation should be investigated to develop methods to mitigate interference. The chemical mechanism for CCSH precipitation should be further explored so that synthesis methods can be tailored to whichever waste products will be used. Additionally, future work should explore different sources of colloidal silica, from premade solutions to crushed, recycled glass used as either a powdered additive or aggregate in mortars and concretes. Mortar and concrete samples should be synthesized to identify which CCSH phases are most desirable for strength and durability as well as which are easiest to produce. Finally, methods to lower the required temperature for precipitation should be investigated to allow for easier incorporation into industrial concrete production.

6. Conclusions

This thesis contains four major findings: (1) The CCSH phases can precipitate directly from solution using TEOS and micro silica combined with CaO, $CaCO_3$ and micro silica, pwol, and combinations of waste slags and ashes; (2) increased $[Na^+]$ in alkaline solutions improves the direct precipitation of CCSH phases; (3) colloidal silica and other elemental additions released from borosilicate glass, pwol, TEOS, or micro silica dissolution impact the CCSH phases precipitated and even improve CCSH precipitation in high $[Na^+]$ solutions; (4) the source and equilibrium direction of CO_2 between gas and solution determines if $CaCO_3$ phases dominate the precipitates. The borosilicate test tubes used in synthesis led to a novel hypothesis to explain the different relationship between NaOH and CCSH precipitation from different reactants. When CaO and micro silica immediately form CSH gel, CCSH crystallization from said gel is hindered by NaOH. When $CaCO_3$, pwol, or slags dissolve slowly, colloidal silica polymerizes and reacts with Ca^{2+} to form CCSH phases. The pathways presented in this thesis could be used to engineer cementitious materials with higher strengths and improved durability via CCSH precipitation and carbon sequestration via carbonate salts. This work also indicates uses for recycled glass as an additive to dissolve and facilitate long term CCSH precipitation and potential self-healing properties, as seen in Roman concrete with volcanic glass aggregates. Using the proposed direct precipitation mechanism to incorporate waste ashes and slags as the main components of cementitious material would reduce CO_2 emissions from the cement industry and help reach climate goals. Additionally, using the waste products for cement would reduce the environmental impact of impounding the otherwise unused materials.

7. References

1. Aïtcin P. 3 - Portland cement. *Sci. Technol. Concr. Admixtures*. Elsevier Ltd; 2016:27–51. https://doi.org/10.1016/B978-0-08-100693-1.00003-5
2. Standard Specification for Portland Cement. 2000 https://doi.org/10.1520/C0150
3. Marchon D, Flatt RJ. 8 - Mechanisms of cement hydration. *Sci. Technol. Concr. Admixtures*. Elsevier Ltd; 2016:129–145. https://doi.org/10.1016/B978-0-08-100693-1.00008-4
4. Chen M, Wang K, Xie L. Deterioration mechanism of cementitious materials under acid rain attack. *Eng Fail Anal*. 2013;27:272–285. https://doi.org/10.1016/j.engfailanal.2012.08.007
5. Hodgson D, Hugues P, Vass T. Cement. *Int Energy Agnecy*. 2021.
6. Golewski GL. Green concrete based on quaternary binders with significant reduced of co2 emissions. *Energies*. 2021;14(15). https://doi.org/10.3390/en14154558
7. Maria Juenger, John L. Provis, Jan Elsen, Winnie Matthes, R. Doug Hooton, Josée Duchesne, Luc Courard, Huan He, Frédéric Michel RS and NDB. Supplementary Cementitious Materials for Concrete: Characterization Needs. *Mater Res Soc Symp Proc*. 2012;1477(August 2016):61–66. https://doi.org/10.1557/opl.2012
8. Kupwade-patil K, Al-aibani AF, Abdulsalam MF. Microstructure of Cement Paste with Natural Pozzolanic Volcanic Ash and Portland Cement at Different Stages of Curing. 2016
9. Jackson MD, Chae SR, Mulcahy SR, *et al.* Unlocking the secrets of Al-tobermorite in Roman seawater concrete. *Am Mineral*. 2012;98(10):1669–1687. https://doi.org/10.2138/am.2013.4484
10. Suprenant BA. Designing concrete for exposure to seawater. 1991
11. Komarneni S, Roy DM. Tobermorites : A New Family of Cation Exchangers. 2014;221(4611):647–648.
12. Walker CS. Characterisation and solubility behaviour of synthetic calcium silicate hydrates. University of Bristol; 2003 https://doi.org/10.13140/RG.2.2.32630.80969
13. Jackson MD, Chae SR, Mulcahy SR, Meral C, Taylor R, Li P, Emwas AH, Moon J, Yoon S, Vola G, Wenk HR, Monteiro PJM. Unlocking the secrets of Al-tobermorite in Roman seawater concrete. *Am Mineral*. 2013;98(10):1669–1687. https://doi.org/10.2138/am.2013.4484
14. Jackson MD, Moon J, Gotti E, Jackson MD, Moon J, Gotti E, Taylor R, Chae SR, Kunz M, Emwas AH, Meral C, Guttmann P, Levitz P, Wenk HR, Monteiro PJM. Material and Elastic Properties of Al-Tobermorite in Ancient Roman Seawater Concrete. 2013;2606(32734):2598–2606. https://doi.org/10.1111/jace.12407
15. Jackson MD, Oleson JP, Moon J, Zhang Y, Chen H, Gudmundsson MT. Extreme durability in ancient Roman concretes. *Am Ceram Soc Bull*. 2018;97(5):22–28.

16. Jackson MD, Mulcahy SR, Chen H, *et al.* Phillipsite and Al-tobermorite mineral cements produced through low-temperature water-rock reactions in Roman marine concrete. *Am Mineral*. 2017;102(7):1435–1450. https://doi.org/10.2138/am-2017-5993CCBY

17. Komarneni S, Roy DM. New tobermorite cation exchangers. *J Mater Sci*. 1985;20(8):2930–2936. https://doi.org/10.1007/BF00553057

18. Komarneni S, Breval E, Miyake M, Roy R. Cation-exchange properties of (Al + Na)-substituted synthetic tobermorites. *Clays Clay Miner*. 1987;35(5):385–390. https://doi.org/10.1346/CCMN.1987.0350509

19. Maeda H, Abe K, Ishada EH. Hydrothermal synthesis of aluminum substituted tobermorite by using various crystal phases of alumina. *J Ceram Soc Japan*. 2011.

20. Gabrovsek R, Kurbus B, Muller D, Wieker W. Tobermorite formation in the system CaO, C3S-SiO2-Al2O3-NaOH-H2O under hydrothermal conditions. *Cem Concr Res*. 1993;23:321–328.

21. Matekonis G, Šiaučiunas R, Vaičiukyniene D. Hydrothermal synthesis and characterization of Na+ and [Al3+ + Na+]-substituted tobermorite in CaO-SiO2 ·nH2O-H2O System. *Medziagotyra*. 2010;16(3):242–248.

22. Wu Y, Pan X, Li Q, Yu H. Crystallization and phase transition of tobermorite synthesized by hydrothermal reaction from dicalcium silicate. *Int J Appl Ceram Technol*. 2020;17(3):1213–1223. https://doi.org/10.1111/ijac.13469

23. Monasterio-Guillot L, Di Lorenzo F, Ruiz-Agudo E, Rodriguez-Navarro C. Reaction of pseudowollastonite with carbonate-bearing fluids: Implications for CO2 mineral sequestration. *Chem Geol*. 2019;524(June):158–173. https://doi.org/10.1016/j.chemgeo.2019.06.011

24. Coleman NJ, Brassington DS. Synthesis of Al-substituted 11 Å tobermorite from newsprint recycling residue: A feasibility study. *Mater Res Bull*. 2003;38(3):485–497. https://doi.org/10.1016/S0025-5408(02)01056-5

25. Plattenberger DA, Ling FT, Peters CA, Clarens AF. Targeted Permeability Control in the Subsurface via Calcium Silicate Carbonation. *Environ Sci Technol Lett*. 2019. https://doi.org/10.1021/acs.est.9b00707

26. Ashraf W. Reaction kinetics, microstructural features and mechanical properties of CO2 activated low-lime calcium silicate binders. University of Purdue; 2017

27. Qian B, Li X, Shen X. Preparation and accelerated carbonation of low temperature sintered clinker with low Ca/Si ratio. *J Clean Prod*. 2016. https://doi.org/10.1016/j.jclepro.2016.01.024

28. Binary diagram CaO-SiO2. 2018.

29. Plattenberger DA, Ling FT, Tao Z, Peters CA, Clarens AF. Calcium Silicate Crystal Structure Impacts Reactivity with CO2 and Precipitate Chemistry. *Environ Sci Technol Lett*. 2018;5(9):558–563. https://doi.org/10.1021/acs.estlett.8b00386

30. Plattenberger DA, Opila EJ, Shahsavari R, Clarens AF. Feasibility of Using Calcium

Silicate Carbonation to Synthesize High-Performance and Low-Carbon Cements. *ACS Sustain Chem Eng*. 2020;8(14):5431–5436. https://doi.org/10.1021/acssuschemeng.0c00734

31. Fuhrman J, Plattenberger DA, Clarens AF. Unpublished life cycle and techno-economic analyis of pseudowollastonite cement and concrete. 2019.

32. Casey WH. Dynamics and durability. *Rev Mod Phys*. 2009;81(2):943–958. https://doi.org/10.1103/RevModPhys.81.943

33. Houston JR, Maxwell RS, Carroll SA. Transformation of meta-stable calcium silicate hydrates to tobermorite: Reaction kinetics and molecular structure from XRD and NMR spectroscopy. *Geochem Trans*. 2009;10:1–14. https://doi.org/10.1186/1467-4866-10-1

34. Guo X, Meng F, Shi H. Microstructure and characterization of hydrothermal synthesis of Al-substituted tobermorite. *Constr Build Mater*. 2017;133:253–260. https://doi.org/10.1016/j.conbuildmat.2016.12.059

35. Siauciunas R, Janickis V, Palubinskaite D, Ivanauskas R. THE SORPTION PROPERTIES OF TOBERMORITE MODIFIED WITH Na + AND Al 3 + IONS. *Ceramics-Silikáty*. 2004;48(2):76–82.

36. Duxon P, Fernandez-Jimenez A, Provis JL, Lukey GC, Palomo A, van Deventer JS. Geopolymer technology : the current state of the art. *Adv Geopolymer Sci Technol*. 2007;(4):2917–2933. https://doi.org/10.1007/s10853-006-0637-z

37. Beaudoin, J. J.; Sato, T.; Tumidajski PJ. The Thermal decomposit ion of Ca(OH)2 polymorphs. *NRC Publ Arch*. 2006.

38. Foldvari M. Handbook of thermogravimetric system of minerals and its use in geological practice. 2011

39. Tajuelo Rodriguez E, Garbev K, Merz D, Black L, Richardson IG. Thermal stability of C-S-H phases and applicability of Richardson and Groves' and Richardson C-(A)-S-H(I) models to synthetic C-S-H. *Cem Concr Res*. 2017;93:45–56. https://doi.org/10.1016/j.cemconres.2016.12.005

40. Farmer VC, Jeevaratnam J, Speakmann K, Taylor HFW. Thermal Decomposition of 14 A Tobermorite From Crestmore. 1966

41. Rimsza JM, Jones RE, Criscenti LJ. Interaction of NaOH solutions with silica surfaces. *J Colloid Interface Sci*. 2018;516:128–137. https://doi.org/10.1016/j.jcis.2018.01.049

42. Dingsøyr E, Christy AA. Effect of reaction variables on the formation of silica particles by hydrolysis of tetraethyl orthosilicate using sodium hydroxide as a basic catalyst. *Prog Colloid Polym Sci*. 2000;116:67–73. https://doi.org/10.1007/3-540-44941-8_11

43. Schneider CA, Rasband WS, Eliceiri KW. NIH Image to ImageJ: 25 years of image analysis. *Nat Methods*. 2012;9(7):671–675. https://doi.org/10.1038/nmeth.2089

44. Galan I, Glasser FP, Andrade C. Calcium carbonate decomposition. *J Therm Anal Calorim*. 2013;111(2):1197–1202. https://doi.org/10.1007/s10973-012-2290-x

45. Manikandan S, Jagannath, Shrikhande VK, Kothiyal GP. Degradation behaviour of borosilicate glass: Some studies. *Anti-Corrosion Methods Mater*. 2006;53(5):303–309. https://doi.org/10.1108/00035590610692581

46. Information about DURAN®. n.d.

47. Murais M, Yamada H, Yamanaka J, *et al.* Unidirectional crystallization of charged colloidal silica due to the diffusion of a base. *Langmuir*. 2007;23(14):7510–7517. https://doi.org/10.1021/la700754s

48. Macphee DE, Luke K, Glasser FP, Lachowski EE. Solubility and aging of calcium silicate hydrates in alkaline solutions at 25 °C. *J Am Ceram Soc*. 1989;54:646–654.

49. Hanein T, Simoni M, Woo CL, Provis JL, Kinoshita H. Decarbonisation of calcium carbonate at atmospheric temperatures and pressures, with simultaneous CO2capture, through production of sodium carbonate. *Energy Environ Sci*. 2021;14(12):6595–6604. https://doi.org/10.1039/d1ee02637b

50. Reinik J, Heinmaa I, Mikkola JP, Kirso U. Hydrothermal alkaline treatment of oil shale ash for synthesis of tobermorites. *Fuel*. 2007;86(5–6):669–676. https://doi.org/10.1016/j.fuel.2006.09.010

51. Warring SL, Beattie DA, McQuillan AJ. Surficial Siloxane-to-Silanol Interconversion during Room-Temperature Hydration/Dehydration of Amorphous Silica Films Observed by ATR-IR and TIR-Raman Spectroscopy. *Langmuir*. 2016;32(6):1568–1576. https://doi.org/10.1021/acs.langmuir.5b04506

52. Ritter SK. A new life for coal ash. *Chem Eng News*. 2019;94(7).

53. US. Geological Survey. Mineral Commodoty Summaries. 2020;(703):86–87.

54. Chi M, Huang R. Effect of montmorillonite as additive on the properties of cement-based composites. *Sci Eng Compos Mater*. 2012;19(1):45–54. https://doi.org/10.1515/secm-2011-0129

55. Akgün Y. A Comparative Study: Blended Cements Containing Analcime and Clinoptilolite. *J Nat Appl Sci*. 2019;23(3):748–758. https://doi.org/10.19113/sdufenbed.457171

56. Benzaazoua M, Quellet J, Servant S, Newman P, Verburg R. Cementitious backfill with high sulfur content physical, chemical, and mineralogical characterization. *Cem Concr Res*. 1999;29(5):719–725. https://doi.org/10.1016/S0008-8846(99)00023-X

A. Appendix

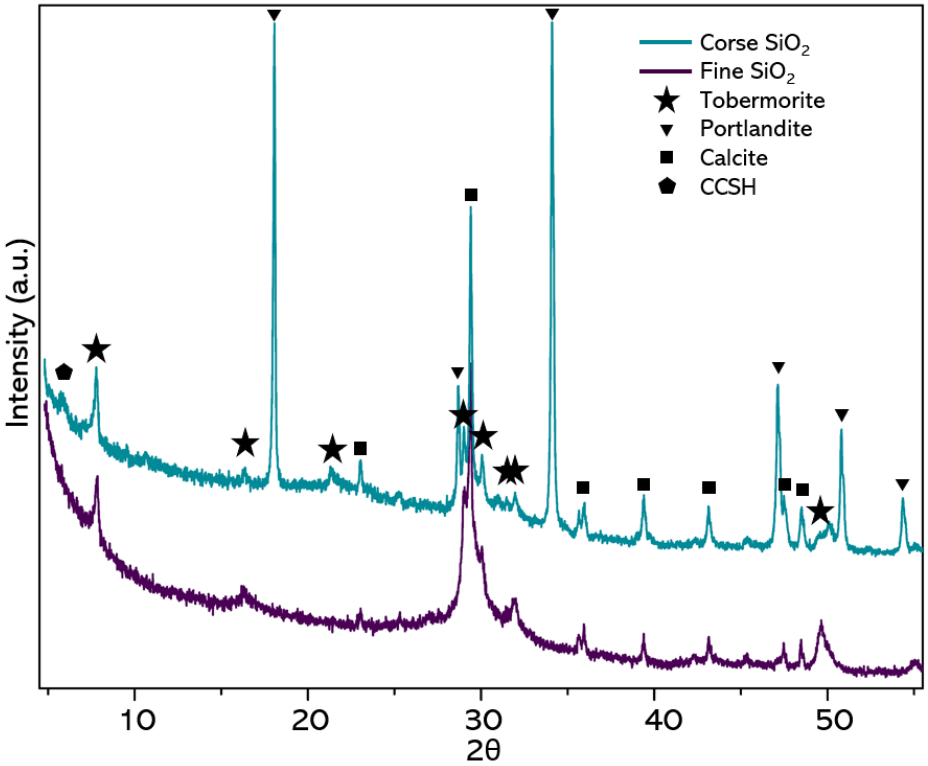

Figure A.1 XRD comparison of CaO + SiO_2 + 0.1M NaOH experiments at 7 days using different SiO_2 particle sizes. Note the presence of portlandite and amorphous SiO_2 broad peak centered around 22 °2θ, indicating the powders did not perfectly mix.

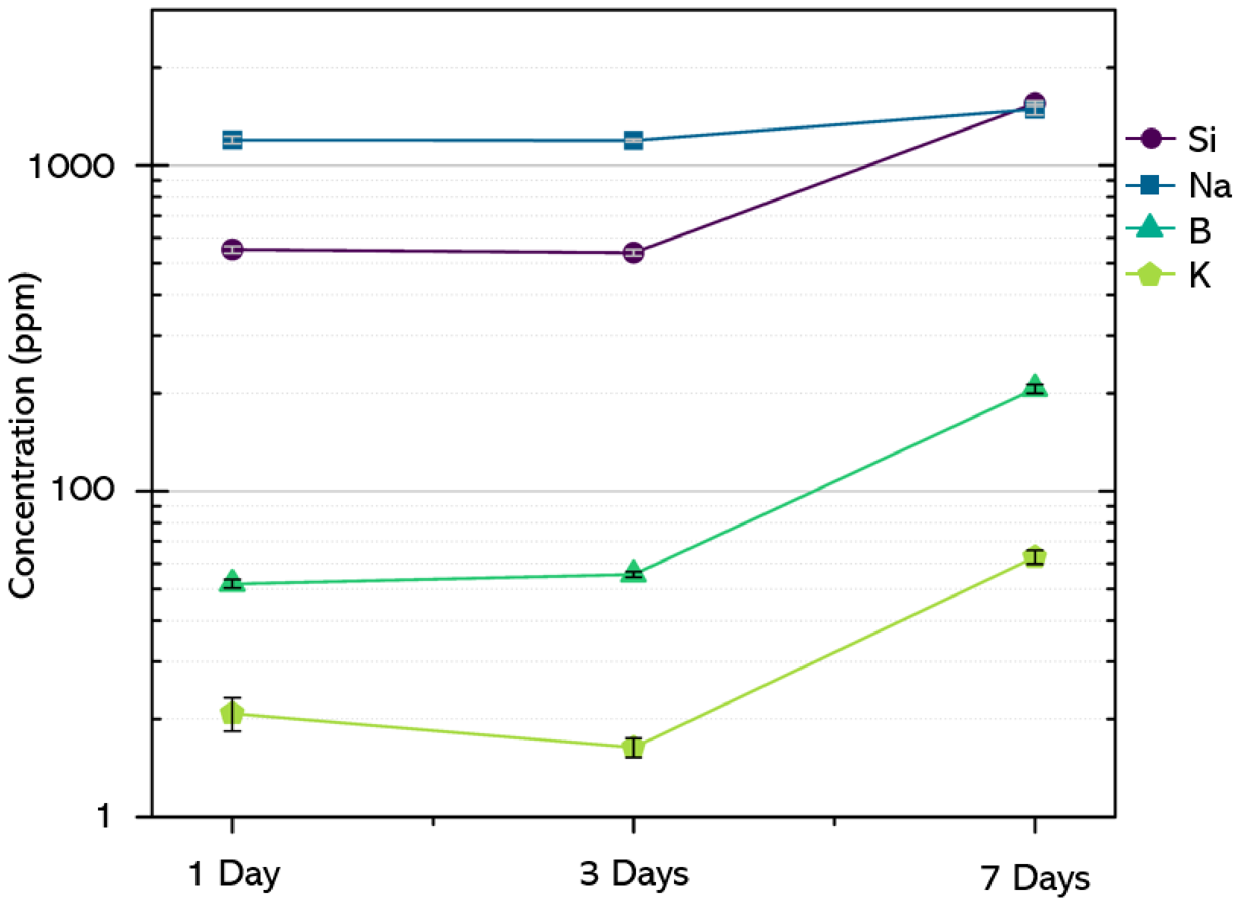

Figure A.2 ICP data of the borosilicate glass dissolution when exposed to 0.1 M NaOH. The error bars indicate 1 standard of deviation.

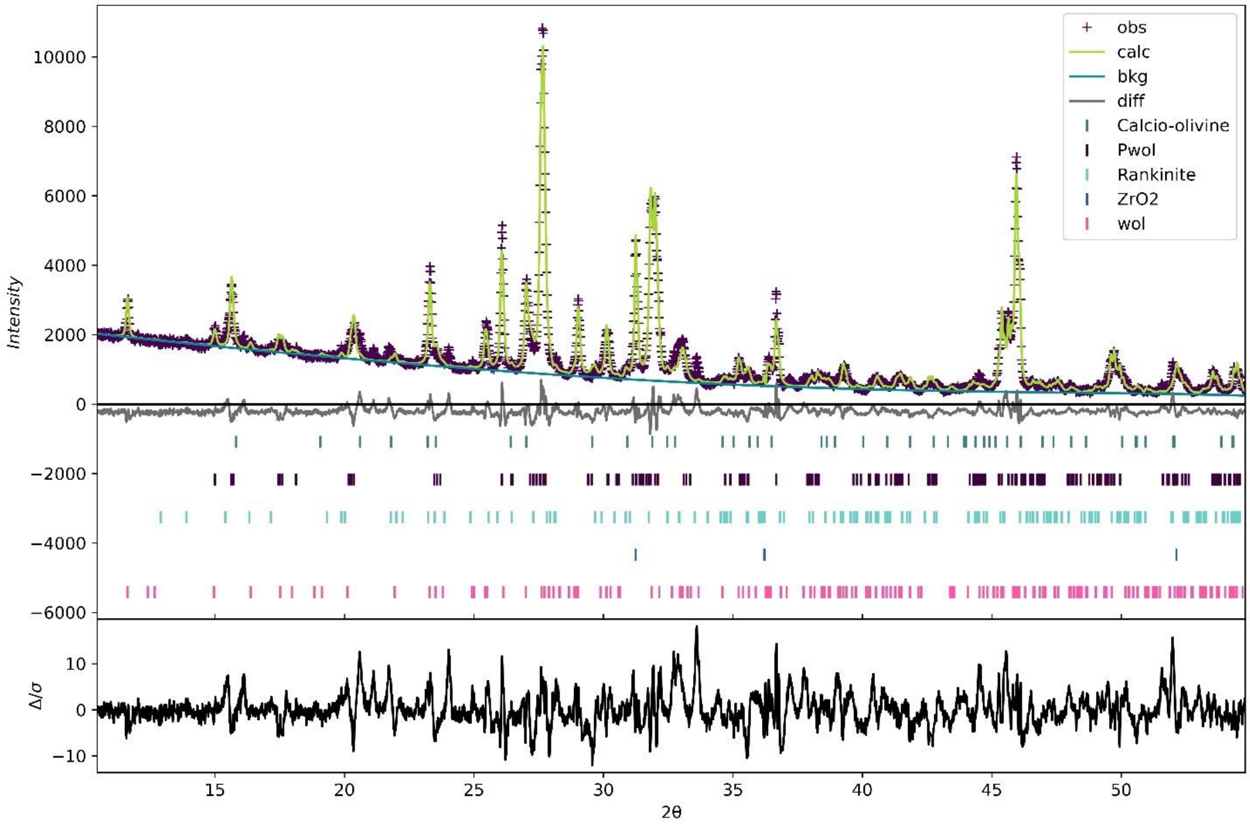

Figure A.3. The fit of the GSAS-II Rietveld refinement of pwol used in Chapter 4.

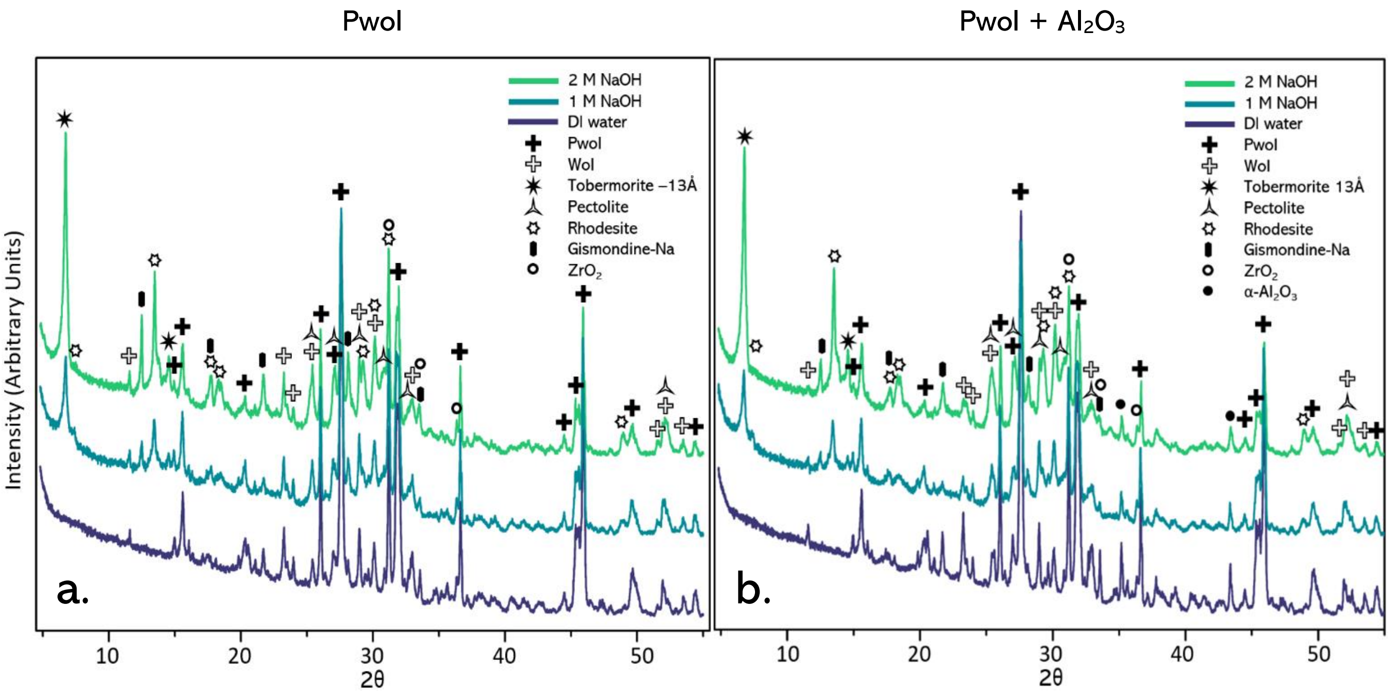

Figure A.4. XRD of 7-day precipitates at varying NaOH concentrations. a. pwol, b. pwol + Al_2O_3

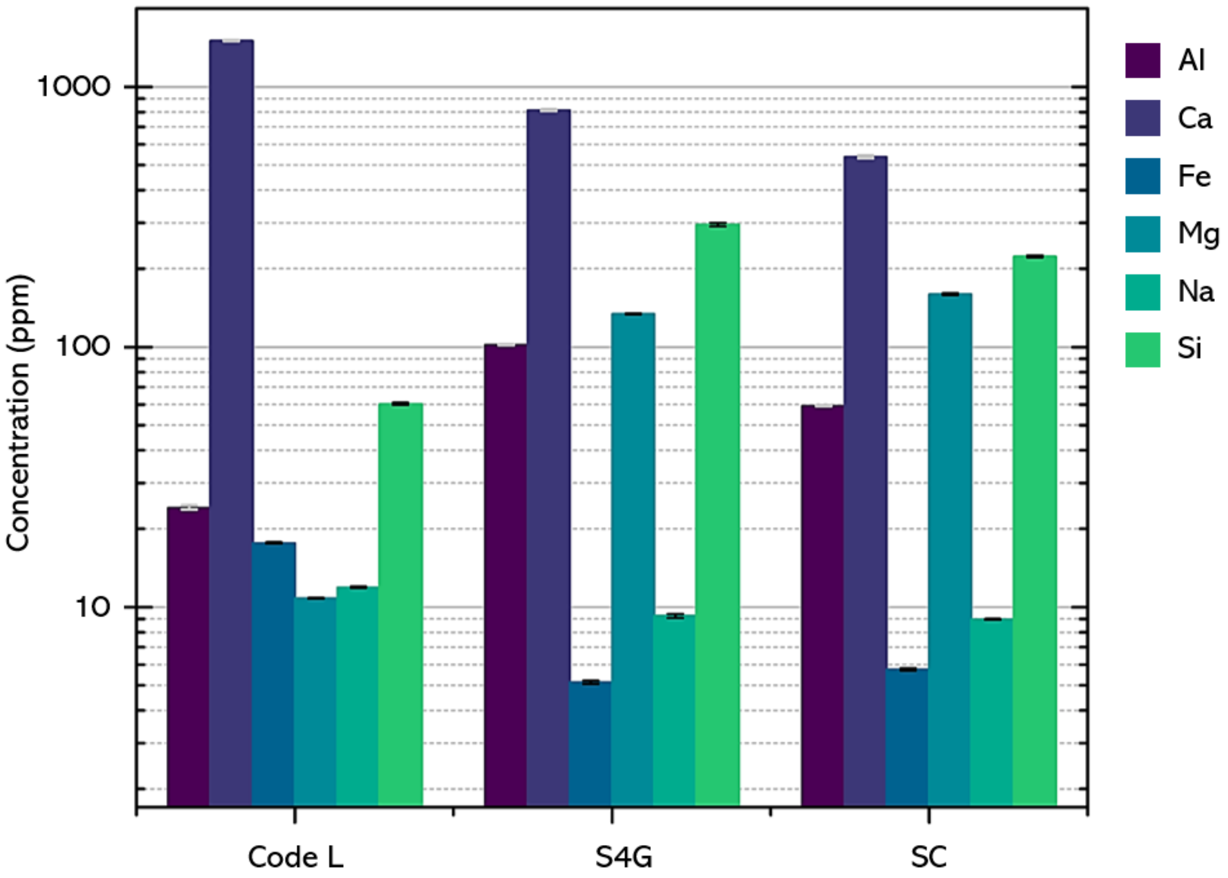

Figure A.5. ICP data of the Ca-rich wastes used in Chapter 5